1-5-2018

Evolution of the Maximum Upper Level Divergence Field in Gulf-Atlantic Tropical Cyclogenesis

Sara A. Ates
Louisiana State University and Agricultural and Mechanical College, sara_f27@yahoo.com

EVOLUTION OF THE MAXIMUM UPPER LEVEL DIVERGENCE FIELD IN GULF-ATLANTIC TROPICAL CYCLOGENESIS

A Thesis

Submitted to the Graduate Faculty of the
Louisiana State University and
Agricultural and Mechanical College
in partial fulfillment of the
requirements for the degree of
Master of Science

in

The Department of Geography and Anthropology

by
Sara Ann Ates
B.S., Louisiana State University, 2014
May 2018

ACKNOWLEDGMENTS

Without the assistance and support of many, the successful completion of this thesis would not have been possible. First and foremost, I thank God for the ability to accomplish this great challenge and for the wonderful people He has put in my path along the way. With God, all things are possible.

I owe my success and motivation to my amazing family. My daughters, Jessica, Kristin, Samantha, and Tessa, gave me inspiration to always do my best. My grandchildren, Jade, Carson, and Mason, reminded me to aim for the stars and succeed beyond them, because children learn by example. For my loving husband, Michael, there aren't enough words. He is my everlasting support, motivation, encouragement, provider, and always lending a shoulder or an ear as needed. Michael always tells me that he would follow me anywhere, even to the ends of the earth. Well, I think we got pretty close. Finally, I thank my parents for believing in me and for always teaching me to work hard, stay honest, and recognize no limits in what I could accomplish. This is for you. I love you all.

I would like to thank my graduate advisor and friend, Dr. Robert V. Rohli, for unending support and motivation. His exceptional teaching and communication skills, vast knowledge of the atmosphere, and meticulous attention to detail during an undergraduate class were my initial motivation to attend graduate school. Those traits, along with securing amazing graduate funding opportunities, were vital to the success of my thesis.

I am also very grateful for the funding provided by the generous Pruitt Fellowship through the Department of Geography and Anthropology which supported my education through the M. S. program. Additionally, Louisiana Geographic Education Alliance (LaGEA) funded through the National Geographic Education Foundation provided additional support and summer work.

A special thanks to fellow students and friends, Jordan Pino and Nazla Bushra, for their unique scientific knowledge, skills, support, and much needed laughs through the years.

Without the R Programing class taught by Dr. Kevin Robbins and statistical analysis advice from fellow student, Rudy Bartels, this research would have never evolved. Thank you.

TABLE OF CONTENTS

ACKNOWLEDGMENTS ii

LIST OF FIGURES iv

LIST OF ABBREVIATIONS vi

ABSTRACT vii

1. INTRODUCTION 1
   - 1.1. Background 1
   - 1.2. Tropical Cyclogenesis (TCG) 1
   - 1.3. Tropical Cyclone Circulation 2
   - 1.4. Research Questions 5
   - 1.5. Summary 5

2. LITERATURE REVIEW 6
   - 2.1. Literature Regarding Study Area Significance for TC Research 6
   - 2.2. Use of 200 hPa 7
   - 2.3. Upper-Tropospheric Analysis at Pressure Levels Other than 200 hPa 11
   - 2.4. Summary 14

3. DATA AND METHODOLOGY 15
   - 3.1. Upper-Level Divergence (ULD) 15
   - 3.2. JRA-55: Japanese 55-Year Reanalysis Data Set 16
   - 3.3. Individual TCG Occurrences 17
   - 3.4. Maximum and Mean ULD 20
   - 3.5. Graphical Display 22
   - 3.6. Summary 22

4. RESULTS 23
   - 4.1. Individual TCG Occurrences 23
   - 4.2. Maximum ULD 54
   - 4.3. Mean ULD 56
   - 4.4. Data Set Comparison 58
   - 4.5. Summary 61

5. CONCLUSIONS 62
   - 5.1. Upper-Level Divergence at Tropical Cyclogenesis 62

6. FUTURE RESEARCH 65

7. REFERENCES 66

8. APPENDIX: EXPANDED TABLES AND ANALYSIS 86

VITA 95

LIST OF FIGURES

Figure 1.1. Secondary circulation of a tropical cyclone. 3

Figure 2.1. Atlantic-Gulf-Caribbean basin. Source: ESRI (2017). 6

Figure 3.1. Anticyclonic upper level divergent outflow visible above Tropical Storm Zeta. 15

Figure 3.2. Nine by nine grid boxes of dimension 1.25º x 1.25º with COC in center box (a). Study area (b)....19

Figure 4.1. Location of each occurrence at time TCG (hurricane symbol) with track....23

Figure 4.2. Arlene ULD at TCG (a) and ULD at TCG with smoothing (b). 24

Figure 4.3. Bret ULD at TCG (a) and ULD at TCG with smoothing (b). 25

Figure 4.4. Cindy ULD at TCG (a) and ULD at TCG with smoothing (b). 26

Figure 4.5. Dennis ULD at TCG (a) and ULD at TCG with smoothing (b)....27

Figure 4.6. Emily ULD at TCG (a) and ULD at TCG with smoothing (b). 28

Figure 4.7. Franklin ULD at TCG (a) and ULD at TCG with smoothing (b)....29

Figure 4.8. Gert ULD at TCG (a) and ULD at TCG with smoothing (b). 30

Figure 4.9. Harvey ULD at TCG (a) and ULD at TCG with smoothing (b). 31

Figure 4.10. Irene ULD at first TCG (a) and ULD at first TCG with smoothing (b). 32

Figure 4.11. Irene ULD at second TCG (a) and ULD at second TCG with smoothing (b). 33

Figure 4.12. Jose ULD at TCG (a) and ULD at TCG with smoothing (b). 34

Figure 4.13. Katrina ULD at TCG (a) and ULD at TCG with smoothing (b). 35

Figure 4.14. Lee ULD at TCG (a) and ULD at TCG with smoothing (b). 36

Figure 4.15. Maria ULD at TCG (a) and ULD at TCG with smoothing (b). 37

Figure 4.16. Nate ULD at TCG (a) and ULD at TCG with Smoothing (b). 38

Figure 4.17. Ophelia ULD at TCG (a) and ULD at TCG with smoothing (b)....39

Figure 4.18. Philippe ULD at TCG (a) and ULD at TCG with smoothing (b). 40

Figure 4.19. Rita ULD at TCG (a) and ULD at TCG with smoothing (b). 41

Figure 4.20. Stan ULD at TCG (a) and ULD at TCG with smoothing (b). 42

Figure 4.21. Unnamed ULD at TCG (a) and ULD at TCG with smoothing (b). 43
Figure 4.22. Tammy ULD at TCG (a) and ULD at TCG with smoothing (b). 44
Figure 4.23. Vince ULD at TCG (a) and ULD at TCG with smoothing (b). 45
Figure 4.24. Wilma ULD at TCG (a) and ULD at TCG with smoothing (b). 46
Figure 4.25. Alpha ULD at TCG (a) and ULD at TCG with smoothing (b). 47
Figure 4.26. Beta ULD at TCG (a) and ULD at TCG with smoothing (b). 48
Figure 4.27. Gamma ULD at first TCG (a) and ULD at first TCG with smoothing (b). 49
Figure 4.28. Gamma ULD at second TCG (a) and ULD at second TCG with smoothing (b). 50
Figure 4.29. Delta ULD at TCG (a) and ULD at TCG with smoothing (b). 51
Figure 4.30. Epsilon ULD at TCG (a) and ULD at TCG with smoothing (b). 52
Figure 4.31. Zeta ULD at TCG (a) and ULD at TCG with smoothing (b). 53
Figure 4.32. Histogram of greatest 2% ULD values between levels 200 hPa and 150 hPa per TCG 54
Figure 4.33. Top 2% of ULD values per TCG occurrence. 55
Figure 4.34. Mean ULD at TCG (a) and ULD at TCG with smoothing (b). 57
Figure 4.35. Same as Figure 4.33 but a single plot of top 2% mean ULD values (73). 58
Figure 4.36. Cross section of mean ULD for JRA-55 data 59
Figure 4.37. Same as Figure 4.36 but for ERA-Interim Project data. 59
Figure 4.38. Same as Figure 4.34 but for ERA-Interim Project data. 60
Figure A.1. Same as Figure 4.32 but for all levels included in study 94

LIST OF ABBREVIATIONS

COC	Center of circulation
ECMWF	European Centre for Medium-Range Weather Forecasts
hPa	Hectopascal (i.e., 100 pascals or 1 millibar of atmospheric pressure)
IBTrACS	International Best Track Archive for Climate Stewardship
LOESS	Locally Weighted Scatterplot Smoothing or LOcal regrESSion
NetCDF	Network Common Data Form
NN	Nearest Neighbor
SC	Subtropical cyclone
SD	Subtropical depression
SS	Subtropical storm
TC	Tropical cyclone
TCG –12 hours	Time 12 hours prior to tropical cyclogenesis
TCG –6 hours	Time 6 hours prior to tropical cyclogenesis
TCG	Tropical cyclogenesis (i.e., tropical storm classification)
TCG +6 hours	Time 12 hours following tropical cyclogenesis
TCG +12 hours	Time 12 hours following tropical cyclogenesis
TD	Tropical depression
TS	Tropical storm
ULD	Upper-level divergence (i.e., outflow)

ABSTRACT

Upper-level (horizontal) divergence (ULD) is an important variable in tropical weather systems. As part of the circulation within a tropical cyclone (TC), it carries air in the upper troposphere away from the center of circulation (COC). To date, most research assumes the 200 hPa pressure level (approximately 12 km, varying with latitude and time of year) as the height for maximum ULD in a TC, possibly because weather observation at the 200 hPa level by radiosonde have remained mandatory for aviation purposes. The more recent availability of gridded, high-spatial-resolution, global "reanalysis" data at multiple levels, along with improvements in spatial interpolation techniques, has allowed for more precise and accurate determination of the heights at which peak ULD actually occurs, how that level varies temporally prior to and after tropical cyclogenesis (TCG), and how the spatial and temporal attributes of the three-dimensional zone of the maximum ULD field vary by storm. This research addresses these questions.

Prediction of TCs is improving rapidly as scientific understanding of the atmospheric and oceanic conditions that characterize TCG, along with tools available for measuring the associated variables, are becoming more advanced and widespread. Results using the 2005 Atlantic tropical cyclone season suggest peak mean ULD during TCG occurs predominantly at 175 hPa and is typically located in the northeastern quadrant of the storm, hundreds of kilometers from the COC. The mean conditions showed a steady increase in magnitude of ULD from TCG –12 hours to TCG +6 hours and levels off or reduces at TCG +12 hours. Mean ULD is less organized on most levels before TCG and becomes more organized and concentrated between 200 hPa and 150 hPa from TCG to TCG +12 hours.

Peak ULD during individual cyclogenesis occurrences varies widely in magnitude, temporally, and vertically. Therefore, each cyclone should be evaluated individually. In general, this research supports the notion that confinement of ULD analysis to a single pressure level could diminish research or model outcome as ULD location is variable in four-dimensional space. These results may be useful in weather and climate modeling as evolution of TC outflow can be better understood.

1. INTRODUCTION

1.1. Background

A tropical cyclone (TC) is defined as a synoptic-scale, non-frontal, warm-cored, low-pressure system that forms over tropical waters and has an enclosed area of low-level wind circulation and organized convection (Hurricane Research Division 2016). Such phenomena are relatively common in much of the low-latitude areas of the Earth. TCs of any magnitude (from weak tropical disturbances to the strongest named storms) can affect inhabitants of coastal zones in the tropics and subtropics. With coastal population growth, urbanization, and density increasing at a faster rate than inland populations (Neumann et al. 2015), the threat to life and property by these storms is an increasing concern (Baker 1979). In addition, as seen with the Galveston Hurricane of 1900, Hurricanes Camille (1969), Opal (1995), and Sandy (2012), and many other TCs around the world, the devastating effects of TCs can reach far inland as well (NHC 2015). According to Nolan (2007) "the inability to accurately forecast TC genesis can be a critical barrier to achieving sufficiently long warning times for landfalling cyclones." Therefore, dynamics of TC formation and intensity has been a topic of study for many decades.

1.2. Tropical Cyclogenesis (TCG)

TC formation is referred to as tropical cyclogenesis (TCG). Some of the conditions widely accepted that favor TCG include; a synoptic-scale, low-level rotation (or vorticity) that exceeds the vorticity imparted on the storm by the rotation of the Earth itself (Gray 1968, Vizy and Cook 2009), small tropospheric vertical wind shear (Landsea et al. 1998), a location of at least 3° to 5° of latitude away from the equator to allow for sufficient Coriolis effect to provide sustained rotational motion within the system (Bracken and Bosart 2000), sea surface temperatures of at least 26 °C (Emanuel 1986) and extending to sufficient depth (Pino 2015), near-surface preexisting atmospheric disturbance (Nolan 2007; Dunkerton et al. 2009), moist mid-tropospheric layers (Yan et al. 2015), statically unstable air, and convection (NHC 2015).

The World Meteorological Organization classifies TCs based on their intensity, with severity increasing from tropical disturbance, to tropical depression (TD), tropical storm (TS), subtropical storm (SS),

hurricane, and major hurricane. A tropical disturbance is an area of low pressure, usually a tropical wave, with increased thunderstorm activity but little organization. A TD forms as winds begin to circulate and become more organized around a center of low pressure. The system becomes more efficient when upper-tropospheric outflow, or upper-level divergence (ULD), begins as a result of convective organization occurring in regions of lowest inertial stability (Mecikalski and Tripoli 2003). As intensity increases, one closed isobar with peak sustained wind exceeding 17 m s^{-1} (HRD 2011) is present as thunderstorms form more organized bands about a center of circulation (COC). This is the TS or SS stage, at which point the storm is generally given a name. The TC is considered a hurricane after the peak sustained winds strengthen and exceed 33 m s^{-1} (Schott et al. 2012). Typically, at this stage the system develops an "eye" near its center. Hurricanes are rated based on the Saffir-Simpson Hurricane Wind Scale with wind speed determining the hurricane category; the thresholds of each category in the scale (from 1 to 5) correspond to wind speeds that damage structures through increasing categories of sturdiness (Schott et al. 2012).

Transitions from tropical disturbance to TD are not as straightforward as the other classification transitions. Without a minimum wind speed requirement (HRD 2011) or other direct measurements identifying the transition, TDs can be difficult to study. In addition, numerous tropical disturbances bypass TD stage and intensify directly into a TS. The TS stage can be measured with more accuracy and generally indicates the continuation of favorable conditions allowing for more intense tropical development (HRD 2011). Briegel et al. (1997) suggests that

> [t]here is nearly universal agreement that when a storm reaches tropical storm intensity, it will intensify into a mature cyclone without external forcing unless it is inhibited by an unfavorable environment (principally strong vertical wind shear and/or moving over land or cold water). (p. 1398)

Therefore, for the purposes of this study, TCG refers to time of transition to a TS or SS.

1.3. Tropical Cyclone Circulation

Through their circulation, TCs are simply one way the Earth regulates its temperature by the transfer of heat from the equatorial region to polar regions by way of the upper troposphere (Prasad 2016). In the Northern Hemisphere, horizontal components of motion within a TC primarily involve a counter-clockwise

(cyclonic) inward-spiral motion toward the interior of the storm at low levels (i.e., convergence), and clockwise (anticyclonic) outward-spiral motion away from the COC at higher levels (i.e., ULD). These horizontal components are part of two circulations (i.e., primary and secondary) required for a TC to develop and become efficient (Sall et al. 2006).

The primary circulation consists of broad-scale horizontal components which respond to pressure gradient force, Coriolis effect, centrifugal force, and (surface) friction, the latter of which affects the speed and therefore the strength of both the Coriolis effect and centrifugal force (Scowcroft et al. 2011). The primary circulation is found throughout the tropospheric depth and consists of azimuthal inward spiraling motion about the vertical axis (i.e., the COC) (Ooyama 1982, Marks and Houze 1987).

Motion also includes a secondary circulation with both radial and vertical components within a TC (Ooyama 1982) and responds to the same forces as the primary circulation (Willoughby 1988). TCs require a strong secondary circulation to maintain the efficiency essential for self-sustainability (Scowcroft et al. 2011). Specifically, heat leaving the system in the upper troposphere must be at a lower temperature than the heat flowing into the system in the lower troposphere (Scowcroft et al. 2011). Moreover, the spatial scale and strength of the secondary circulation largely controls TC intensity (Fang and Zhang 2011, Rappin et al. 2011). The secondary circulation in a TC (Figure 1.1) can be compared to a thermodynamic heat engine (Willoughby 1999, Denur 2011), or a Carnot engine (Ge et al. 2008).

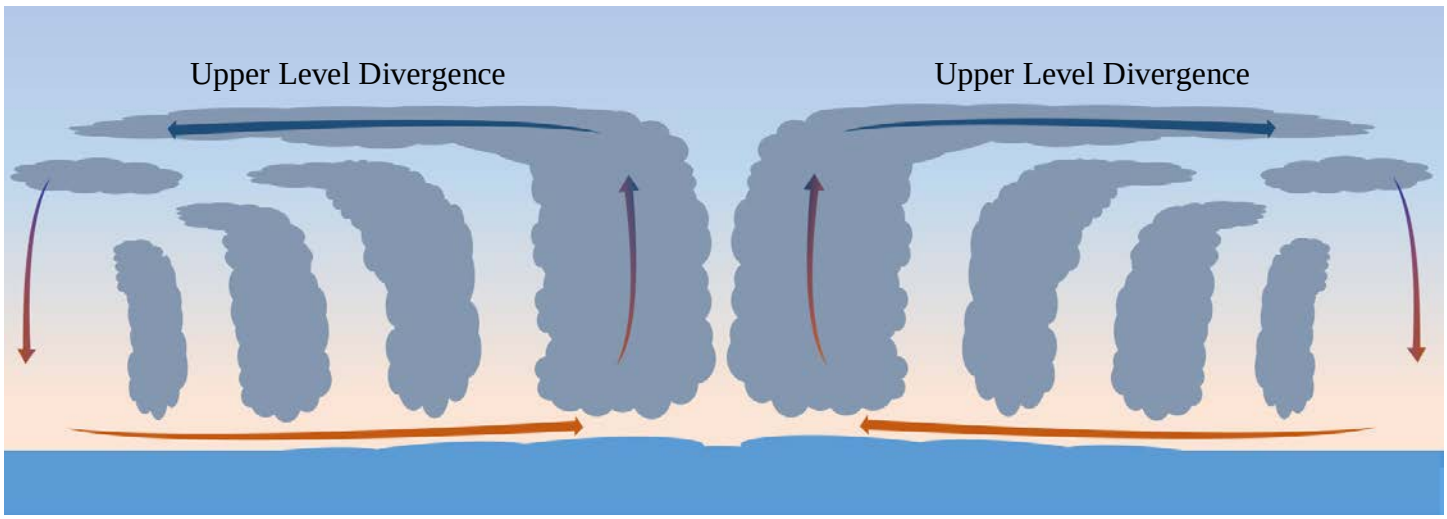

Figure 1.1. Secondary circulation of a tropical cyclone.

The cycle requires heat energy to be lost (i.e., mainly radiational cooling) at the low temperatures of the upper troposphere and gained at warmer temperatures near the surface, increasing the thermodynamic heat engine efficiency (Denur 2011, Ozawa and Shimokawa 2015) and creating a positive feedback.

This "engine" process begins as air flows over the ocean surface toward the central lower pressure of the system and isothermal expansion of air occurs (Willoughby 1999, Tang and Emanuel 2010). At this point the work (W) done by friction at higher temperatures (TH) near the surface releases kinetic energy of the winds (Denur 2011). Next, air ascends adiabatically within the deep convection (updrafts) occurring toward the center of the storm (Willoughby 1999, Tang and Emanuel 2010). This buoyancy is due to the difference in temperature between the ocean surface (TH) and the upper troposphere (TC) where outflow occurs. The difference (i.e., TH – TC) must be sufficient to promote continued lifting at the moist adiabatic lapse rate (Denur 2011, Emanuel 1986). Intensification relies on the cooler upper level to promote the unstable atmosphere needed to maintain the convection (Rai et al. 2016) which can reach approximately 13 to 19 km (i.e., 150 hPa to 75 hPa) in height (Dessler 2002).

Air is subsequently radiated outward (i.e., ULD) in the upper troposphere away from the storm and isothermal compression occurs (Willoughby 1999, Tang and Emanuel 2010). The removal of air above surface convergence reduces surface pressure, increasing the pressure gradient, and promoting large-scale ascending motion (Ge et al. 2010). Eventually, the cooler air subsides from height away from the COC and warms by adiabatic compression (Willoughby 1999, Tang and Emanuel 2010). The process begins again as the warmer air, now near the surface, flows toward the central lower pressure of the system, allowing the TC to maintain itself (Scowcroft et al. 2011).

Many variables contributing to primary circulations are studied extensively, as they are either related to conditions favorable for TC or subtropical cyclone (SC) development or intensification. Other variables, such as ULD, however, have not been studied as extensively, particularly in the days when only sparse data were available for upper-levels at a coarse spatial and temporal resolution. The resulting trend was less study of secondary circulation variables, leading to more assumptions regarding them in TC research.

A long-established assumption that ULD in TCs is best represented at 200 hPa atmospheric pressure level has followed the science as far back as the 1960s. Today, however, with aircraft equipped to fly through TCs, the increased availability of measurements, models to make estimates where measurements are unavailable, and ability to process such measurements has facilitated an examination of the extent to which ULD at the 200 hPa level actually represents a TC's peak divergence.

1.4. Research Questions

Specifically, this research seeks to address the following research questions:

1. To what extent does the atmospheric pressure level and temporal evolution for the maximum ULD field vary during TCG?
2. To what extent does the vertical and temporal evolution of the maximum ULD field vary within individual TCs?
3. To what extent does the mean ULD field vary within a TC's evolution around TCG?
4. Is it reasonable to assume that the 200 hPa level is most appropriate for identifying ULD during TCG?

1.5. Summary

This chapter has provided background on ULD, an important feature affecting TCG. It also described the objectives for the present study of the spatial and temporal evolution, in four dimensions, of the ULD during the 28 storms of the 2005 Atlantic-Gulf of Mexico TC season. The next chapter will review the scholarly literature on the 2005 Atlantic-Gulf of Mexico TC season and ULD in TCs in more detail.

2. LITERATURE REVIEW

2.1. Literature Regarding Study Area Significance for TC Research

The 2005 Atlantic Basin hurricane season was chosen as the study area due to frequency and variety in intensity of named storms (Beven et al. 2008). The 2005 season produced 28 named cyclones (NHC 2015) ranking 2.56 times the TC frequency of the 1944–2003 long-term mean (Beven et al. 2008). As the most active and costliest season on record in the Atlantic-Gulf-Caribbean basin (Figure 2.1), including the production of its strongest recorded hurricane (Wilma; Beven et al. 2008), the season has been widely studied. Moreover, the season is recent enough that high-quality measurements are available. As a result, much research has focused on individual storms within the 2005 season and on the season as a whole.

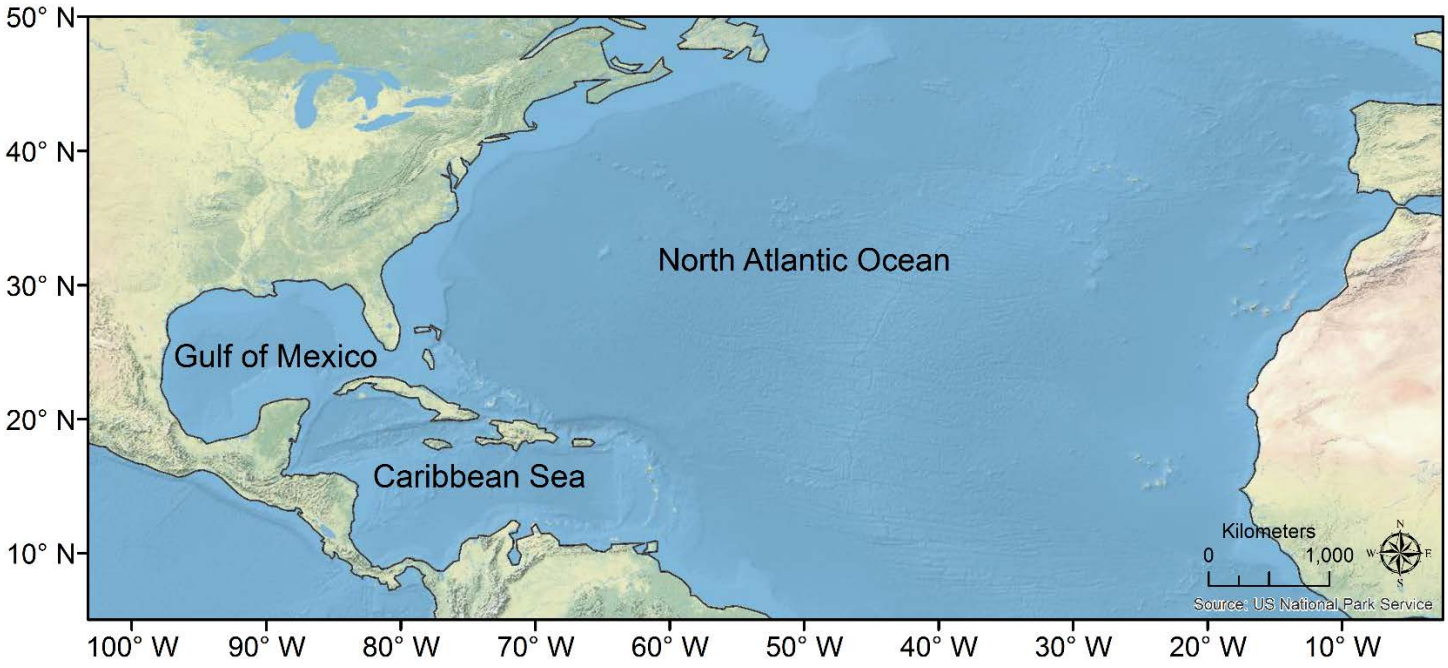

Figure 2.1. Atlantic-Gulf-Caribbean basin. Source: ESRI (2017).

Examples of research on individual storms within the 2005 season include sea surface temperatures (Foltz and McPhaden 2006), the life cycle of Hurricane Katrina (McTaggart-Cowan et al. 2007a, 2007b), Hurricane Dennis landfall damage assessments (Czajkowski and Done 2014), and TCG of Hurricane Cindy (Yoo et al. 2014). Other research that focused on the entire season includes discussions in Beven et al. (2008), anomalies of sea surface temperature between the 2005 and 2006 seasons (Chiodi and Harrison 2008), and impacts of Saharan dry air and dust on the season (Sun et al. 2008). The hurricane response of the U. S.

Geological Survey in 2005 is thoroughly documented in a USGS comprehensive report (Farris et al. 2007). Therefore, with a plethora of available data and previous research, this season was chosen as a proxy in determining vertical and horizontal extent of ULD at cyclogenesis.

Often, predicted TC impacts relative to population centers determine the amount of research on a particular storm. For example, data for some 2005 storms, such as Ophelia and Wilma, are more abundant than for others and included multiple data surveillance missions (Aberson 2008). In order to capture the full extent of ULD, this study includes all 2005 Atlantic-Gulf of Mexico storms regardless of their impact or landfall location.

2.2. Use of 200 hPa

Current literature has sparse coverage of divergence field evolution on a climatic time scale or its relationship to other atmospheric variables. Use of 200 hPa for upper-level outflow for TCs has been the widely-accepted assumption in scientific literature. Although many additional papers exist regarding different aspects of TC dynamics, motion, and thermodynamics, only a few have included sufficient examination of ULD not confined to 200 hPa (Section 2.3).

Previous research has examined wind and ULD around the 200 hPa level because it was assumed to represent the most important level for wind fields. Riehl (1948) may have been among the first to use 200 hPa for TC analysis while researching the formation of typhoons. Riehl (1948) recognized 200 hPa to 150 hPa as the levels of greatest intensity in upper systems and where the westerlies were the strongest. Upon review of upper level cyclonic circulation, Riehl (1948) determined: “It is indeed a fact that tropical storms of great intensity … display an unquestionable affinity for the 200 [hPa] high-pressure cells. [Therefore] the 200 [hPa level was] chosen as the basic level for high-altitude analysis”. Colón and Nightingale (1963) examined hurricane seasons 1956–1962 to produce preliminary results in identifying favorable patterns in upper-level flow at 200 hPa associated with TCG. Conclusions identified a need of further study on TCG “in relation to circulation patterns at the 200 [hPa] level” (Colón and Nightingale 1963). Additional research by Gray (1968) concludes:

> Divergent mass acceleration is stimulated in the upper troposphere at the level where, jointly 1) the deep cumulus updraft velocities are decreasing due to sharp increase of stability, and 2) [the] compensating outward pressure accelerations are very large. These two effects combine best near 200 [hPa]. This is the primary level of divergent mass compensation. (p. 697)

The 1718 citations compiled by Google Scholar indicate that Gray (1968) has been used as an important source for TC research and has "been accepted as the standard genesis criteria" for over 40 years (Agudelo et al. 2011). Therefore, many authors have applied the 200 hPa level as the uppermost height in TC analysis.

In part, this assumption is made because the 200 hPa level was one of the few, preselected mandatory vertical levels at which radiosondes would collect and report atmospheric measurements (Ellrod and Knapp 1992) and the 200 hPa maps were typically included in most atlases (Krishnamurti 1971a). However, over the ocean, the network of rawinsondes for wind data collection was sparse, leading to a lack of data in evaluating the TC outflow layer (Black and Anthes 1971). TC in situ research was limited to aircraft coverage of only short high-level data accumulation with restrictions on the aircraft capabilities to hundreds of kilometers outside the COC and the exiguous rawinsonde data (Black and Anthes 1971). Beginning in 1970, photographs from the ATS-III satellite allowed for flow fields to be constructed at levels with traceable clouds (Black and Anthes 1971). Despite this technological advancement, it remained impossible to determine the pressure at which these cloud traces were located when viewed from space. In an effort to validate the satellite images to the corresponding pressure level, methods employed by Black and Anthes (1971) compared cirrus cloud motions viewed from space to available 200 hPa rawinsonde data and showed a comparable agreement. Still though, Black and Anthes (1971) also cautioned that cirrus motions may not be occurring at maximum outflow levels.

Arpe (1989) recognized that although systematic errors in the European Centre for Medium-Range Weather Forecast (ECMWF) models had been reduced, they were at that time of unreliable quality regarding divergent wind. Baray (1999) noted that available data resolution is weak both in the vertical and horizontal, but upper-level clouds observed in the satellite imagery of TC Marlene (1995) correspond with the 150 hPa level. The TC outflow layer by 1997 was still plagued with minimal observations; therefore, results including ULD analysis underscore its importance (Dengler and Reeder 1997). Furthermore, Dengler and Reeder (1997) recognized "a pressing need to obtain such data in order to assess the theories." Even a review of tropical

convection by Houze (1997) mentions 200 hPa as the height extent of reliably measured divergence (i.e., ULD), but data show cloud tops several kilometers higher in the atmosphere.

Gray (1998) reported that in his Gray (1968) research, upper-level influences on TC development can be underrepresented due to lack of sufficient satellite and upper-air data in the study area (McTaggart-Cowan et al. 2013). However, reevaluation of commonplace upper-level assumptions possibly based on Gray (1968) are not evident in the following paragraphs.

Zehr (1992) analyzed 200 hPa divergence for developing and non-developing disturbances to classify synoptic-scale patterns relating to TC formation in the western North Pacific. Hurricane outflow structure is analyzed with flow fields produced from a model by Wu and Emanuel (1994) with an uppermost vertical pressure of 200 hPa. Elsberry and Jefferies (1996) analyze vertical wind shears between 200 hPa and 850 hPa to determine a threshold for wind shears unfavorable for TC development. However, they mention that the difference between 200 hPa and 850 hPa for vertical wind shear analysis is commonplace due to limited marine atmospheric data and the inability to evaluate it in more detail. In an analysis of Hurricane Wilma (2005), Chen and Zhang (2013) "...recommend that more attention should be paid to the upper-tropospheric flows, rather than just [vertical wind shear] in the typical 850–200-hPa layer, in order to reasonably predict the [rapid intensification] of TCs."

Wind field data with respect to a TC's COC were used in Briegel et al. (1997) to form composites of 200 hPa upper-level troughs possibly triggering cyclogenesis. Analysis determining upper-level anticyclonic outflow effects on a computer-generated vortex produced potential vorticity fields at 200 hPa using a model simulating cyclone vertical structure in Wang (1998). Divergence was layer-averaged between 300 hPa and 200 hPa by Bosart et al. (1999) for evaluation of Hurricane Opal's (1995) unexpected intensification. Bracken and Bosart (2000) used ~900 hPa to 200 hPa winds to model flow patterns during North Atlantic Ocean TCG with composite results for divergence at 200 hPa. Largest outflow (ULD) magnitudes were found between 250 hPa and 100 hPa in Barrett et al. (2016) but 200 hPa was the only level selected for analysis due to more frequent 200 hPa clustering in the two included case studies over their entire life cycle.

Research on the TC environment has similarly assumed a 200 hPa maximum vertical level. For instance, DeMaria et al. (2001) developed a North Atlantic TC genesis parameter that includes vertical wind shear and temperature difference analysis between 850 hPa and 200 hPa. Cheung (2004) looked for mean values of environmental parameter thresholds to determine favorable TCG locations with the use of 200 hPa divergence. Chand and Walsh (2009) calculated seasonal threshold averages for favorable TCG conditions, including cyclonic relative vorticity, environmental vertical wind shear, and divergence at 200 hPa. The development of a rapid intensity index for rapid intensification of TCs by Kaplan et al. (2010) used 200 hPa divergence averaged over a zero to 1000 km radius.

Likewise, intensification of TCs has also been studied with the assumption of 200 hPa as the "top" of the storm. For example, Davidson and Kar (2002) examined upper-tropospheric flow during intensification and used a model "initialized with objective analysis at the 200 hPa level" and even suggest that the absence of enhanced ULD during intensification could mean that ULD may not be crucial to intensification. Bhatia and Nolan (2013) compared hurricane intensity forecast models to address which environmental conditions lead to better forecasts, but limited the data analysis to 200 hPa and below in the atmosphere. Lee et al. (2015) developed a model predicting intensity changes in TCs related to certain environmental conditions but limits the divergence variable to only 200 hPa.

Even easterly wave development into TCs has assumed a 200 hPa vertical maximum. Vizy and Cook (2009) analyzed 200 hPa divergence during comparison of two African easterly wave-initiated TSs. Peng et al. (2012) investigated developing versus nondeveloping disturbances in the North Atlantic including calculations of the wind shear between 850 hPa and 200 hPa in addition to vertical divergence profiles that do not extend vertically higher than 200 hPa. Leppert et al. (2013) distinguished between non-developing and developing waves (i.e., TCs) by the presence of three conditions, one of which is "large-scale, upper-level (~200 hPa) divergence." Vertical wind shear in Didlake and Houze (2013) was calculated from 850–200 hPa although cross sections show ULD reaching well above 12 km (i.e., 200 hPa). Brammer and Thorncroft (2015) used ULD from 300 hPa – 200 hPa at TD stage to model variability and evolution of African easterly waves.

This trend of using 200 hPa upper-air data for variables related to ULD is not limited to studies, models, and research. It can be found in textbooks as well, such as Introduction to Tropical Meteorology (Laing and Evans 2011) in which winds were only considered up to 200 hPa. Even the (U.S.A.) Climate Prediction Center's Climate Diagnostics Bulletin provides monthly mean values and anomalies for vector wind, streamfunction, divergence, and velocity potential with divergent wind vectors all at 200 hPa (CPC 2017). The 2005 North Atlantic hurricane season climate perspective overview by Bell et al. (2006) incorporated 200 hPa data from the above-mentioned Climate Prediction Center.

These references identify a misconception of the importance and location of outflow associated with TCs. It is not the intention of this research to show error, but only to express the need to revisit commonplace assumptions that have become a standard. One horizontal slice of the atmosphere will not be sufficient to capture useful ULD values for use in models or research. Therefore, future research should reevaluate the 200 hPa assumption on relevant variables and implement a more encompassing use of available upper-air data. Table A.1 in the Appendix consists of a more extensive list of references that represent ULD at 200 hPa and/or use other variables related to or included in calculations of ULD.

2.3. Upper-Tropospheric Analysis at Pressure Levels Other than 200 hPa

Despite the overwhelming volume of research assuming that ULD occurs at the 200 hPa level, some research has examined ULD at other vertical levels. Jordan (1952) obtained an upper level wind-circulation pattern for TCs and recognizes anticyclonic outflow patterns beginning around 300 hPa and extending to above 150 hPa. In the 1960s, the U.S. Air Force initiated the High Altitude Clean Air Turbulence program (HICAT) to measure ~12 to ~21 km atmospheric conditions (Waco 1970). Measurements taken during Hurricane Beulah (1967) recorded anticyclonic outflow from 100 hPa to 57 hPa with the visual cirrus outflow layer top ranging between 147 hPa and 121 hPa mostly on the northern and eastern side of the COC (Waco 1970).

By 1976 satellite images and rawinsonde data had become readily available and aircraft capabilities had improved. Data for 300 hPa, 250 hPa, and 200 hPa are mentioned in Sadler (1976) as levels where wind observations by aircraft are more numerous. Sadler (1976) selected 250 hPa for the best level to analyze the

tropical upper-tropospheric trough (TUTT) associated with tropical cyclones, comparing it to the satellite observed cloudiness. With the use of aircraft wind observation data from the 300 hPa and 200 hPa levels combined with the 250 hPa and 200 hPa rawinsonde data, Sadler (1976) minimized voids in the observations. In a comparison between equatorial Western Pacific waves with ULD occurring around 175 hPa (Reed and Recker 1971) and Eastern Atlantic waves, Thompson et al. (1979) reported that ULD is of similar size and position as ULD in the Pacific, except it occurs around 250 hPa. Emanuel (1986) discussed the importance and contribution of the upper-level outflow temperature in relation to TC formation and intensity and its correlation to the ratio between radius of maximum winds to the outer radius. The temperatures used in Emanuel (1986) were taken from 300 hPa.

In a study of TC structure and evolution during explosive cyclogenesis in the North Atlantic, Wang and Rogers (2001) applied ULD data from 250 hPa. Brayshaw et al. (2009, 2011) also applied 250 hPa ULD to TC track studies in the North Atlantic. Agudelo et al. (2011) recognized that macro-scale environmental conditions in Gray (1968) (Section 2.2) are representative of the regional climatology of TC formation and not the individual TCG factors, and introduced a divergence index for African easterly waves based on differences between divergence at 850 hPa and 300 hPa. Using a reduced model to evaluate turbulence induced TC formation, Schecter (2011) was vertically limited at 300 hPa. Kerns and Chen (2015) related sea level pressure changes to a TC's warm core with available dropsonde data from aircraft flying no higher than ~350 hPa. ULD at 250 hPa was displayed in storm-centered composites by Rios-Berrios et al. (2016b) for the intensification of Ophelia (2011) in a sheared environment.

Kasahara et al. (1994) used satellite radiometric imagery data to conclude that maximum divergence occurs between 175 and 150 hPa. Davidson (1995) found in a review of vorticity budget diagnostics in tropical weather situations that ULD peaks at ~ 150 hPa. Merrill and Velden (1996) found that the outflow layer of Supertyphoon Flo (1990) was located between 180 and 120 hPa through various stages of development. Liu et al. (1997) modeled intense outflows above 300 hPa in Hurricane Andrew, with ULD appearing to extend above 200 hPa. In a separate analysis of Hurricane Andrew, Liu et al. (1999) modeled horizontal wind velocity taken

from 900 hPa to 150 hPa and intense outflows above 12 km (i.e., the approximate assumed mean height of the 200 hPa constant pressure surface). Bender (1997) analyzed the ULD of Hurricane Gilbert (1988) up to 22 km while comparing a hurricane model to a case study. Using the Advanced Microwave Sounding Unit (AMSU) data, a satellite analysis of TCs by Kidder et al. (2000) revealed the anticyclonic flow (ULD) structure between 13 km and 20 km (i.e., 175 hPa to 50 hPa). Prior to the extratropical transition of Typhoon Vicki in 1998, Kitabatake (2002) found that maximum clustered ULD was located around the 150 hPa level.

Möller and Shapiro (2002) and Shapiro and Möller (2003) used the Geophysical Fluid Dynamics Laboratory (GFDL) model forecast to simulate radial outflow up to 15 km during intensification of Hurricane Opal (1995). Liu et al. (2009) analyzed divergence up to 100 hPa for Typhoon Longwang with graphs showing ULD varying through time from 200 hPa to above 100 hPa, but the temporal mean determined 200 hPa as the contributing level. Xu and Wang (2010) extended analysis to 16 km showing radial outflow between 13 km and 16 km looking at sensitivity of TCs to entropy flux. Gopalakrishnan et al. (2011) showed that the radial wind component of the secondary circulation's outflow (ULD) extends upwards of 13 km to above 15 km, using an experimental atmosphere-ocean coupled Hurricane Weather Research and Forecast (HWRF) system. The 13 km to 16 km height was recognized statistically as the maximum cloud top height in Kubokawa et al. (2012) (i.e., the location of anvil cirrus formation resulting from the spread of outflow as deep convection reaches the tropical tropopause layer) using Nonhydrostatic Icosahedral Atmospheric Model (NICAM) data. ULD location varies between 230 hPa to 150 hPa in an evaluation of the upper-level warm core associated with Hurricane Wilma (2005) in Chen and Zhang (2013). Chen and Zhang (2013) also noted the ULD contribution to the TC's warm core in protecting it from environmental flow ventilation.

Horizontal divergence of TC-generated gravity waves was evaluated in Kim et al. (2014) to the height 16 km above ground level. Riemer and Laliberté (2015) limited secondary circulation trajectories to a height of 12 km in one experimental setup, but recognized outflow layer upper areas to be around 14 km – 15 km in height. Bentley (2017) produced layer-averaged upper-tropospheric divergent outflow from 250 hPa to 150 hPa. Komaromi and Majumdar (2014, 2015) used 200 hPa divergence to evaluate ensemble-based error for

TCG. However, Komaromi and Doyle (2017) recognized the lack of observations at higher altitudes in the first decade of the 21st century. According to Komaromi and Doyle (2017) the top of ULD may remained undetected even with observations up to 150 hPa, as the outflow can range from 300 hPa to 100 hPa; therefore, they used the mean of the combined levels. Tang (2017) suggested "setting [z (i.e., elevation)] just above the initial height of the tropopause allows for the full secondary circulation to be captured."

2.4. Summary

This chapter has traced the development of the idea for using 200 hPa level as the representative height for identifying ULD. Then, some of the most important research that has made use of the 200 hPa assumption was reviewed. The chapter concluded by mentioning ULD research at levels other than 200 hPa. This review was important as a prelude to addressing the research questions identified in Chapter 1. The next chapter will describe the data and methods used to address those research questions.

3. DATA AND METHODOLOGY

3.1. Upper-Level Divergence (ULD)

As part of the TC's secondary circulation, divergent outflow (i.e., ULD) of air from the top of a storm is an important variable. It is easily recognizable in satellite images as the widespread circulation moving outward out from the COC (Figure 3.1). ULD refers to the rate (in m s^{-1} m^{-1}, or s^{-1}) at which horizontal velocity (in m s^{-1}) changes per unit horizontal distance (in m), with positive (negative) values representing a net increase (decrease) in horizontal velocity across a distance, or horizontal divergence of air. It is a measure of whether the air is piling up (i.e., convergence, or negative ULD) or spreading out (i.e., divergence, or positive ULD) laterally in a given area.

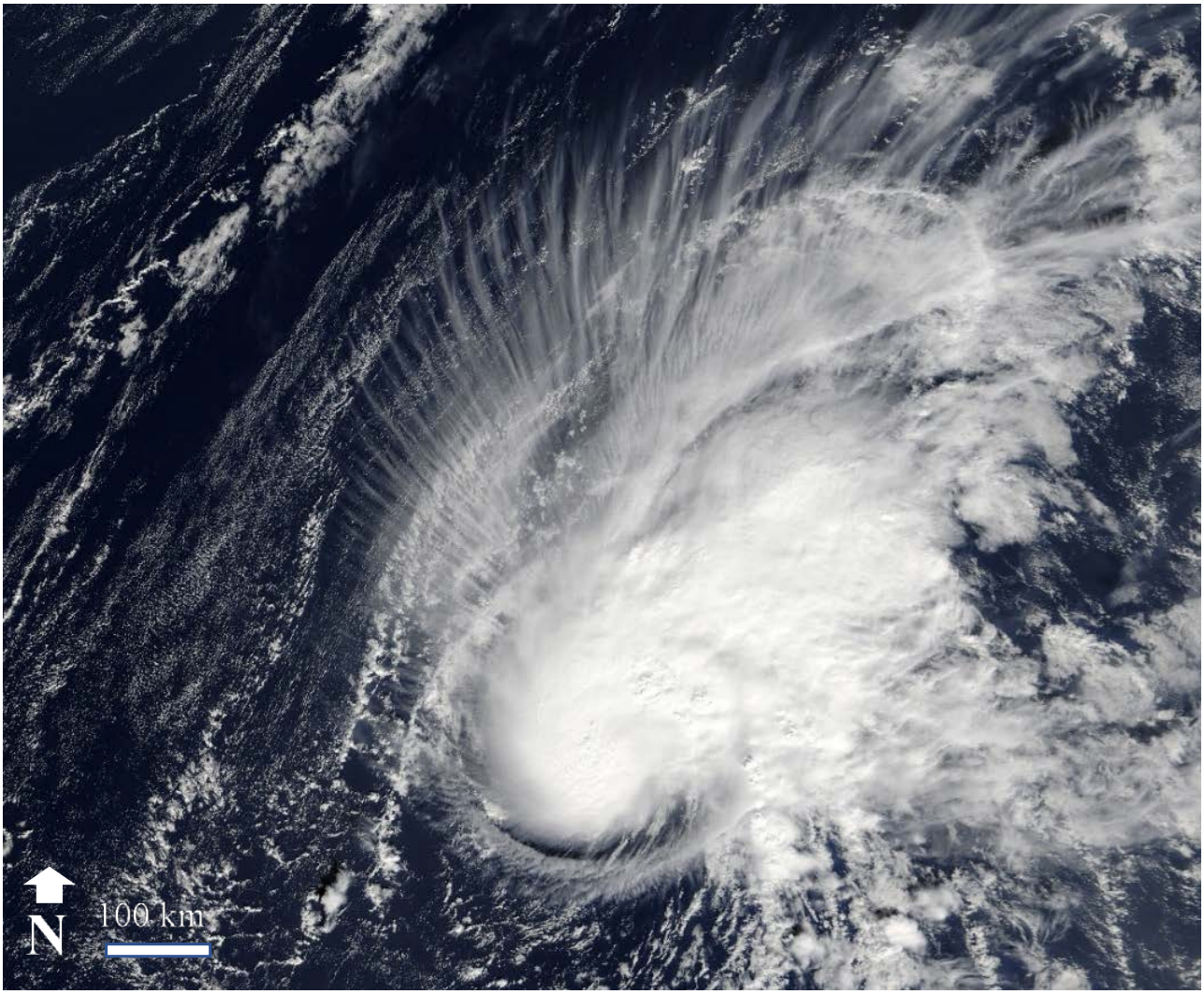

Figure 3.1. Anticyclonic upper level divergent outflow visible above Tropical Storm Zeta. Date: 03 January 2006 (NASA 2017).

Mathematically, divergence is defined as the dot product of the del operator (∇, i.e., the three-dimensional gradient vector)

$$\nabla = \vec{\vec{v}} = \vec{i}\frac{\partial}{\partial x} + \vec{j}\frac{\partial}{\partial y} + \vec{k}\frac{\partial}{\partial z}$$

of the variable of interest, where $\vec{\imath}$, $\vec{\jmath}$, and $\vec{k}$ are unit vectors in the directions of the *x*, *y*, and *z* axes, respectively, and the velocity vector

$$\vec{v} = u\vec{\imath} + v\vec{\jmath} + w\vec{k}$$

where *u*, *v*, and *w* are the west-to-east, south-to-north, and down-to-up components of the velocity, respectively. Thus, three-dimensional divergence of a vector field can be written as

$$ULD = \vec{\vec{v}} \cdot \vec{v} = \frac{\partial u}{\partial x} + \frac{\partial v}{\partial y} + \frac{\partial w}{\partial z}$$

where ∂ represents the partial derivative of the velocity components, with respect to distance in the *x*, *y*, and *z* directions. In modern data sets, *u*, *v*, and *w* are provided at multiple levels in the atmosphere, based on measured or modeled data, at a series of grid points. Therefore, ULD is derived easily from available information.

3.2. JRA-55: Japanese 55-Year Reanalysis Data Set

Divergence data were downloaded from the Japanese 55-year Reanalysis (JRA-55) project carried out by the Japan Meteorological Agency (Japan 2013, Kobayashi 2017). This data set was chosen in lieu of the more widely-used NCAR/NCEP Reanalysis (Kalnay et al. 1996) due to finer spatial resolution and additional model capabilities. Specifically, JRA-55 applies a four-dimensional variational analysis (4D-Var) with Variational Bias Correction (VarBC) and "improves the representation of atmospheric flow and the temporal consistency" (Harada et al. 2016). A preliminary analysis of the Japanese TC Vera (1959) shows high potential for use of the JRA-55 Reanalysis on TC research (Ebita et al. 2011). Moreover, the JRA-55 has improved representation of TCs in areas with limited data through its use of a wind profile retrieval method (Wood et al. 2013). At the time of initial research and data retrieval, JRA-55 provided ULD on a spatial grid of 1.25° latitude by 1.25° longitude over the research area while the NCAR/NCEP Reanalysis spatial

resolution was available only on a 2.5° latitude by 2.5° longitude spatial grid. In recent years, NCAR/UCAR Research Data Archive includes ULD data on a 0.7° latitude by 0.7° longitude spatial grid through the ERA-Interim Project (ECMWF 2009, Berrisford et al. 2011). Although Murakami (2014) found that JRA-55 was the best reanalysis data set to evaluate TCs among six available, a brief comparison of both JRA-55 and ERA-Interim Project can be found in Section 4.4. Both data sets are modeled data; therefore, this research is based on the validity of data generated by these models.

Reanalysis data for divergence are provided in Network Common Data Form (NetCDF) every 6 hours at 0000 UTC, 0600 UTC, 1200 UTC, and 1800 UTC from the JRA-55 (Japan 2013). All divergence data within a bounding box of 5° N to 50° N latitude and 103.25° W to 2.5° W longitude were downloaded to cover the relevant basin areas (Figure 2.1). The data points occur at intervals of 1.25° latitude by 1.25° longitude, creating grid blocks covering an approximate area of 139 km in the north/south direction and 138 km in the east/west direction in latitudes closest to the equator and decreasing to 89 km in the northernmost portion of the study area at latitude 50° N. The JRA-55 data set includes 37 atmospheric levels from 1000 hPa to 1 hPa. Only data from June through December 2005 were included; TS Zeta, although lasting into 2006, achieved TS status early 30 December 2005, so divergence data for 2006 were not needed.

3.3. Individual TCG Occurrences

Data retrieval, subsetting, sorting, statistical analysis, and plotting used the open source edition of R Studio, which is an integrated environment for the R Project for Statistical Computing (R 2014). International Best Track Archive for Climate Stewardship (IBTrACS; Knapp et al. 2010) best track COC data are provided to the tenth of a degree of latitude and longitude, while the JRA-55 data are provided in multidimensional NetCDF on a 1.25° latitude by 1.25° longitude grid. R programming code was written to determine which JRA-55 grid coordinates would represent the IBTrACS COC coordinates most accurately. Using the R Program's nearest neighbor (NN) formula, the minimum distance was calculated from each set of latitude/longitude coordinates in IBTrACS to the closest set of latitude/longitude coordinates on the JRA-55 1.25° grid. The result was a set of grid coordinates matching JRA-55 data for every record in the 2005 season.

Additional code produced the time of TCG based on IBTrACS wind speed, and verified with NHC (2015) Atlantic cyclone reports for 2005.

Evaluation of the time series covering 12 hours before to 12 hours after the system acquired TS status (i.e., when TCG is considered to have occurred) allowed for 24 hours of continuous ULD data throughout development. Thus, the reporting times are labeled TCG –12 hours, TCG –6 hours, TCG (time at cyclogenesis), TCG +6 hours, and TCG +12 hours. For storms in which TCG occurred so quickly that data for times prior to TCG were not included in IBTrACS, a manual review of the disturbance movement and direction prior to record were evaluated to determine the coordinates used in this study. With time and location of TCG identified, latitude and longitude coordinates for 6 and 12 hours before and after TCG could be identified in the JRA-55 data set.

Divergence (i.e., ULD) values were extracted from the JRA-55 data set using a latitude/longitude grid covering approximately 11.25° x 11.25° (i.e., nine values across and nine down, each of dimension 1.25° x 1.25°). To produce the 11.25° x 11.25° grid, four coordinates to the east and to the west, and four coordinates to the north and to the south, of the COC were used. Therefore, each grid includes 81 (9 x 9) ULD values, with the center grid box (5, 5) representing COC location as shown in Figure 3.2 (a). Total area covered in each 9 x 9 box is between approximately 1.0 million and 1.5 million km2 (depending on latitude) to capture the spatial distribution of ULD. The large 81-point gridded area provides the spatial extent necessary to obtain an accurate representation of ULD in TCs. This “grid box” method enables analysis of ULD in relation to the TC’s center of circulation (COC). A similar approach using eye-centered data for TC’s was employed by Briegel et al. (1997), Babu et al. (2015), and Rios-Berrios et al. (2016a).

The above data collection procedure was repeated for the five individual times and on each of the pressure levels. After review of the primary vertical locations of the divergence field for each TC, it was determined that nine pressure levels (350, 300, 250, 225, 200, 175, 150, 125, and 100 hPa) would be included in the evaluation. These isobaric levels cover a range of altitudes that encompass vertical extent of ULD throughout TCG.

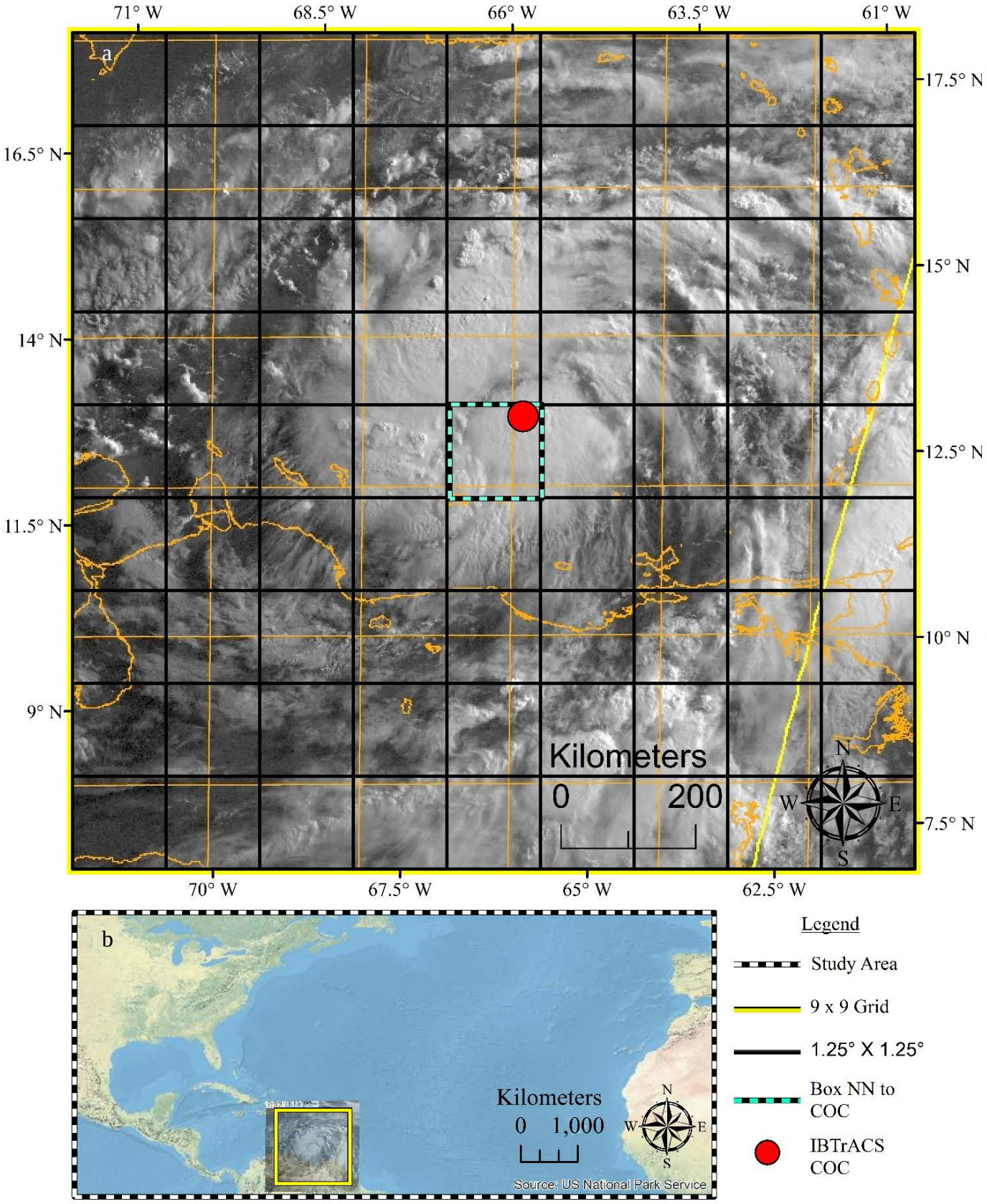

Figure 3.2. Nine by nine grid boxes of dimension 1.25º x 1.25º with COC in center box (a). Study area (b). Overlain on Tropical Storm Dennis for scale. Program ESRI. Image: Tropical Storm Dennis 07/07/05 12:00 UTC 13º N 65.9º W. GOES-12 VIS Satellite. Source: https://www.nrlmry.navy.mil/TC.html.

Originally, the season produced 27 named storms until one unnoted (subsequently named "Unnamed") SS was included in an after-season review, leading to the listed 28 (Beven et al. 2008; Knapp et al. 2010; NHC 2015). Irene, Stan, and Gamma reached TS status (i.e., achieved TCG, as defined in this research) twice in their lifespan. Of the 28 recorded storms, both TCG occurrences for Irene and Gamma were due to favorable atmospheric conditions for strengthening and are both included in this study (NHC 2015). Stan briefly weakened to a TD while crossing the Yucatán Peninsula, accounting for only one six-hour interval as a TD after (and not included in) the analyzed time series. Therefore, only the first occurrence of TCG for Stan is used, as the second was a result of land interference which caused slight deterioration of the cyclone. In total, 30 TCG occurrences (i.e., two TCGs each for Irene and Gamma and 26 named storms) are included in this study (Table 3.1). A full list appears in the Appendix Table A.2.

By incorporating the 24 hours of observations for each of the nine pressure levels centered on the time of TCG, a visualization of the ULD time series was created using the R program "levelplot" package. Individual storm plots consist of data for 81 points horizontally during the five times (i.e., TCG –12, TCG –6, TCG, TCG +6, TCG +12) and vertically through nine pressure levels. All 30 occurrences of TCG from the Atlantic-Caribbean-Gulf of Mexico basin 2005 hurricane season were analyzed, resulting in a data set of 109,350 observations (9 vertical levels x 5 temporal observations x 30 TCG x 81 grid points each).

3.4. Maximum and Mean ULD

The maximum 2% of ULD values were used in subsequent analysis to determine the pressure levels best representing ULD during TCG. This ensures the examination of peak ULD while still incorporating a sufficient number of observations to reach robust conclusions. The maximum 2% of ULD values were extracted for each individual TCG occurrence, resulting in the top 73 ULD values for each occurrence (109360 / 30 x 0.02). Of these 109350 values, 61259 are positive (i.e., divergence) and 48091 are negative (convergence). Analyzing 2% of the total data produces evaluations of ~3.6% of positive (i.e., divergence) values for each of the 30 TCGs, thereby eliminating negative values (i.e., convergence rather than divergence) to represent the peak ULD times and pressure levels (hPa).

Table 3.1. TCG occurrences in 2005 for Gulf-Atlantic-Caribbean basin. NN to JRA-55 coordinates listed.

TCG	Name	Classification	Lat °N	Long °W	Date 2005	Time	Lat °N (NN)	Long °W (NN)
1	Arlene	TCG	18.20	83.90	09-Jun	06:00	18.75	83.75
2	Bret	TCG	20.00	95.80	29-Jun	00:00	20.00	96.25
3	Cindy	TCG	25.10	90.20	05-Jul	06:00	25.00	90.00
4	Dennis	TCG	13.00	65.90	05-Jul	12:00	12.50	66.25
5	Emily	TCG	11.00	46.80	12-Jul	00:00	11.25	46.25
6	Franklin	TCG	25.70	75.90	22-Jul	00:00	26.25	76.25
7	Gert	TCG	20.80	95.00	24-Jul	06:00	21.25	95.00
8	Harvey	TCG	29.50	68.60	03-Aug	06:00	30.00	68.75
9	Irene (1)	TCG	20.20	45.00	07-Aug	12:00	20.00	45.00
10	Irene (2)	TCG	23.30	59.30	11-Aug	00:00	23.75	58.75
11	Jose	TCG	19.60	95.00	22-Aug	18:00	20.00	95.00
12	Katrina	TCG	24.50	76.50	24-Aug	12:00	25.00	76.25
13	Lee	TCG	29.00	50.40	31-Aug	12:00	28.75	50.00
14	Maria	TCG	21.10	49.40	02-Sep	12:00	21.25	50.00
15	Ophelia	TCG	27.90	78.80	07-Sep	06:00	27.50	78.75
16	Nate	TCG	28.40	66.60	06-Sep	00:00	28.75	66.25
17	Philippe	TCG	13.50	54.90	17-Sep	18:00	13.75	55.00
18	Rita	TCG	22.20	72.30	18-Sep	18:00	22.50	72.50
19	Stan	TCG	19.50	87.20	02-Oct	06:00	20.00	87.50
20	Unnamed	TCG	35.90	28.50	04-Oct	12:00	36.25	28.75
21	Tammy	TCG	27.30	79.70	05-Oct	06:00	27.50	80.00
22	Vince	TCG	32.90	20.60	08-Oct	06:00	32.50	20.00
23	Wilma	TCG	16.90	79.60	17-Oct	06:00	17.50	80.00
24	Alpha	TCG	16.50	68.50	22-Oct	18:00	16.25	68.75
25	Beta	TCG	11.00	81.30	27-Oct	06:00	11.25	81.25
26	Gamma (1)	TCG	14.30	66.00	15-Nov	06:00	13.75	66.25
27	Gamma (2)	TCG	15.70	85.60	18-Nov	18:00	16.25	85.00
28	Delta	TCG	30.70	40.50	22-Nov	18:00	31.25	40.00
29	Epsilon	TCG	31.50	49.20	29-Nov	06:00	31.25	48.75
30	Zeta	TCG	24.20	36.10	30-Dec	06:00	23.75	36.25

This analysis eliminates noise (negative values of divergence) created from the large 81-point gridded area that was necessary to ensure a large enough spatial extent to capture relevant ULD and to obtain the unique visual representation of individual TCG occurrences and mean ULD in Section 4. Mean divergence around TCG relative to the COC (i.e., the mean for each grid point averaged to a single value at each pressure level and every time stamp) calculations use the R program and include all 30 TCG occurrences, resulting in 3645 (81 grid points x 9 vertical levels x 5 instants in time) mean observations.

Due to the recent availability of better-resolution ULD data on the NCAR/UCAR Research Data Archive, identical COC centered subsetting and analysis was performed on the data to offer results comparable

to the JRA-55 data set. The ULD data are provided on a 0.7° latitude by 0.7° longitude spatial grid through the ERA-Interim Project (ECMWF 2009, Berrisford et al. 2011). The extracted data contain 289 observations per time stamp (i.e., 17 values across and 17 down), with a total of 390,150 producing a 11.9° x 11.9° latitude/longitude grid (Section 4.4). Vertical cross sections of mean ULD through the COC for each time stamp are used to compare the two data sets.

3.5. Graphical Display

Individual and mean plots are colored on a scale diverging at zero to represent areas of divergence (positive), nondivergence (i.e., values around zero), and convergence (negative). Plots are provided for exact data values as well as a smoothed plot for a simpler interpretation. In the histograms displaying level vs. time counts, the standard error of the mean with 95% confidence intervals of the standard mean is rounded to the nearest 5.0×10^{-6} s^{-1} to represent mean value intervals. Distinct colors also represent values 1) below mean, 2) near mean, and 3) above mean. Maximum 2% ULD plots use distinct colors to differentiate between ULD found 1) 200 hPa and below and 2) above 200 hPa. The R program "local regression smoothing" (LOESS) is applied to maximum 2% ULD plots with a 95% confidence interval within the shaded area. LOESS is a local polynomial regression fitting and was chosen due to the low number of points (73) for each TCG. The smoothing is fit based on distance-weighted points in the neighborhood of each point (R 2014). In an effort to prevent overplotting, some graphs use "jitter" to spread the points within the areas designated for vertical level and time series. Although the ULD data are continuous, the data points are taken on a discrete scale with only nine pressure levels and five time stamps. Therefore, slight displacement and 50% transparency of the values at each set point are necessary to visualize the quantity of the values.

3.6. Summary

This chapter has detailed the data used to address research questions in Chapter 1. It also described the methods used to evaluate the individual, mean, and maximum evolution of ULD during TCG. It concluded with a brief description of the visual tools used to display the research data. The next chapter will review results of the analysis described in Chapter 3.

4. RESULTS

4.1. Individual TCG Occurrences

The following section is a brief review of synoptic history related to storm intensification conditions within the 24-hour time period analyzed (Figure 4.1 and Appendix Table A.2). Additional synoptic information can be found on the National Hurricane Center website (NHC 2015).

ULD in each storm is displayed on a plot with the 24-hour time scale on the x-axis and pressure levels from 350 hPa up to 100 hPa on the y-axis. ULD values are displayed as a ramped color palette showing divergence (convergence) in blue (brown) and darker (lighter) as stronger (weaker) values. The area of non-divergence (ULD ~ 0.0 s^{-1}) is pale. The COC is located in the center of each individual grid box, represented by a small red dot. The COC coordinates can vary in latitude and longitude through time depending on the TC translation speed and direction. Therefore, it is important to note that each time stamp has its own unique set of coordinates using the best track data location (IBTrACS, Knapp et al. 2010) of COC at a given time. These graphs are intended to show the temporal and three-dimensional spatial maxima, range, and concentrated areas of ULD for each storm.

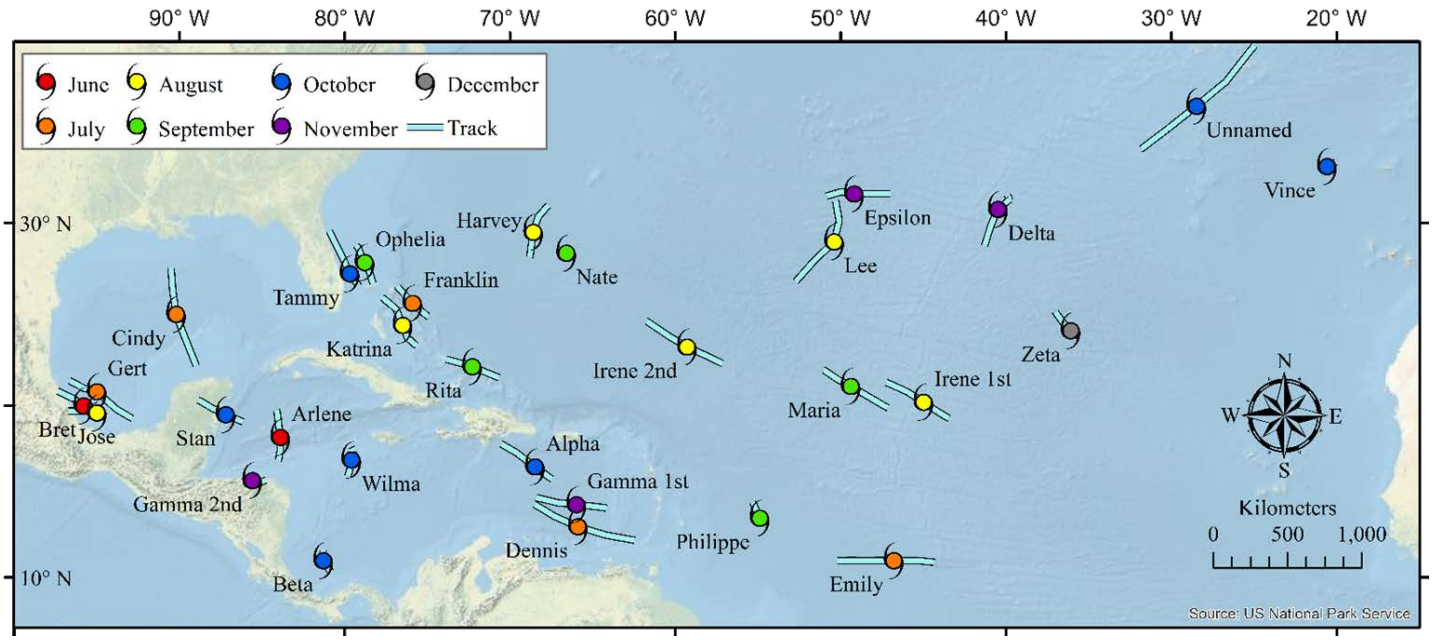

Figure 4.1. Location of each occurrence at time TCG (hurricane symbol) with track of location through the 24 hours included in study. Colors indicate month of TCG occurrence.

4.1.1. Tropical Storm Arlene

Arlene is the first named TS of the 2005 Atlantic Hurricane Season. Arlene achieved TS status at 0600 UTC on 9 June 2005 at 18.2° N, 83.9° W (Knapp et al. 2010) due to cyclonically curved very deep convection forming northeast of the COC (NHC 2015). Throughout the lifetime of Arlene, various centers rotating around a larger gyre (NHC 2015) occurred. These "centers" are noticeable in Figure 4.2 at time TCG predominantly occurring at 150 hPa and 6 hours after TCG at 200 hPa. The ULD values tend to be concentrated northeast of the COC. Arlene displayed steady intensification during this period. Concentrated ULD values reach to 125 hPa at TCG –6 hours and become less organized through time. Maximum ULD concentrations also move lower in the atmosphere through time.

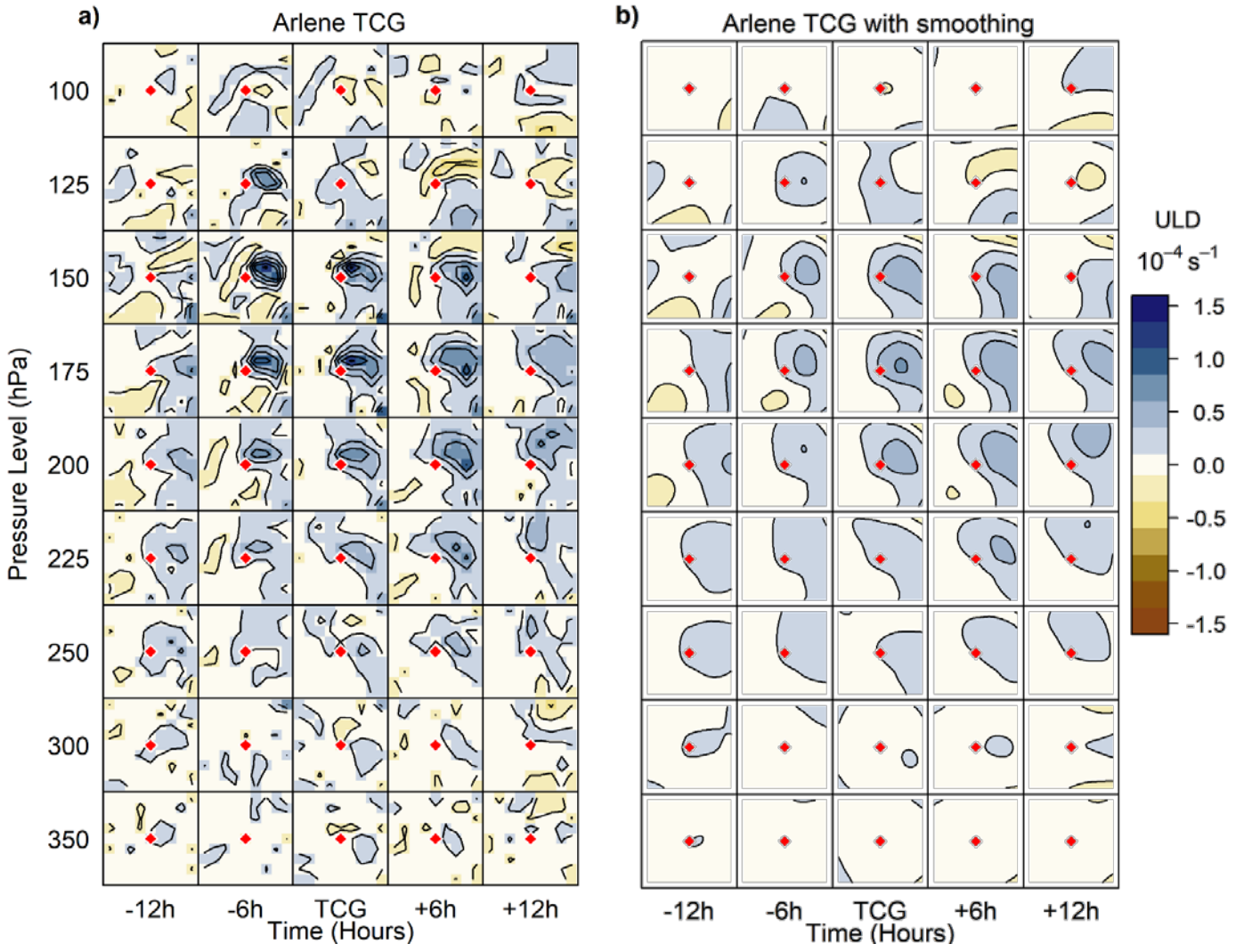

Figure 4.2. Arlene ULD at TCG (a) and ULD at TCG with smoothing (b).

4.1.2. Tropical Storm Bret

Bret achieved TS status between 1800 UTC on 28 June 2005 and 0000 UTC on 29 June 2005 at 20.0° N, 95.8° W (Knapp et al. 2010). The 0000 UTC report on 29 June 2005 was used for TCG. Bret formed very near the coast of Mexico and was small and short-lived but maintained increasing organization and strengthening until landfall at 1200 UTC on 29 June (NHC 2015). Storm tracking records for Bret began with TCG –6 hours when it was categorized as a TD. Therefore, time for TCG –12 hours was estimated back from initial movement and location records of the storm. The concentrated ULD values reach 100 hPa six hours after TCG in Figure 4.3, with strongest ULD organized between the 175 hPa and 150 hPa heights six hours before and at TCG.

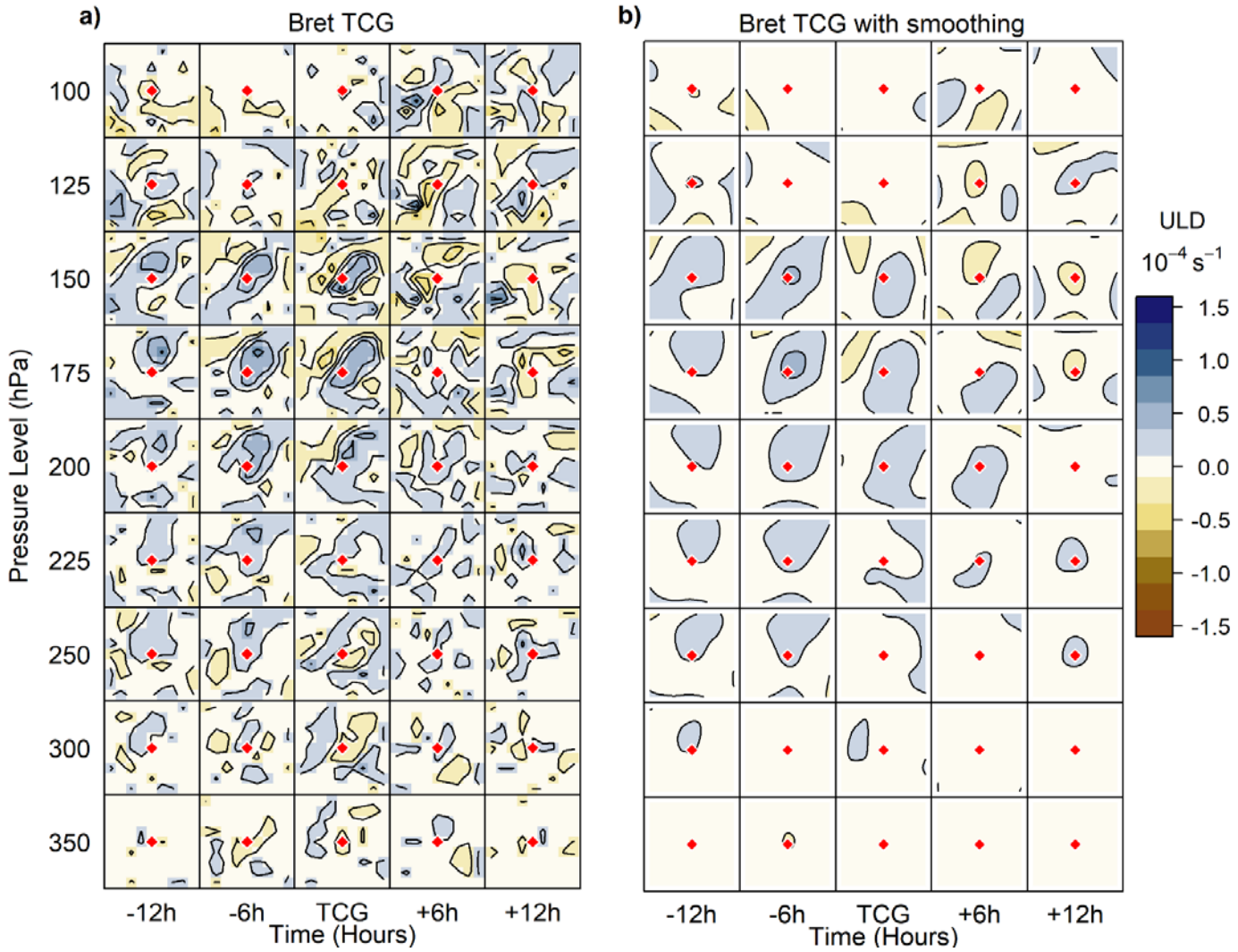

Figure 4.3. Bret ULD at TCG (a) and ULD at TCG with smoothing (b).

4.1.3. Tropical Storm Cindy

Cindy achieved TS status at 0600 UTC on 5 July 2005 at 25.1° N, 90.2° W (Knapp et al. 2010). The high translation speed of Cindy and decrease in southerly wind shear aided in the rapid development of a hurricane within the next 18 hours (NHC 2015). Maximum concentrated ULD values reach the 125 hPa level at most times during TCG. The area of ULD stretches vertically, with the peak value rising higher in the atmosphere over time (Figure 4.4). The remarkable strengthening during the 24 hours surrounding TCG as Cindy was about to move onshore is evident in Figure 4.4 and appears to indicate the makings of a major hurricane. In post-season re-analysis, Cindy was upgraded from a TS to a hurricane only 40 nautical miles SSW of Grand Isle, Louisiana, and subsequently maintained hurricane status hours after landfall (NHC 2015).

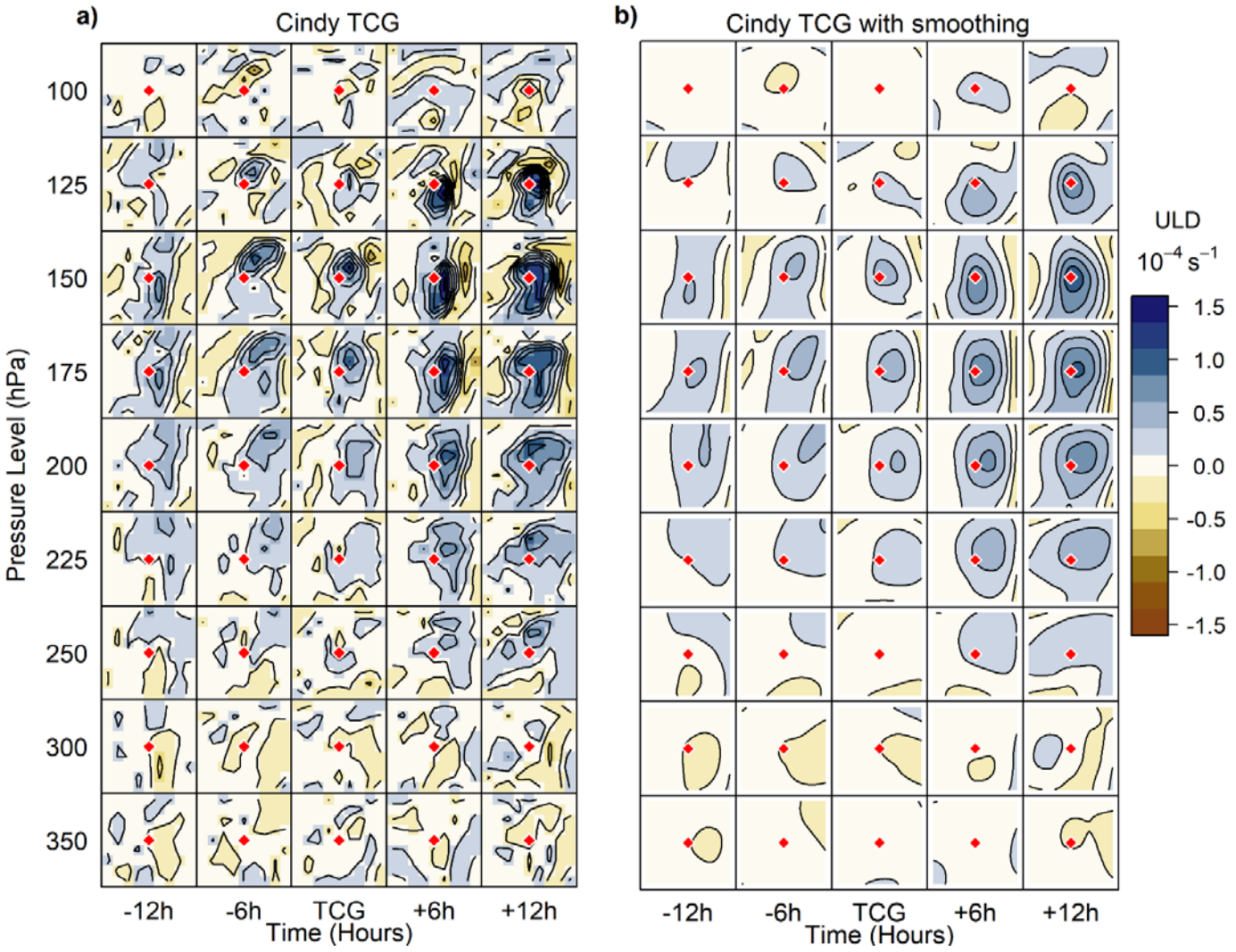

Figure 4.4. Cindy ULD at TCG (a) and ULD at TCG with smoothing (b).

4.1.4. Tropical Storm Dennis

Dennis achieved TS status at 1200 UTC on 5 July 2005 at 13.0° N, 65.9° W (Knapp et al. 2010). From TD to Category 4 hurricane, Dennis continued steady to rapid intensification in favorable conditions (NHC 2015). The largest concentrations of ULD values remain above the 200 hPa level during the 24 hour time series and extend up to 125 hPa (Figure 4.5). ULD magnitude gradually increases from TCG –12 hours till after TCG, then begins to decrease between TCG +6 hours and TCG +12 hours. Dennis appears fairly well organized throughout the time series and the ULD field is maintained very near the COC from approximately 225 hPa to 125 hPa.

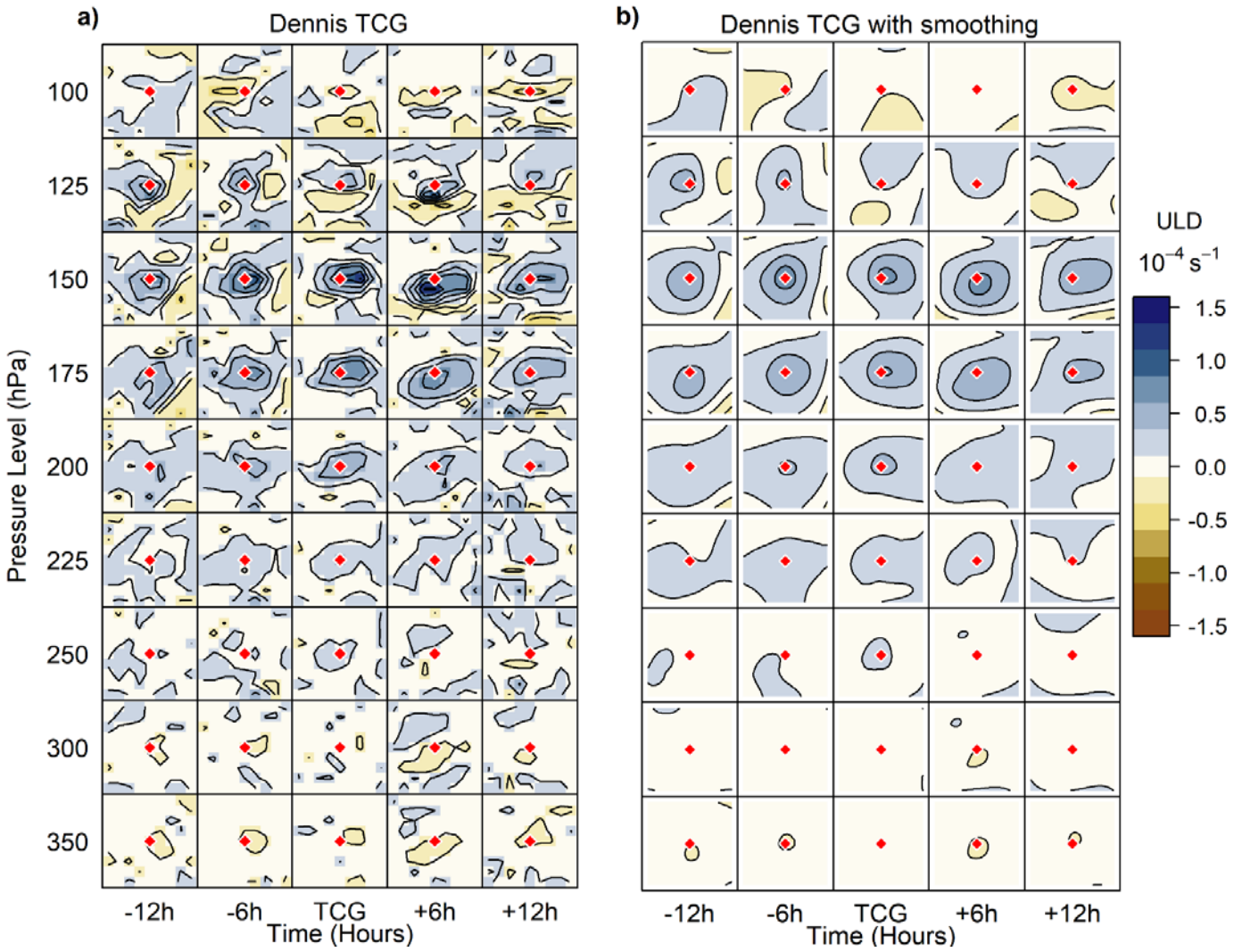

Figure 4.5. Dennis ULD at TCG (a) and ULD at TCG with smoothing (b).

4.1.5. Tropical Storm Emily

Emily reached TS status at 0000 UTC on 12 July 2005 at 11.0° N, 46.8° W despite a broad circulation and poorly-organized convection (NHC 2015, Knapp et al. 2010). A dry environment and easterly shear slowed Emily's initial development (NHC 2015). Forward speed increased due to a low-level surge and later the COC reformed to the northeast (NHC 2015). Maximum ULD values are between the 250 hPa and 150 hPa geopotential heights (Figure 4.6). The ULD field contains numerous smaller pockets of more intense concentrations and is located more to the west and north of the COC. This is most likely due to the presence of easterly shear during formation. A steady maintenance of the ULD field is apparent through time with an average level near 200 hPa.

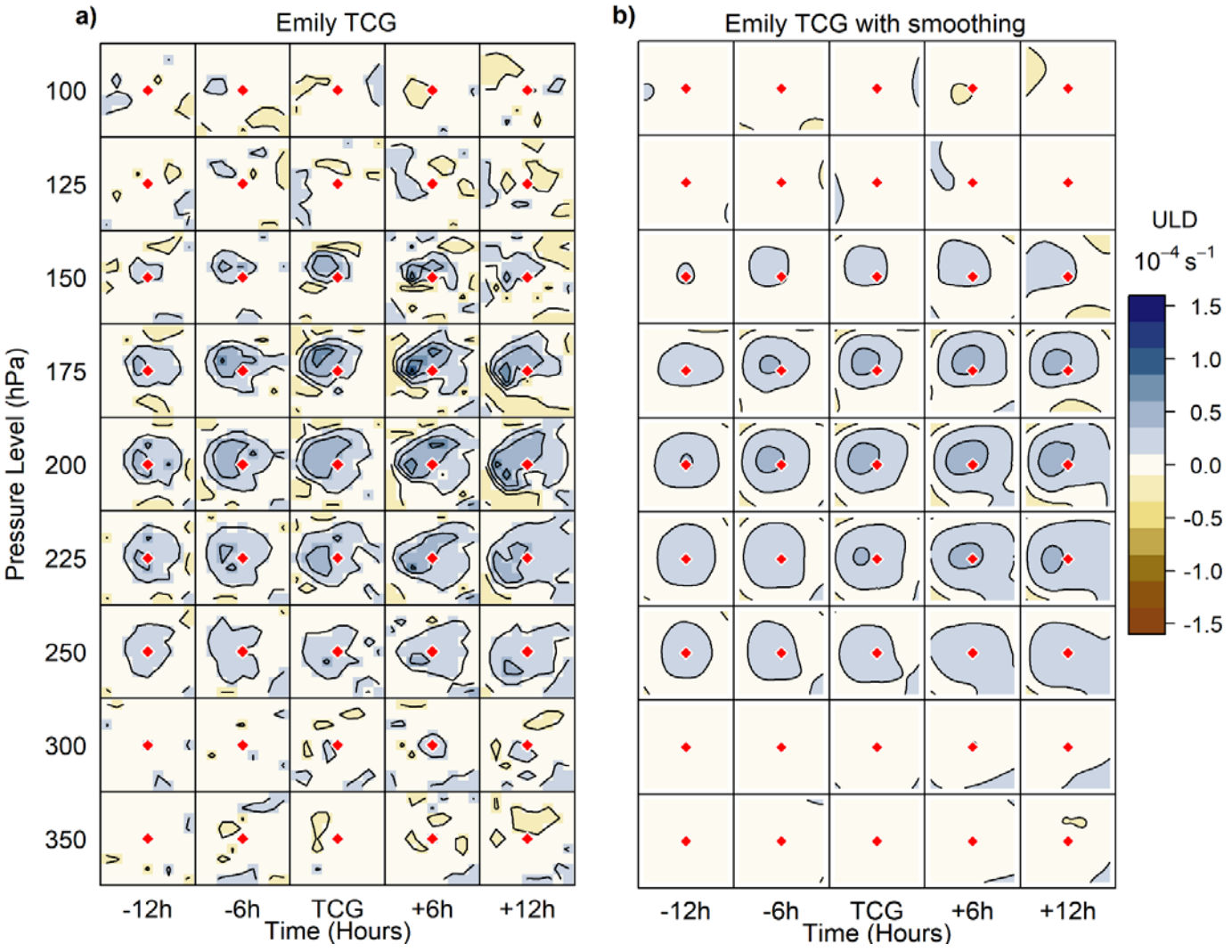

Figure 4.6. Emily ULD at TCG (a) and ULD at TCG with smoothing (b).

4.1.6. Tropical Storm Franklin

Franklin and the subsequent storm, Gert, both developed from the same tropical wave: Franklin from the northern portion and Gert from the southern portion (NHC 2015). In hours prior to TD development, the system displayed deep convection and curved banding due to northwestward migration (NHC 2015). Still only a disturbance at time TCG –12 hours, coordinates 25.0° N, 75.0° W are used in analysis for the initial disturbance. Franklin achieved TS status at 0000 UTC on 22 July 2005 at location 25.7° N, 75.9° W (Knapp et al. 2010), but westerly shear from Gert's (still only a disturbance) ULD hindered strengthening (NHC 2015). Figure 4.7 shows more organized ULD from 225 hPa to 150 hPa prior to TCG, partial decay at TCG, an obvious interference in organization at TCG +6 hours, then an attempt to reorganize at TCG +12 hours.

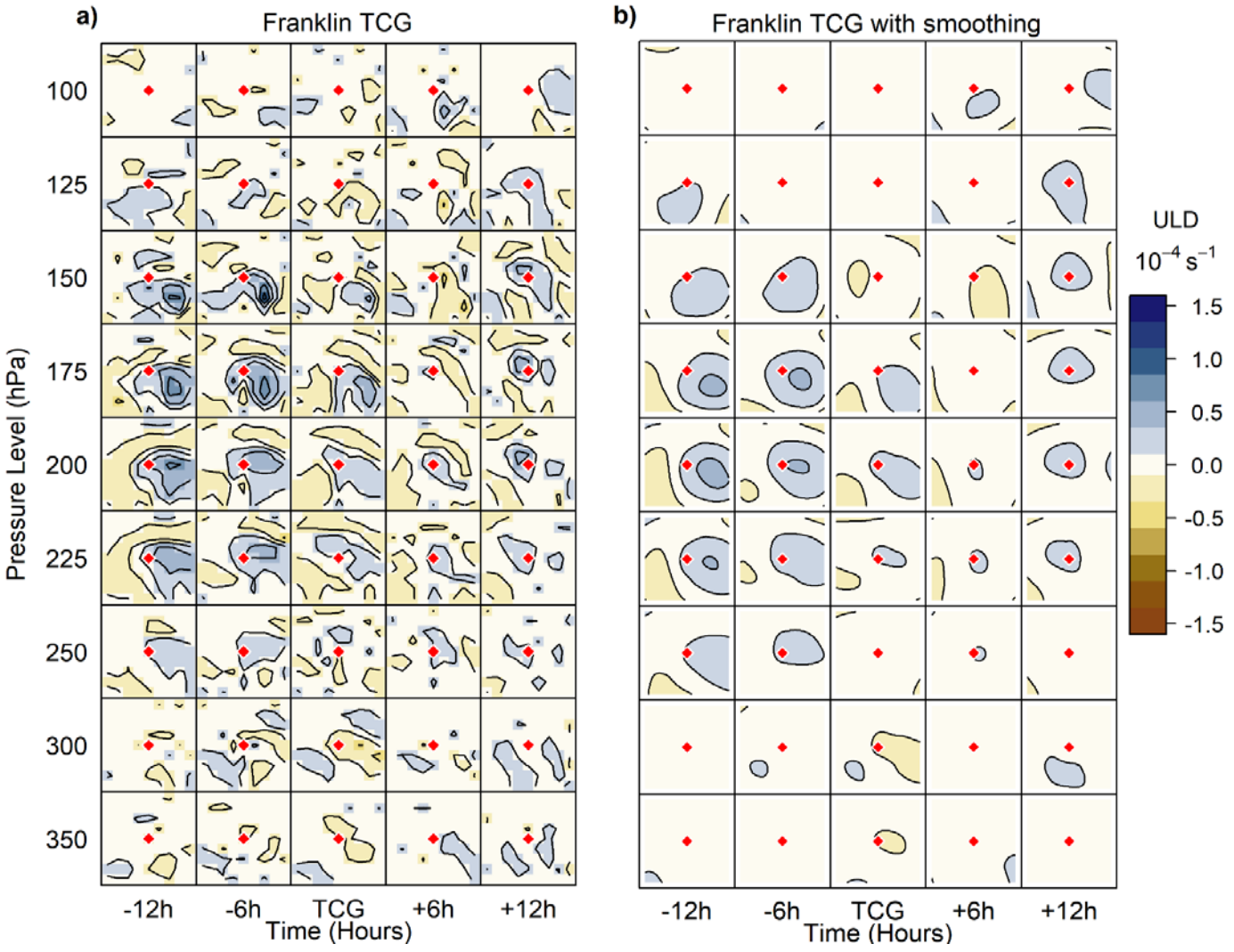

Figure 4.7. Franklin ULD at TCG (a) and ULD at TCG with smoothing (b).

4.1.7. Tropical Storm Gert

Gert achieved TS status at 0600 UTC on 24 July 2005 at 20.8° N, 95.0° W (Knapp et al. 2010). The system maintained steady development from TD stage until landfall at 0000 UTC on 25 July (NHC 2015). Gert formed from the southern portion of the same tropical wave whose northern portion produced Franklin (NHC 2015). Gert had multiple smaller COCs accompanying a larger circulation (NHC 2015). They all rotated within a gyre; therefore, best track data from IBTrACS for COC was constructed using the mean of the gyre (NHC 2015). The numerous circulations are most pronounced in Figure 4.8 at time TCG –6 hours. ULD values fluctuate mainly between 200 hPa and 125 hPa heights. It is apparent in Figure 4.8 that the area of concentrated ULD moves lower in the atmosphere and gains better organization as time progresses.

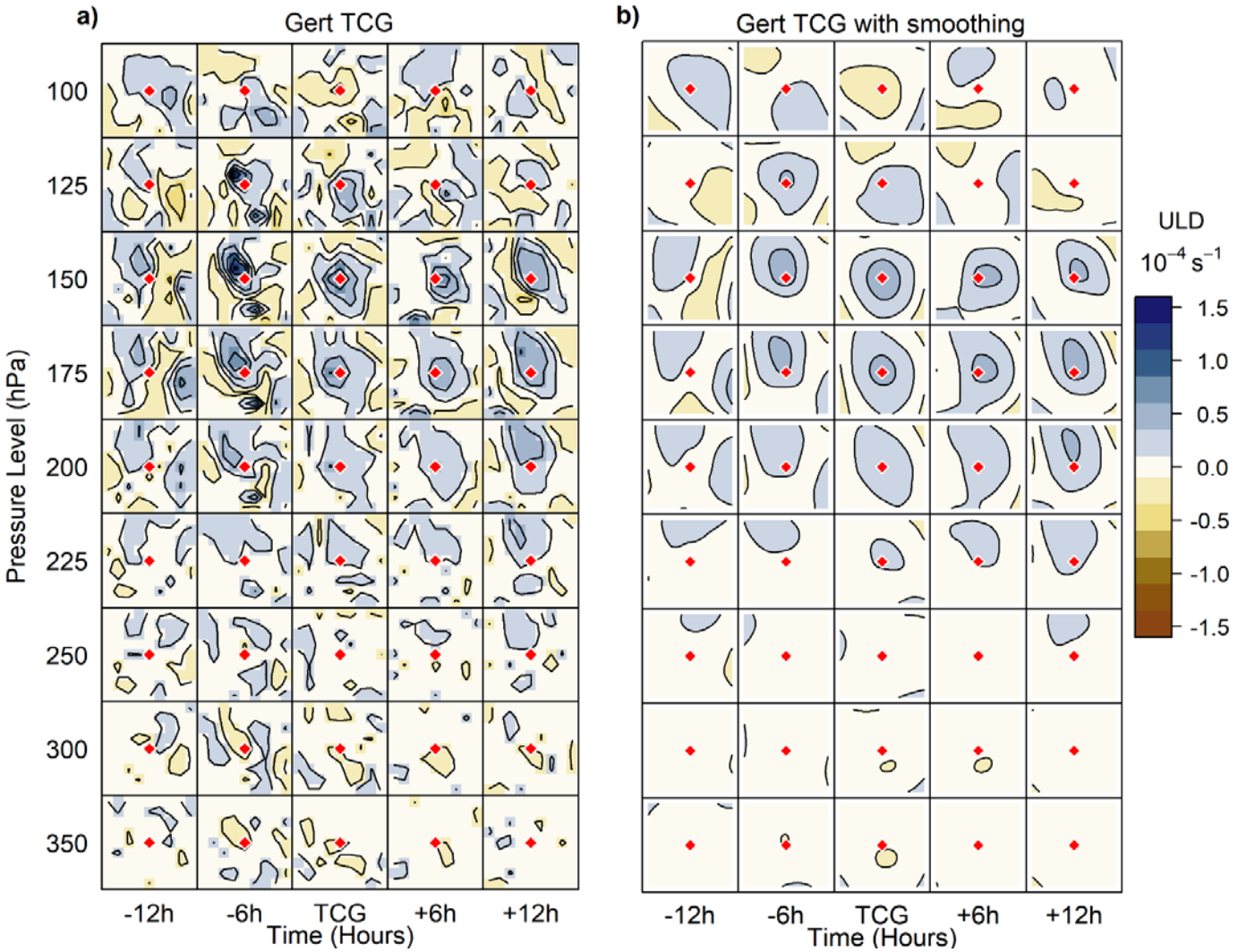

Figure 4.8. Gert ULD at TCG (a) and ULD at TCG with smoothing (b).

4.1.8. Tropical Storm Harvey

Harvey began as an African tropical wave on 22 July 2005, but the disturbance remained disorganized due to southerly wind shear from an upper-level low to the west (NHC 2015). Circulation was poorly organized when Harvey became a TD, and despite the satellite imagery appearance seeming subtropical, the location of deep convection was close enough to the low-level COC to allow a tropical designation (NHC 2015). The upper-level low assisted in moving the disturbance northward (NHC 2015) allowing Harvey to strengthen to TS at 0600 UTC on 3 August 2005 at 29.5° N, 68.6° W (Knapp et al. 2010). Harvey continued slow intensification and turned east-northeast due to a mid- to upper-level trough to the north (NHC 2015). Disorganized ULD in Figure 4.9 ranges from 250 hPa to 150 hPa with a lack of significant closed contours.

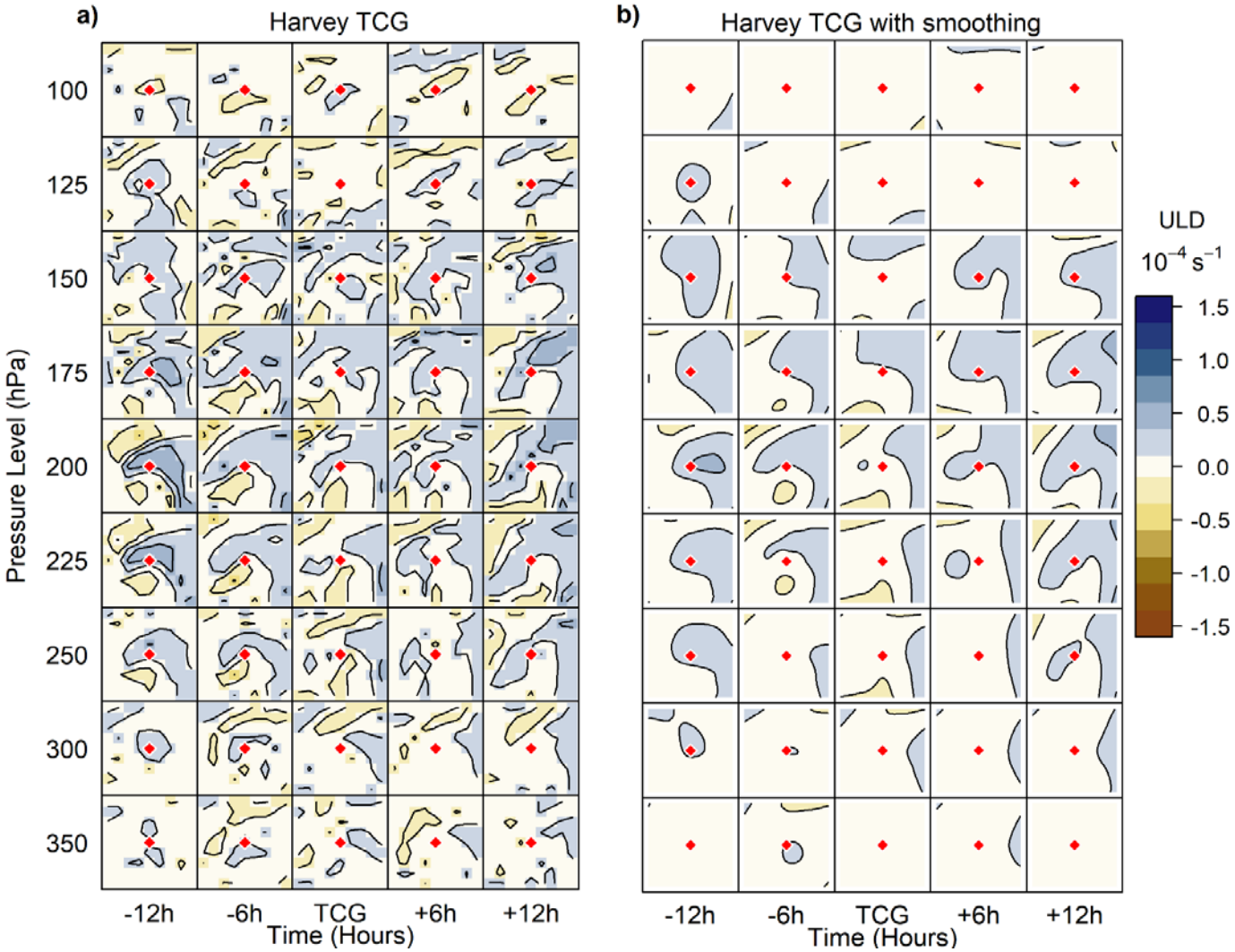

Figure 4.9. Harvey ULD at TCG (a) and ULD at TCG with smoothing (b).

4.1.9. Tropical Storm Irene

Irene achieved TS status twice and both are included in this analysis. For two days prior to TCG, Irene experienced unfavorable environmental conditions that thwarted further development (NHC 2015). Strong stable trade wind flow and cooler water temperatures caused a decrease in organized convection, but surprisingly, Irene slowly strengthened (NHC 2015). Irene was embedded in the upper-level northwesterly winds and it is speculated that enough barotropic instability existed for Irene to derive sufficient energy and become a TS (NHC 2015). Irene first achieved TS status at 1200 UTC on 7 August 2005 at 20.2° N, 45.0° W (Knapp et al. 2010) as it moved west-northwestward (NHC 2015). In Figure 4.10, ULD is focused substantially more northeast of the COC for TCG –12 hours and values are widespread vertically from 350 hPa

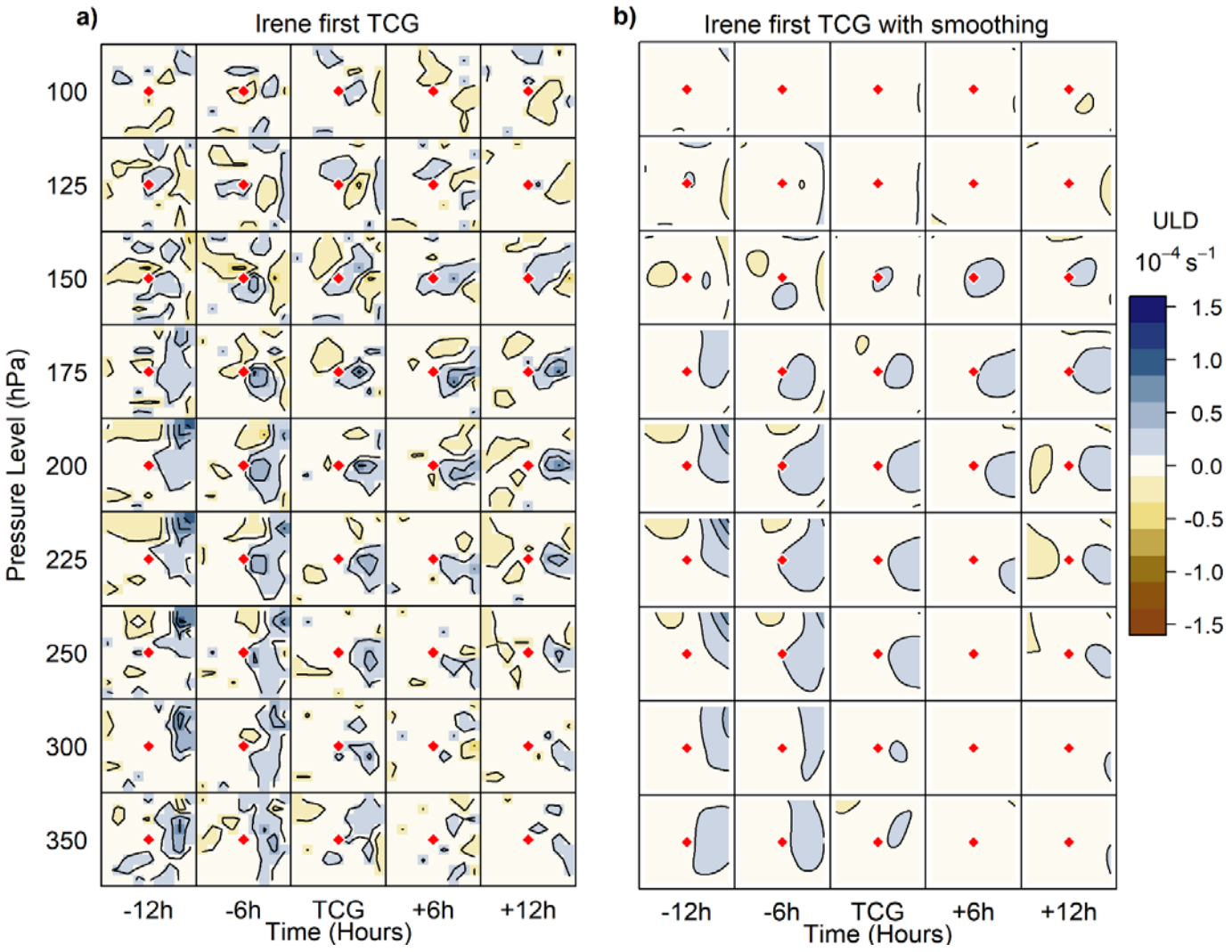

Figure 4.10. Irene ULD at first TCG (a) and ULD at first TCG with smoothing (b).

to 150 hPa before time TCG. Starting at time TCG the small ULD field is concentrated east of the COC and more around 200 hPa to 175 hPa. Irene only maintained TS status for 24 hours before a dry stable environment and upper-level shear hindered convection (NHC 2015).

Irene redeveloped into a TS a second time 0000 UTC on 11 August 2005 at 23.3° N, 59.3° W (Knapp et al. 2010) as convection increased due to decreased vertical shear (NHC 2015). Irene then made a turn northwestward, assisted by a deep southeasterly steering flow (NHC 2015). The clustered ULD field was maintained between the 225 hPa and 175 hPa levels and rose to 150 hPa for times TCG –6 hours to TCG in Figure 4.11.

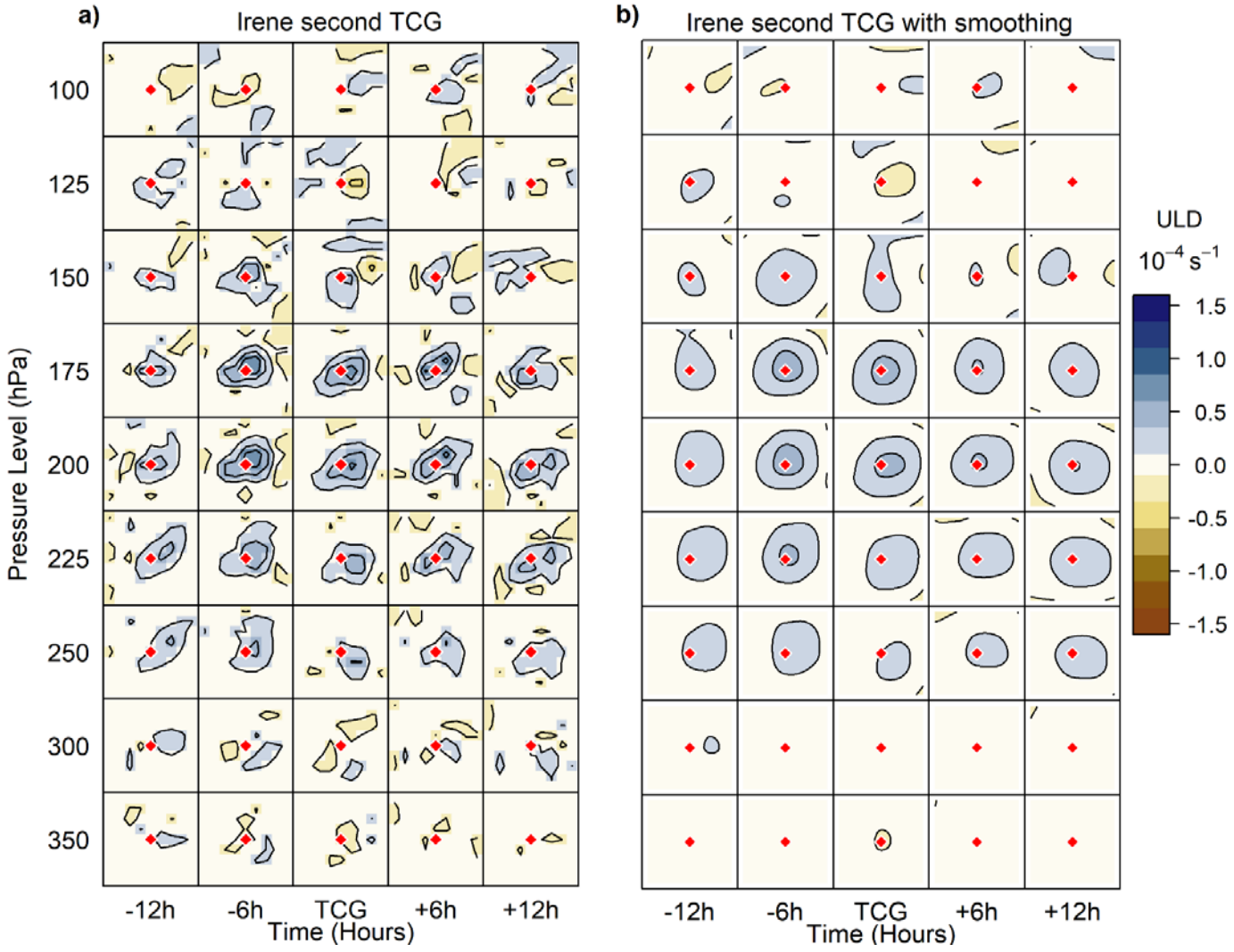

Figure 4.11. Irene ULD at second TCG (a) and ULD at second TCG with smoothing (b).

4.1.10. Tropical Storm Jose

Jose was a very brief TC progressing from disturbance, to TD, to TS, then landfall in under 24 hours (NHC 2015). According to the NHC (2015) "under a very favorable divergent upper-level anticyclonic flow, convection exploded" early 22 August 2005 and classified Jose a TS 1800 UTC on 22 August 2005 at 19.6° N, 95.0° W (Knapp et al. 2010). Jose made landfall between times TCG +6 hours and TCG +12 hours. An eyewall appeared just before landfall (NHC 2015) as Jose was shaping up to become a hurricane. Pockets of intense ULD at TCG +12 hours in Figure 4.12 could be related to regional topographic features, the Sierra Madres, suspected to have enhanced the strongest winds southwest of the COC (NHC 2015). During the study time, the ULD field decreases in height and magnitude from 125 hPa, to below 225 hPa then increases again.

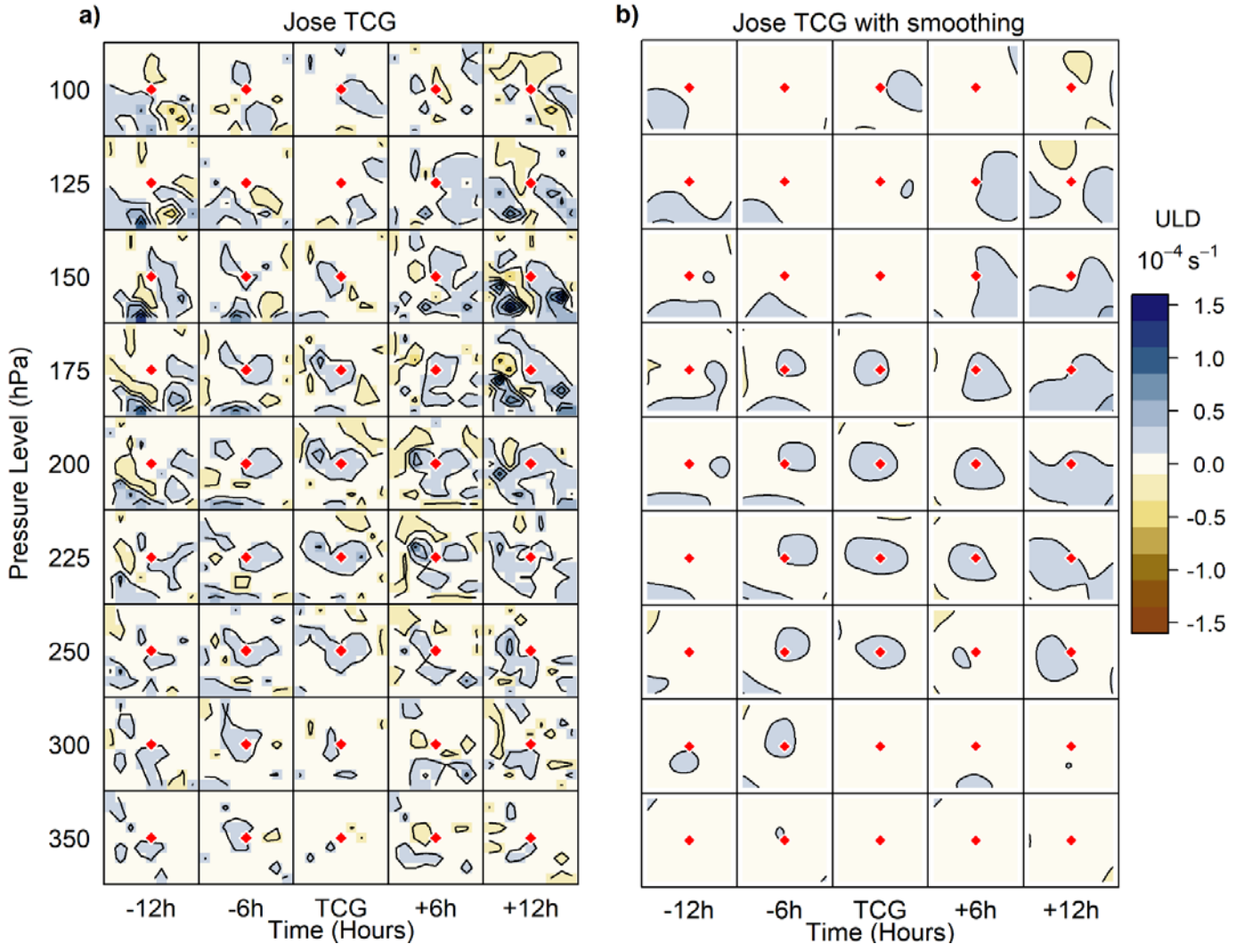

Figure 4.12. Jose ULD at TCG (a) and ULD at TCG with smoothing (b).

4.1.11. Tropical Storm Katrina

Katrina resulted from a convergence of remnants from Tropical Depression 10 (middle tropospheric circulation) and a tropical wave (NHC 2015). To the north and east of the COC, a well-defined band of deep convection formed (NHC 2015), initiating TS status at 1200 UTC on 24 August 2005 at 24.5° N, 76.5° W (Knapp et al. 2010). As seen in Figure 4.13, the ULD field is disorganized and scattered between 250 hPa and 100 hPa. Values tend to be located to the north and east of the COC with apparent strengthening and organization at time TCG +12 hours. Katrina evolved into a deeper cyclone at TS status and continued steady intensification (NHC 2015).

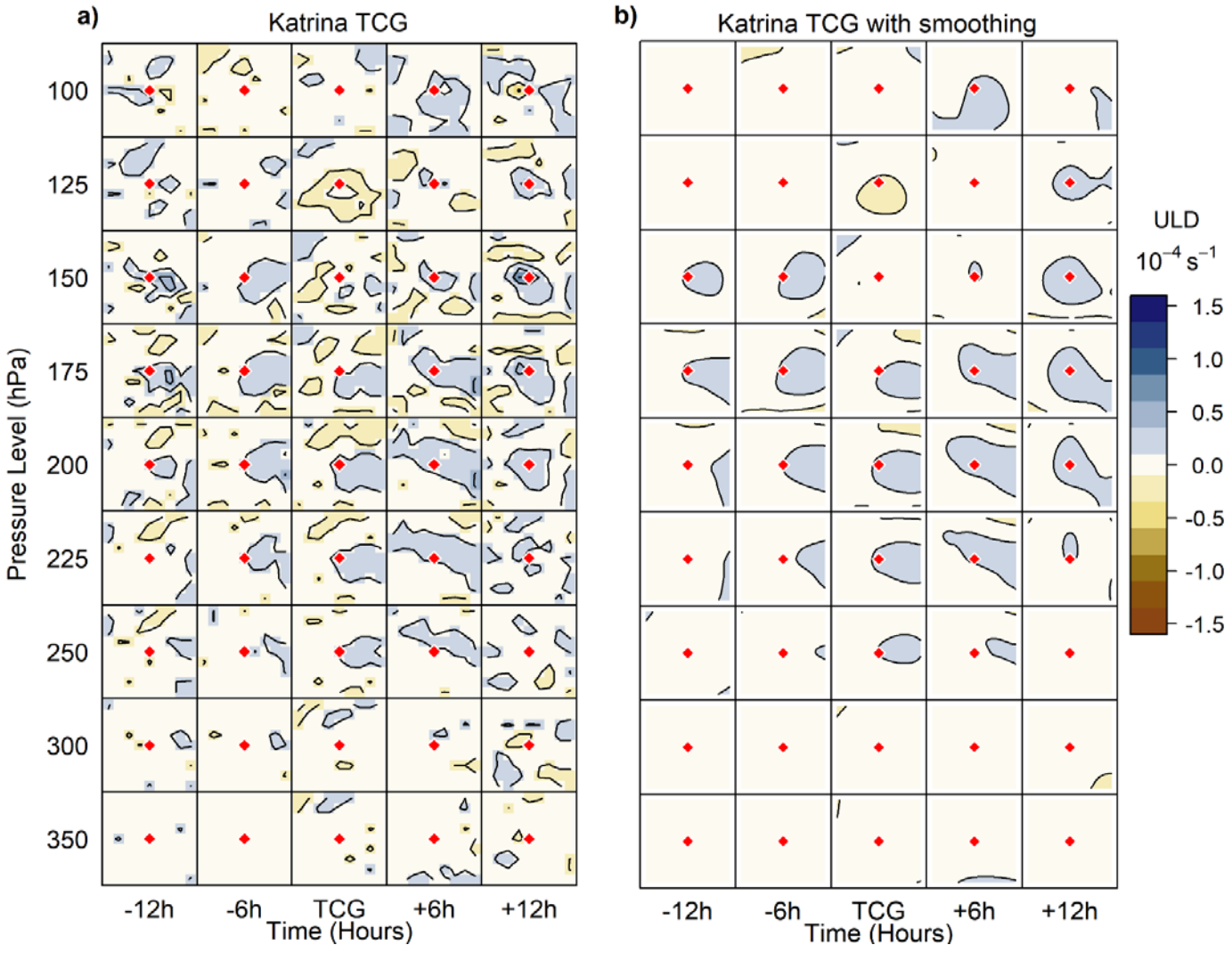

Figure 4.13. Katrina ULD at TCG (a) and ULD at TCG with smoothing (b).

4.1.12. Tropical Storm Lee

Lee achieved TS status at 1200 UTC on 31 August 2005 at 29.0° N, 50.4° W (Knapp et al. 2010). Small circulations were embedded in the larger gyre after northeasterly wind shear displaced the main COC on the day before TCG (NHC 2015). Lee was then considered only an area of low pressure until banding features developed and upgraded the cyclone to a TD at TCG –6 hours (NHC 2015). Lee only briefly strengthened enough to be classified a TS (Knapp et al. 2010, NHC 2015). This lasted for 12 hours and by time +12 TCG, Lee was again a TD (NHC 2015). For a struggling TC, the ULD patterns are interesting, as they seem more organized than those of strengthening cyclones like Katrina. Highest ULD values reach the 125 hPa height (Figure 4.14) and larger ULD values are maintained above 200 hPa.

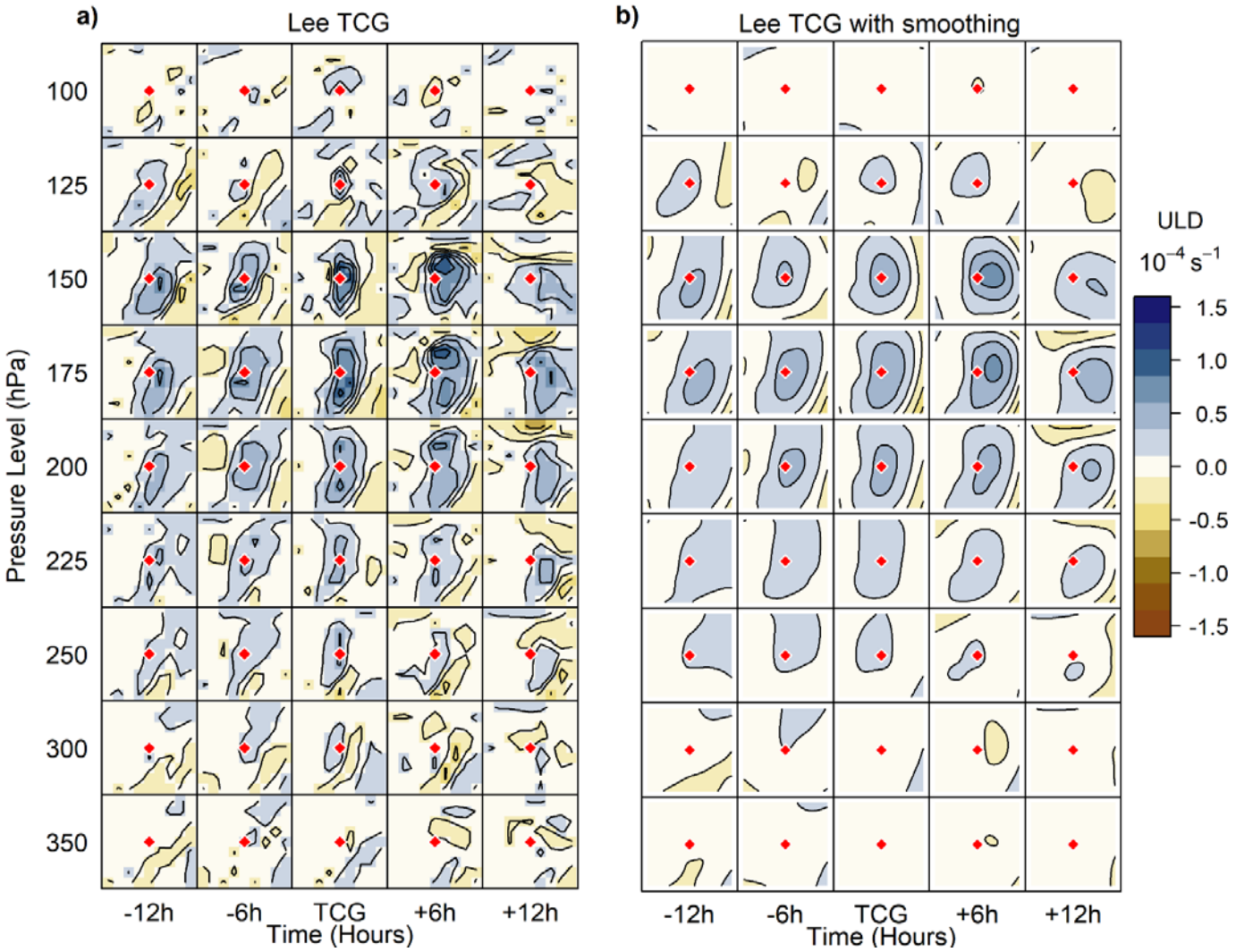

Figure 4.14. Lee ULD at TCG (a) and ULD at TCG with smoothing (b).

4.1.13. Tropical Storm Maria

Maria achieved TS status at 1200 UTC on 2 September 2005 at 21.1° N, 49.4° W (Knapp et al. 2010). A reduction in shearing from a nearby upper-level low that originally hampered formation in the days prior to TCG allowed Maria to gain strength (NHC 2015). Environmental conditions were not ripe for rapid intensification, so strengthening progressed slowly (NHC 2015). The largest area of maximum ULD occurs before TCG and above 200 hPa. Figure 4.15 (a) exhibits a trend of the ULD field moving from higher vertical heights (175 hPa and 150 hPa) to lower vertical heights (300 hPa and 250 hPa) with a decrease in structure and size through time. Smoothing in Figure 4.15 (b) did not detect the small areas of ULD between 350 hPa and 250 hPa shown in Figure 4.15 (a) after TCG.

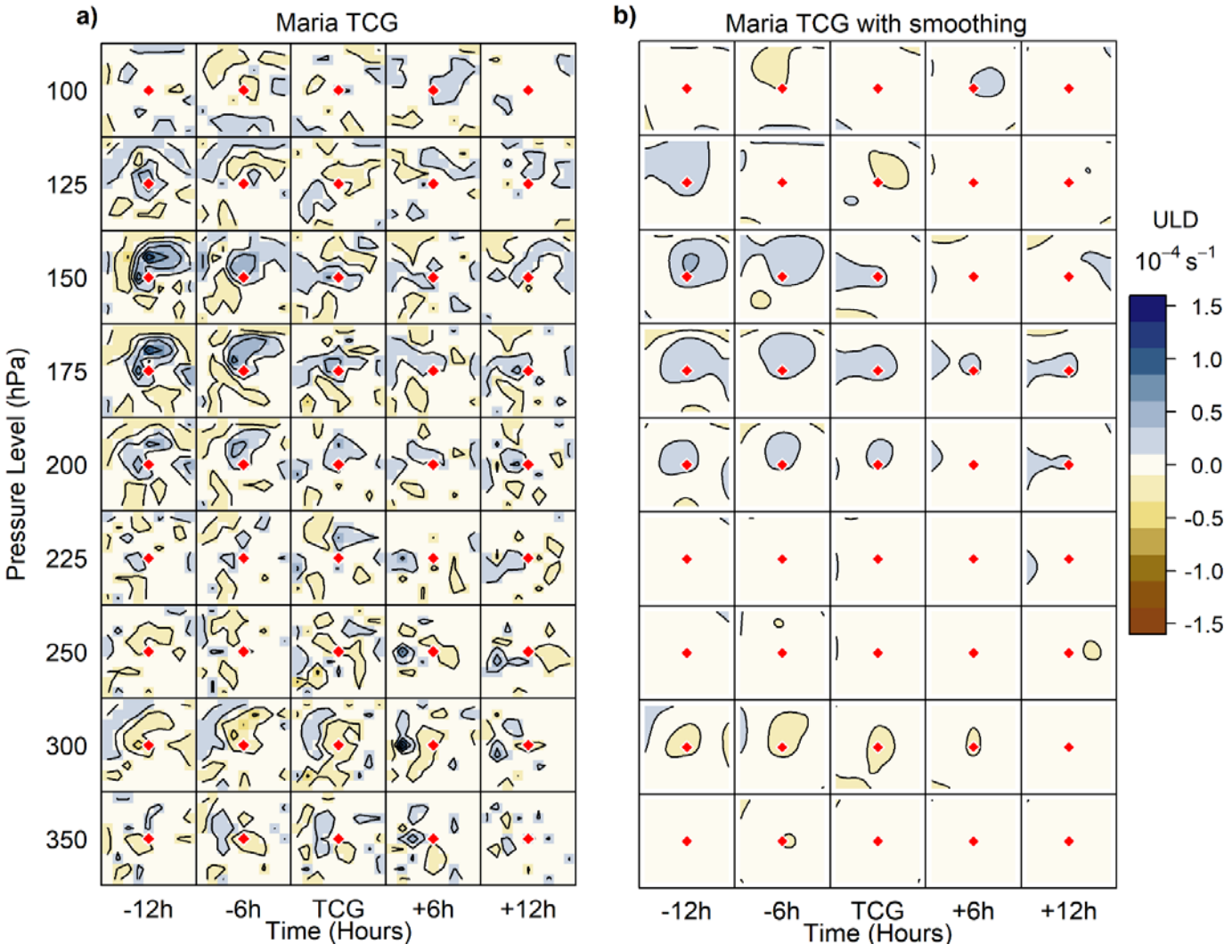

Figure 4.15. Maria ULD at TCG (a) and ULD at TCG with smoothing (b).

4.1.14. Tropical Storm Nate

Nate originated from the northern portion of a split tropical wave and a cold front (NHC 2015). As convection organized along the wave axis, convective banding was observed on satellite data and the disturbance was given TD status (NHC 2015). The cyclone developed into a TS only six hours after it was classified as a TD due to weak wind shear (NHC 2015). Nate achieved TS status at 0000 UTC on 6 September 2005 at 28.4° N, 66.6° W (Knapp et al. 2010). The coordinates for TCG –6 hours were used for TCG –12 hours due to a relatively stationary cyclone. Maximum ULD values start around 250 hPa and reach up to 150 hPa. Progression of increasing ULD organization and height through time is clear in Figure 4.16, but magnitude decreases slightly after TCG.

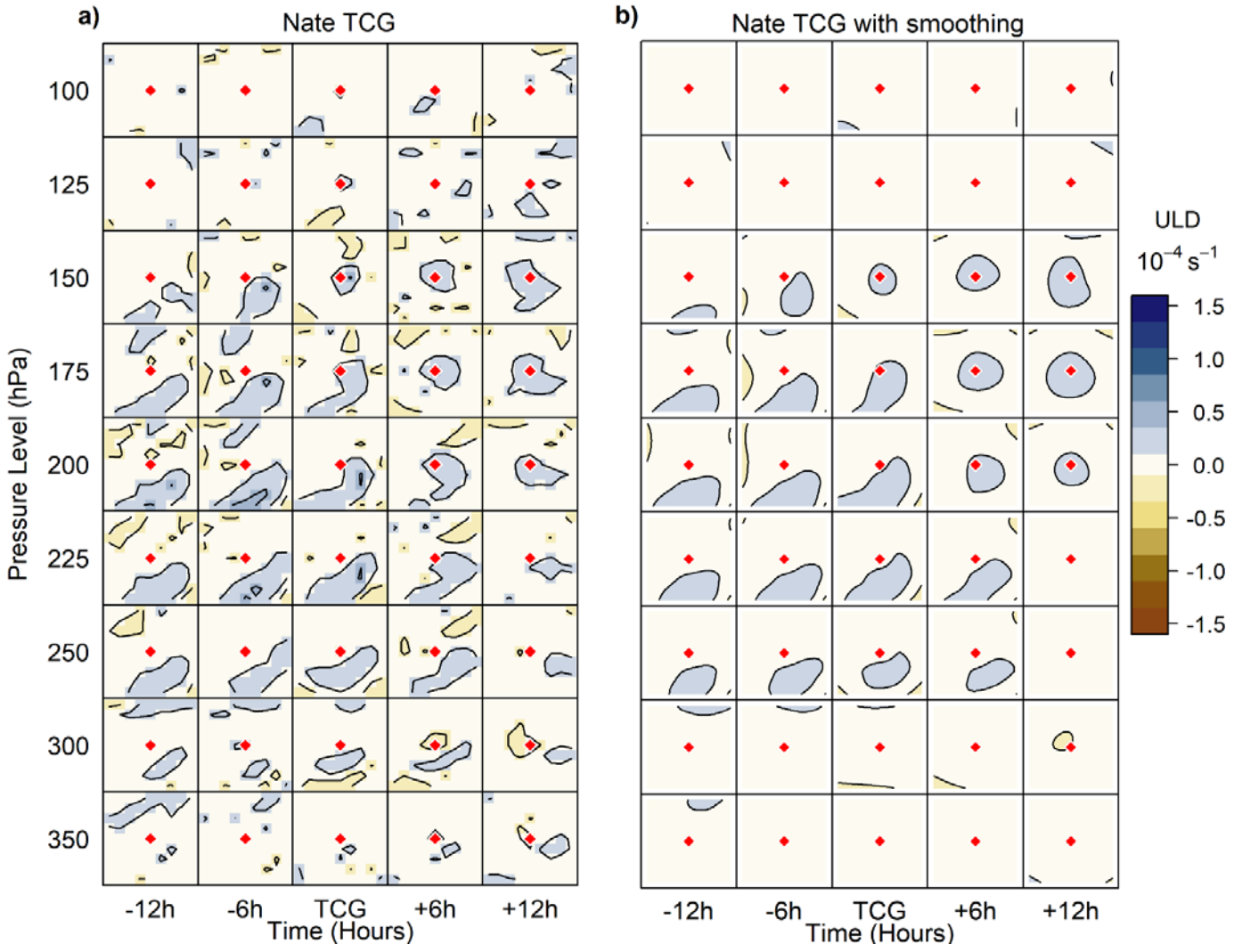

Figure 4.16. Nate ULD at TCG (a) and ULD at TCG with Smoothing (b).

4.1.15. Tropical Storm Ophelia

A low-pressure trough off Lee interacted with a non-tropical cold front to produce Ophelia. The split tropical system formed Nate from the northern portion and Ophelia from the southern portion (NHC 2015). Paralleling the east Florida coast (NHC 2015), Ophelia was designated as a TS at 0600 UTC on 7 September 2005 at 27.9° N, 78.8° W (Knapp et al. 2010). Ophelia made a counter-clockwise loop, the first of two (second loop clockwise farther northeast the following week), while strengthening over the next 24 hours (NHC 2015). The area of ULD is apparent north of COC and gradually moves closer to the COC through time (Figure 4.17). Substantial maximum ULD values are maintained between 175 hPa and 150 hPa while averages range between 250 hPa to 125 hPa.

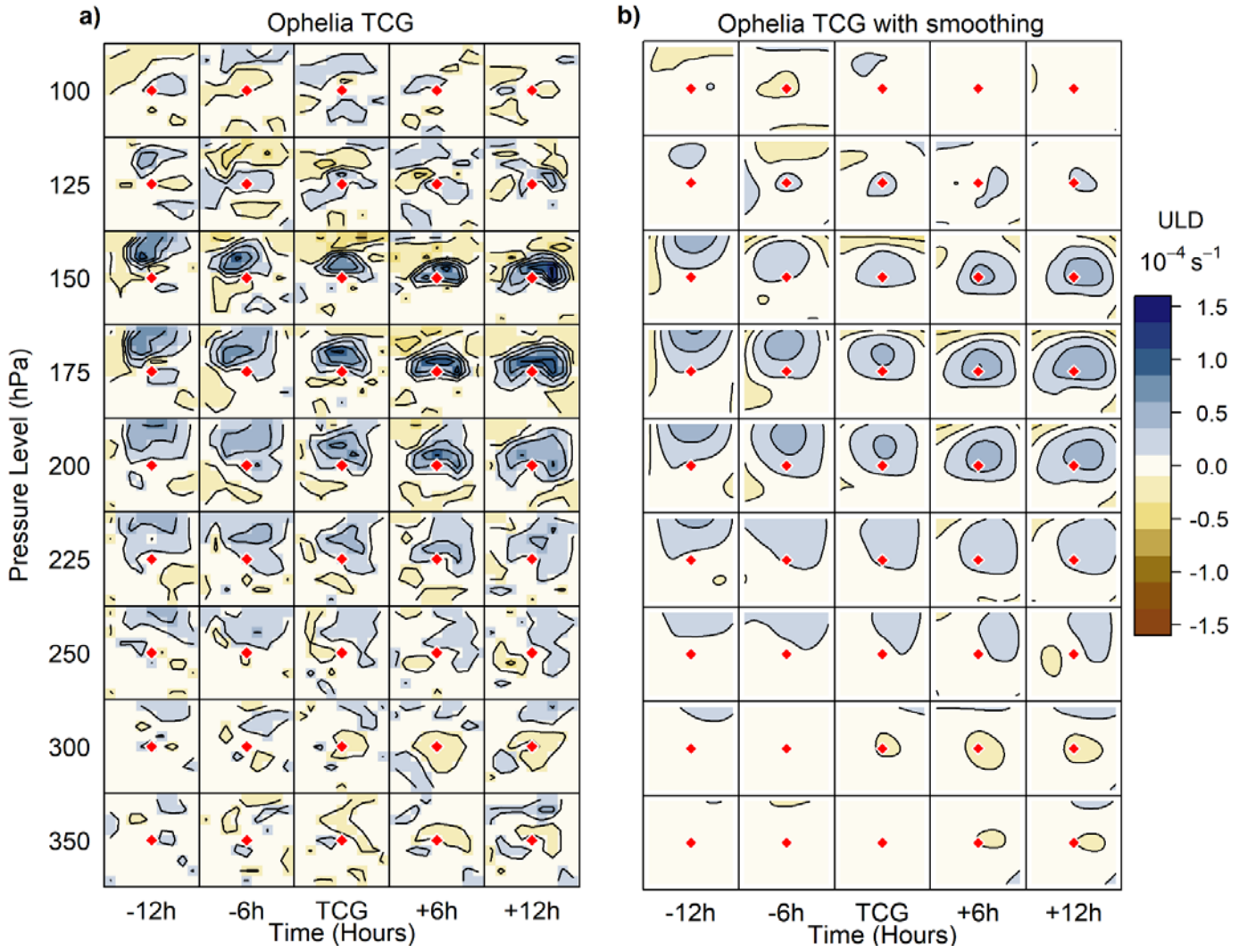

Figure 4.17. Ophelia ULD at TCG (a) and ULD at TCG with smoothing (b).

4.1.16. Tropical Storm Philippe

Philippe was a large disturbance with convection concentrating south as the COC became better defined (NHC 2015). The cyclone formed in low latitudes with weak steering currents and meandered northwestward (NHC 2015) while strengthening to TS status at 1800 UTC on 17 September 2005 at 13.5° N, 54.9° W (Knapp et al. 2010). Transition from tropical disturbance to TS occurred over only 12 hours (NHC 2015); therefore, TCG –12 hour coordinates were estimated from relative disturbance movement. Moving toward a weakness in the nearby subtropical ridge allowed for the steady strengthening of Philippe (NHC 2015). In Figure 4.18, through time the ULD increases in organization and magnitude while expanding vertically between 250 hPa to 125 hPa.

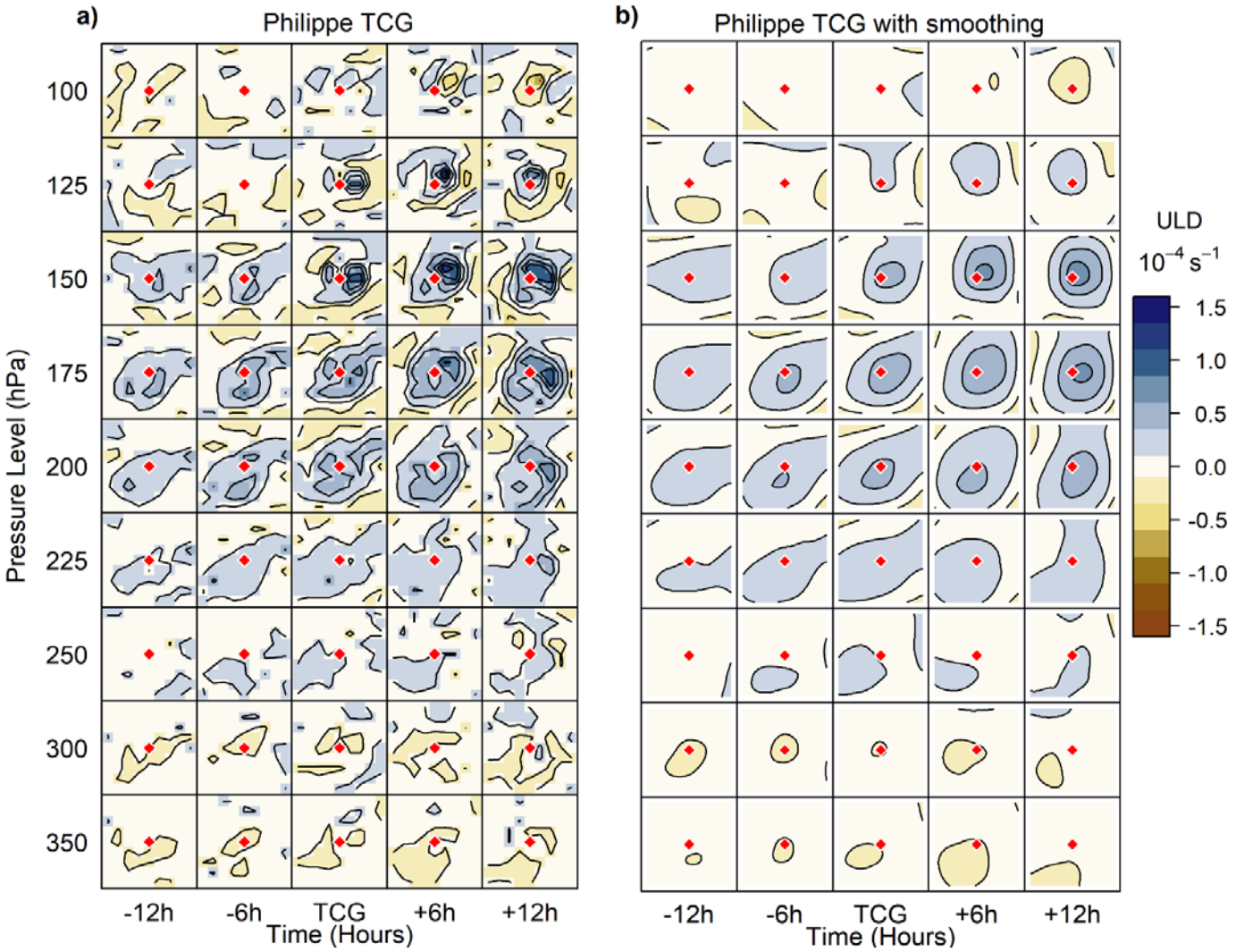

Figure 4.18. Philippe ULD at TCG (a) and ULD at TCG with smoothing (b).

4.1.17. Tropical Storm Rita

As a TD, the cyclone exhibited a low-level COC with increasing strong convection more to the north of the COC (NHC 2015). This northerly confinement occurred under the influence of southerly vertical shear (NHC 2015). Organization continued, and Rita became a TS 1800 UTC on 18 September 2005 at 22.2° N, 72.3° W (Knapp et al. 2010). Vertical shear continued to affect the system until after TCG +12 hours when convection became more symmetric allowing for further strengthening (NHC 2015). Concentrations of ULD are seen north of the COC during the study period (Figure 4.19). Maximum values reach 150 hPa while the strongest concentrations occur at TCG and TCG +6 hours.

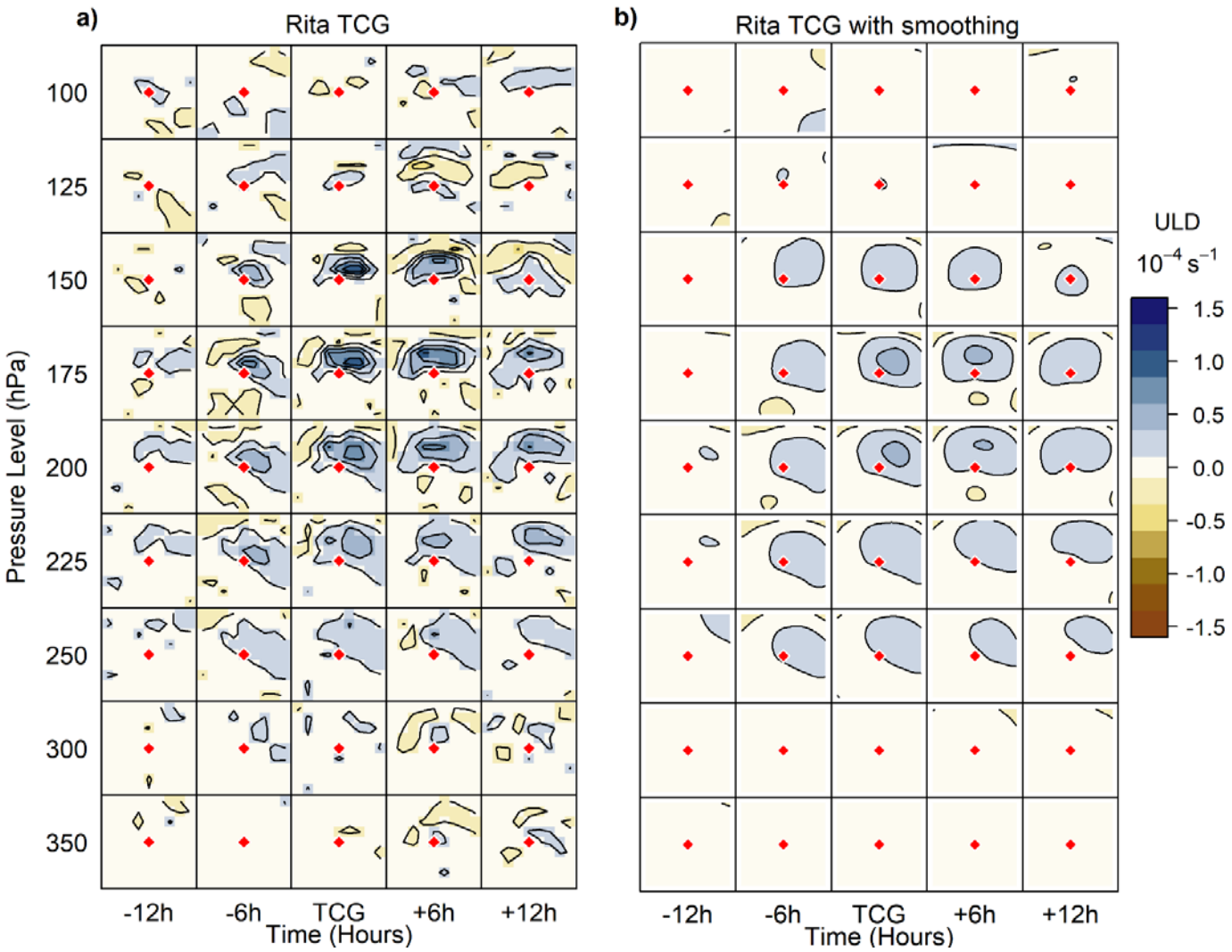

Figure 4.19. Rita ULD at TCG (a) and ULD at TCG with smoothing (b).

4.1.18. Tropical Storm Stan

After days of struggling, deep and organized convection development permitted characterization as a TD on 1 October (NHC 2015). Establishment of an upper-tropospheric anticyclone aided in the cyclone's strengthening (NHC 2015) and Stan became a TS 0600 UTC on 2 October 2005 at 19.5° N, 87.2° W (Knapp et al. 2010) just two hours prior to making landfall (NHC 2015). Stan traveled west over the Yucatán peninsula and weakened briefly to a TD before regaining strength once back over water (NHC 2015). TD classification occurred six hours after TCG +12 hours and only held six hours before returning to TS classification (NHC 2015). During both TCG +6 hours and TCG +12 hours, Stan was over land (NHC 2015). Maximum ULD values reach the 125 hPa height and average around 150 hPa in Figure 4.20.

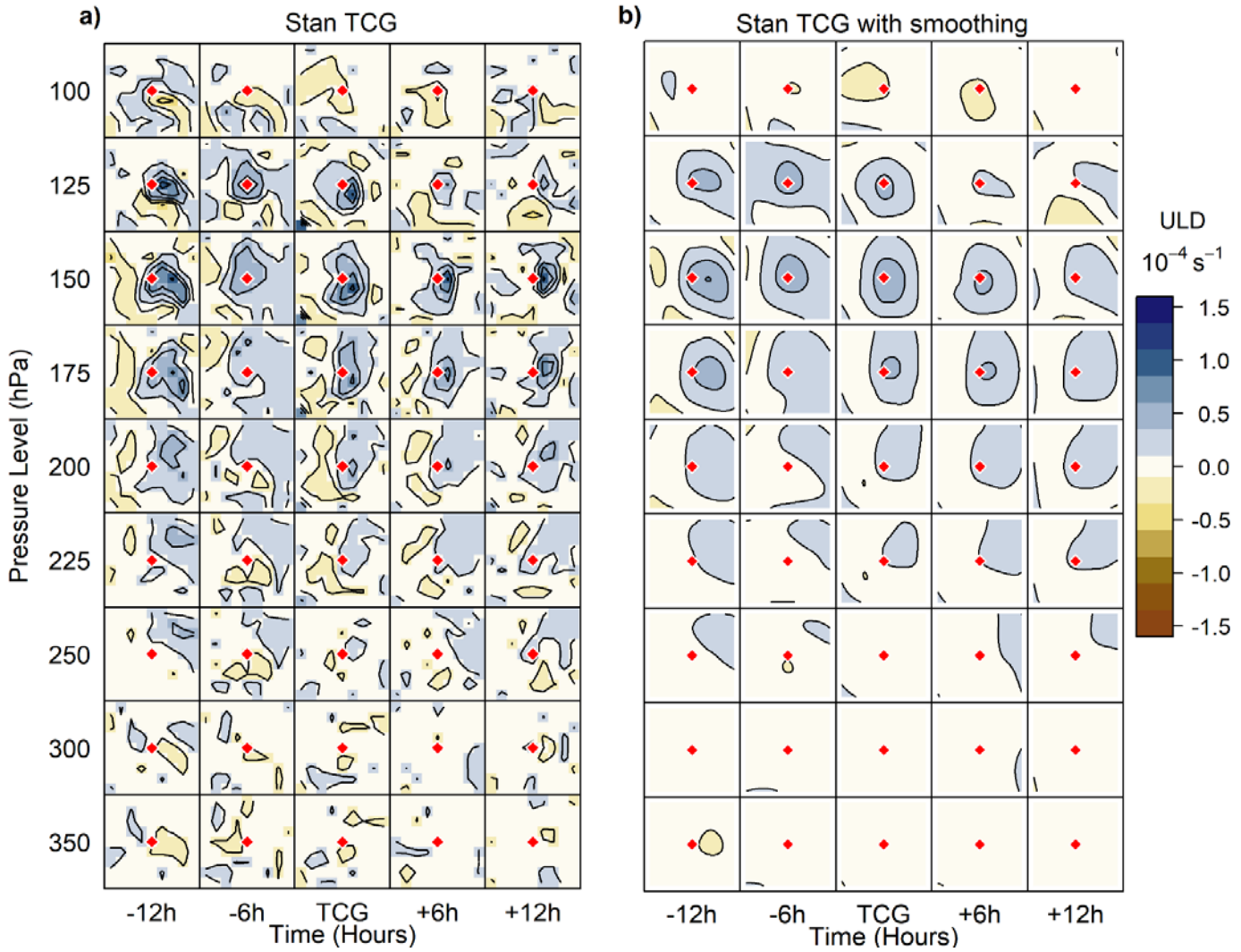

Figure 4.20. Stan ULD at TCG (a) and ULD at TCG with smoothing (b).

4.1.19. Unnamed Tropical Storm

Identified in a post-season re-analysis as a SC instead of a non-tropical low, Unnamed was a surface low at TCG –12 hours and subtropical depression (SD) at TCG –6 hours (NHC 2015). The cyclone achieved SS status at 1200 UTC on 4 October 2005 at 35.9° N, 28.5° W (Knapp et al. 2010). Continued development occurred through the next day when it merged with a cold front that was subsequently absorbed by a non-tropical low, which eventually evolved into Vince (NHC 2015). A 200 hPa warm core suggested a possible fully tropical nature but an upper-level trough after TCG suggested a subtropical nature (NHC 2015). ULD values reach to about 175 hPa with the best signature of maximum values between 250 hPa and 200 hPa occurring from TCG to TCG +6 hours (Figure 4.21).

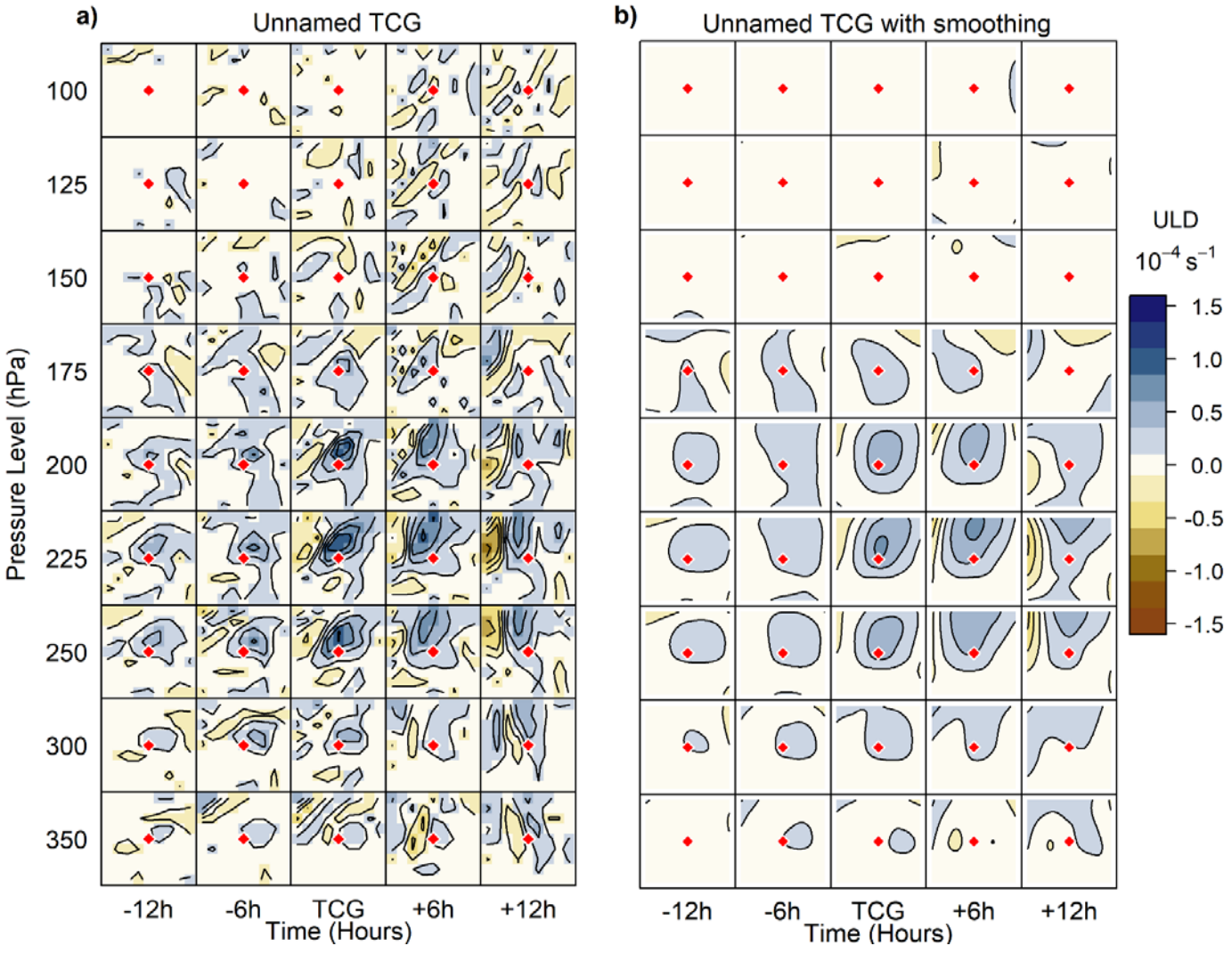

Figure 4.21. Unnamed ULD at TCG (a) and ULD at TCG with smoothing (b).

4.1.20. Tropical Storm Tammy

Tammy began as the northern portion of a split tropical wave that found favorable conditions in a low vertical shear environment (NHC 2015). As a surface trough, the system moved near a large central Atlantic Ocean surface high, causing the pressure gradient to increase and creating gale-force winds (NHC 2015). A low-pressure center developed along with deep convection and low to mid-level cyclonic circulation (NHC 2015). Gale-force winds over 17 m s^{-1} allowed Tammy's classification to begin with TS status (NHC 2015). Therefore, a centralized location for TCG –12 hours and TCG –6 hours are based on previous location and movement. TCG occurred 0600 UTC on 5 October 2005 at 27.3° N, 79.7° W (Knapp et al. 2010). ULD values weaken before TCG then increase vertically, spatially, and in magnitude after TCG (Figure 4.22).

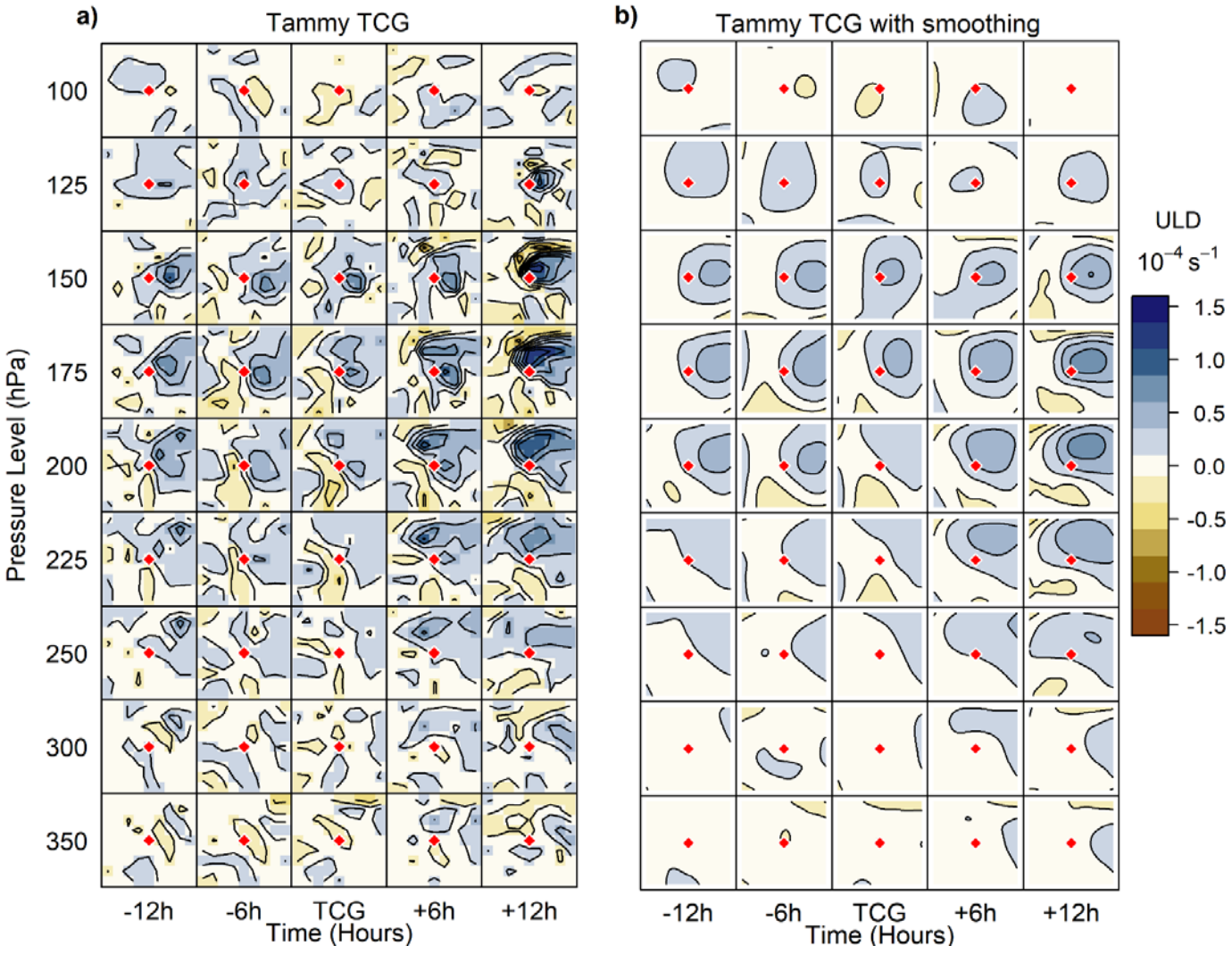

Figure 4.22. Tammy ULD at TCG (a) and ULD at TCG with smoothing (b).

4.1.21. Tropical Storm Vince

The system began 0600 UTC on 8 October 2005 at 32.9° N, 20.6° W (Knapp et al. 2010) as a SS that resembled the structure of a TS, both with the surface wind field and the core convective structure, but with a notable upper tropospheric cold-core circulation (NHC 2015). Like Tammy, Vince's complete formation and cyclogenesis occurred within 6 hours, and a centralized location for the disturbance twelve hours prior to cyclogenesis was estimated using the available location and movement. Vince maintained steady development over the next 18 hours and a warm core developed in the mid- to upper-levels upgrading the classification to TS at 1200 UTC on 9 October 2005 (NHC 2015). Figure 4.23 shows disorganized ULD clusters from 350 hPa to 125 hPa and a very concentrated ULD area occurring at TCG +6 hours between 250 hPa and 225 hPa.

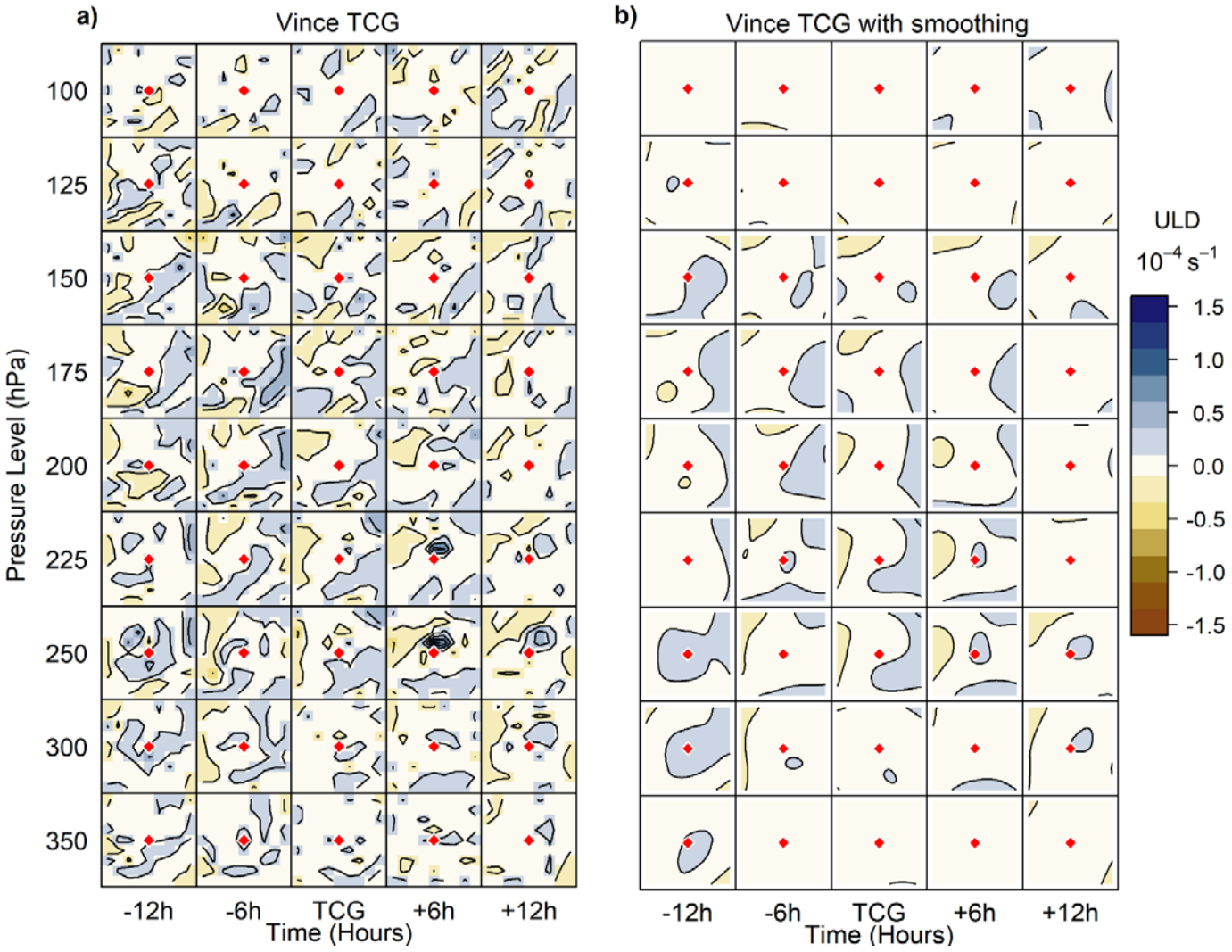

Figure 4.23. Vince ULD at TCG (a) and ULD at TCG with smoothing (b).

4.1.22. Tropical Storm Wilma

Wilma started as a surface low and an area of disturbed weather approximately 14 October (NHC 2015). After becoming a TD the next day, Wilma displayed slow strengthening for the next two days and eventually became a TS 0600 UTC on 17 October 2005 at 16.9° N, 79.6° W (Knapp et al. 2010). The cyclone had a rather dull beginning compared to what it eventually became. As a note, Wilma's explosive episodes, record-breaking eye diameter, and record-breaking minimum pressure were well past the time analyzed for this study (NHC 2015). Wilma gradually strengthened during the study period and Figure 4.24 (a) reflects a fairly uniform structure. ULD values seem to be the most consistent between 175 hPa and 125 hPa and expand vertically from 250 hPa to 125 hPa.

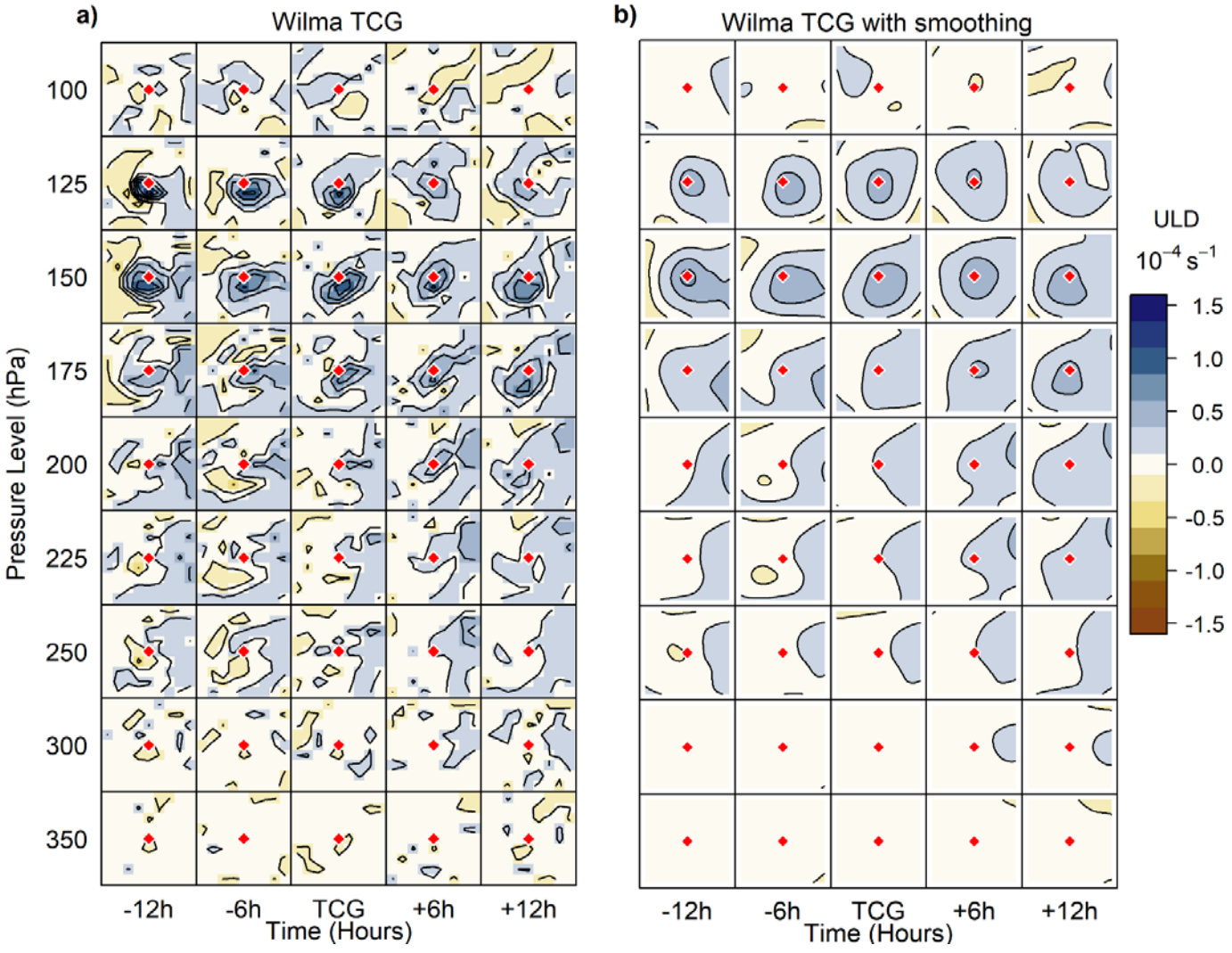

Figure 4.24. Wilma ULD at TCG (a) and ULD at TCG with smoothing (b).

4.1.23. Tropical Storm Alpha

Alpha began as a tropical wave that developed a low-pressure center along with organized convection (NHC 2015). It had a well-defined COC prior to depression stage and continued to intensify until landfall (NHC 2015). Classification to a TS occurred 1800 UTC on 22 October 2005 at location 16.5° N, 68.5° W (Knapp et al. 2010) after it developed tightly clustered banding features seen on microwave images (NHC 2015). Coordinates for time TCG –12 hours, while the storm was still a disturbance, were estimated using available data. In Figure 4.25 (b), the ULD field appears to shift from a southeast to a more northwest direction through time while the strongest ULD magnitudes in Figure 4.25 (a) are limited to very small areas throughout the levels 200 hPa to 125 hPa.

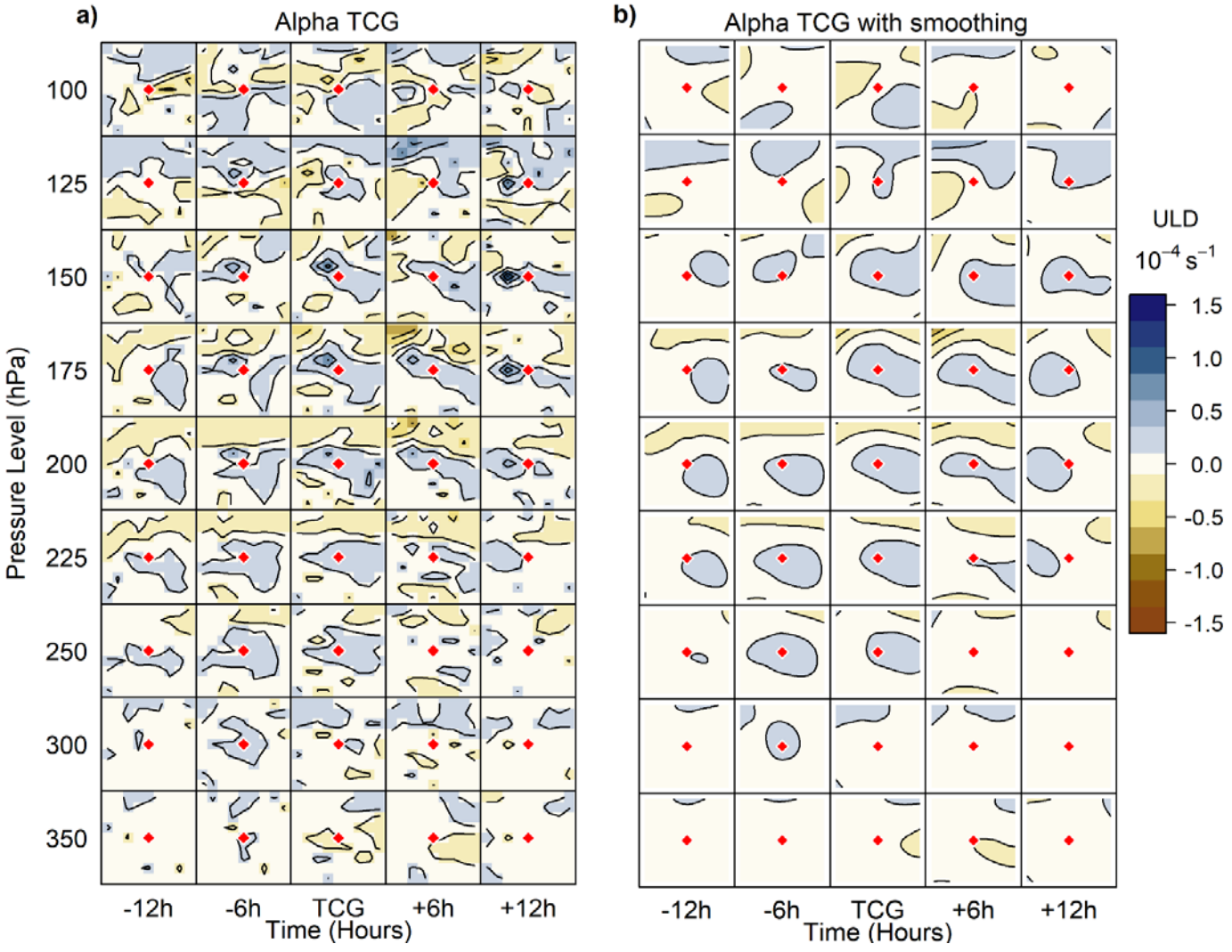

Figure 4.25. Alpha ULD at TCG (a) and ULD at TCG with smoothing (b).

4.1.24. Tropical Storm Beta

Spawned from the same tropical wave as Alpha, Beta began to organize, displaying banding features and deep convection 12 hours prior to TCG (NHC 2015). Under favorable conditions of 29 °C sea surface temperature and minimal vertical wind shear (NHC 2015), the cyclone became a TS at 0600 UTC on 27 October 2005 at 11.0° N, 81.3° W (Knapp et al. 2010). A slight increase in northeasterly shear permitted only slow strengthening (NHC 2015) for the duration of this study. Figure 4.26 shows ULD ranging from 250 hPa to 150 hPa and is more disorganized during times TCG and TCG +6 hours. Small concentrations of ULD prior to TCG and at TCG +12 hours are very compact and found close to or directly on the IBTrACS coordinates for COC location.

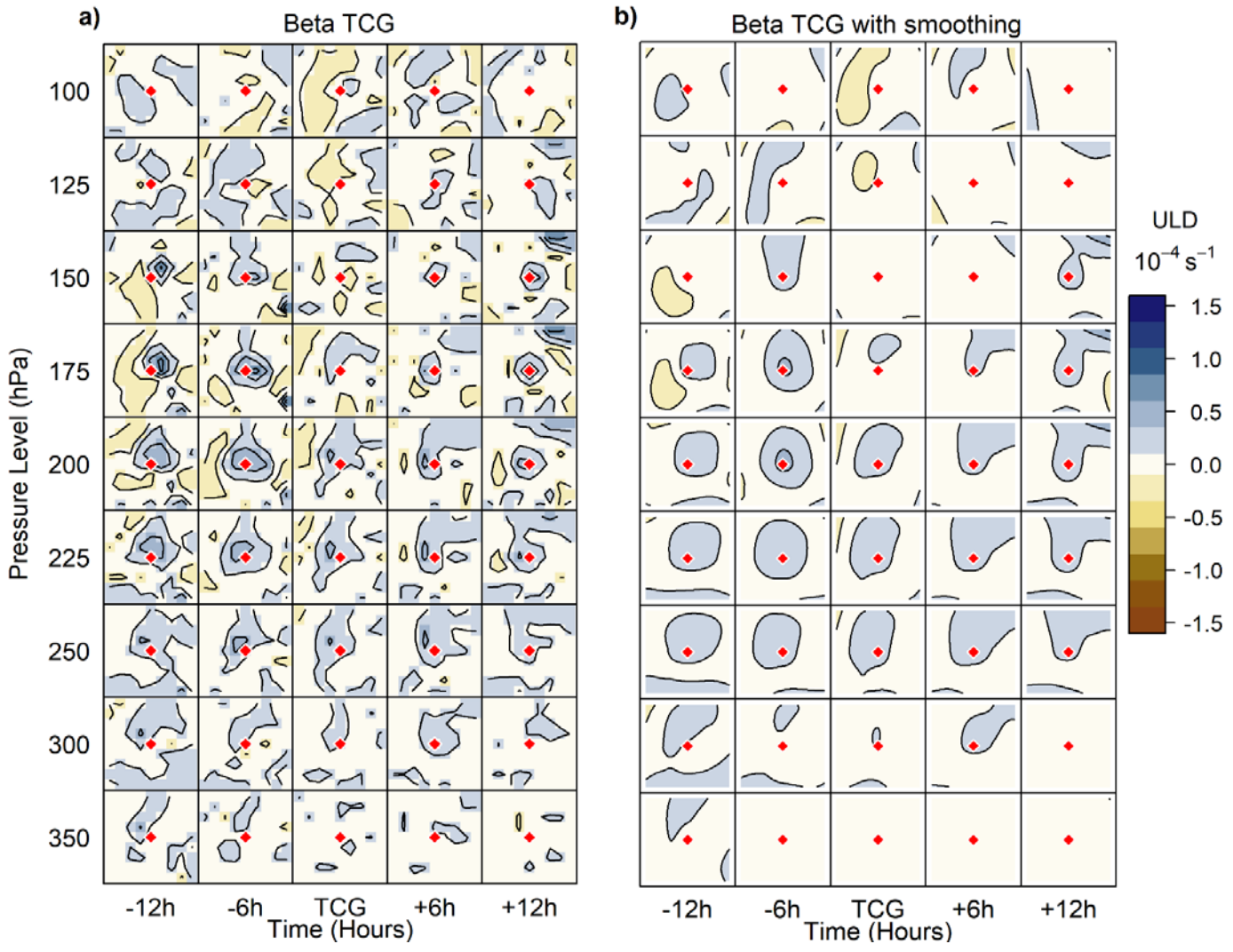

Figure 4.26. Beta ULD at TCG (a) and ULD at TCG with smoothing (b).

4.1.25. Tropical Storm Gamma

Throughout the TC's lifespan, Gamma maintained deep convection (NHC 2015). It reached TS status twice in its lifespan. Both are included in this analysis. It first achieved TS classification briefly at 0600 UTC on 15 November 2005 at 14.3° N, 66.0° W and maintained it for twelve hours (Knapp et al. 2010). An increase in westerly vertical shear caused the cyclone to weaken and TCG +12 hour data reflects a TD (NHC 2015). Very intense and compact areas of ULD reach the 125 hPa level in Figure 4.27. The largest maximum values of all ULD data included in this study occur during Gamma's first TCG occurrence at 125 hPa between TCG –6 hours and TCG. Although actual ULD values are not the focus of this research, these maximum rates should be mentioned. Gamma was a mid-November cyclone and produced values exceeding 1.5 x 10^{-4} s^{-1}.

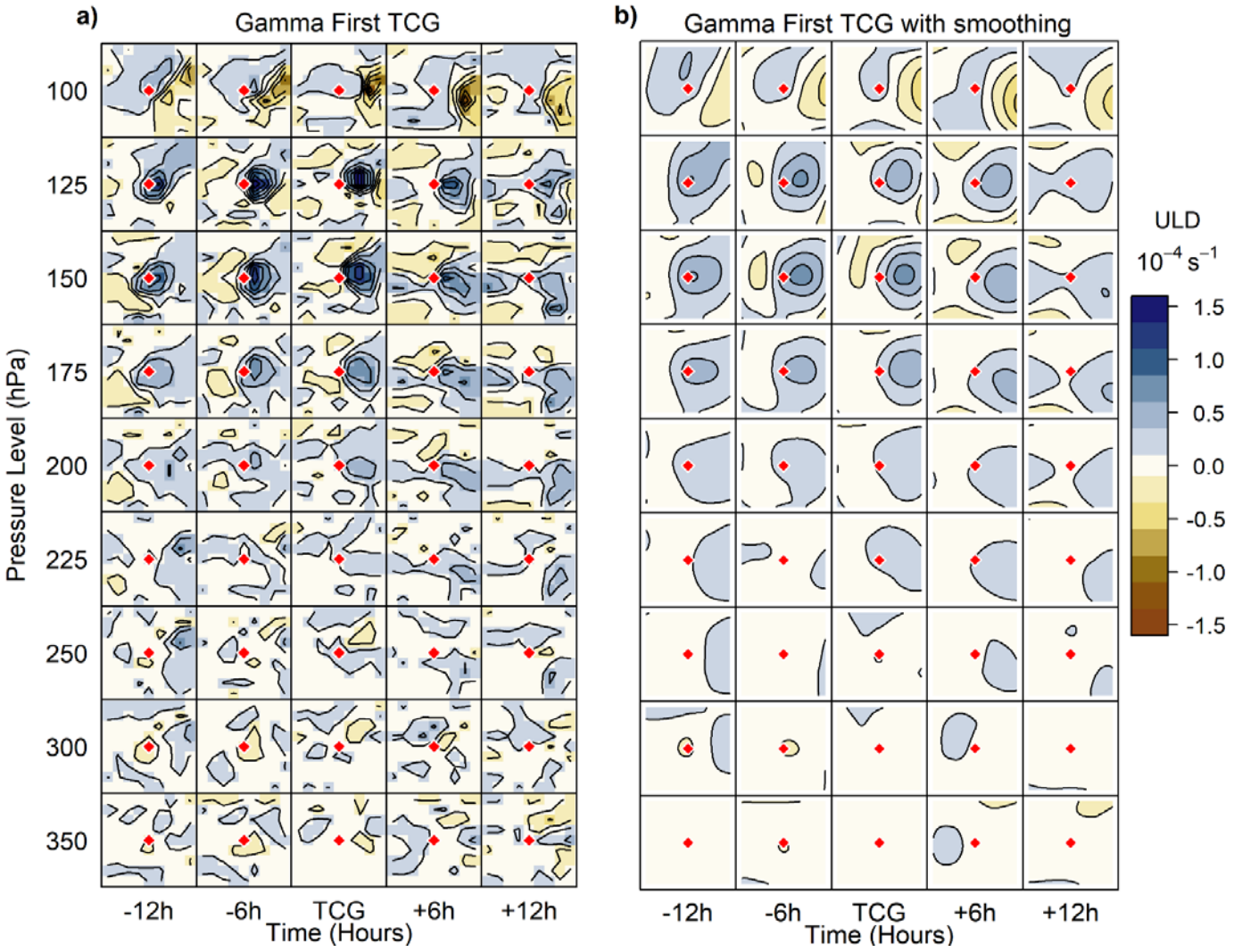

Figure 4.27. Gamma ULD at first TCG (a) and ULD at first TCG with smoothing (b).

Gamma regenerated from a remnant low while interacting with a non-convective low-pressure system over the topographical elevations of the Sierra La Esperanza (NHC 2015). The low-level circulation of both systems merged (NHC 2015), allowing TS status to occur a second time at 18:00 on 18 November 2005 at 15.7° N, 85.6°W (Knapp et al. 2010). The classification upgrade occurred while the COC was over land just south of the Honduran coastline. Most ULD is dispersed north and northeast of the COC, which is over water during the time series in Figure 4.28. ULD extends vertically to 125 hPa and is concentrated between the levels 250 hPa and 150 hPa. Starting at TCG –12 hours values increase in magnitude till TCG when values begin decreasing in magnitude through TCG +12 hours.

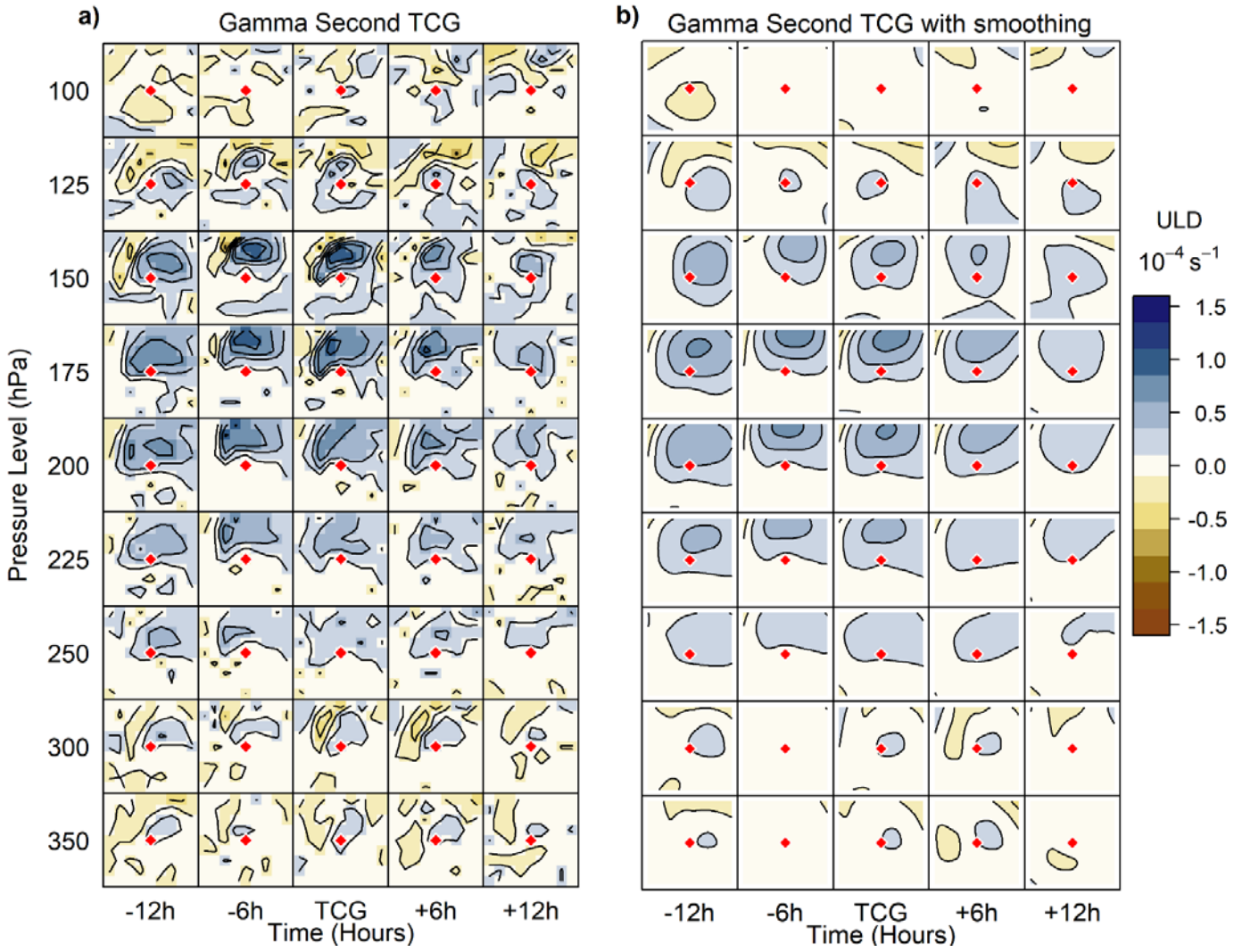

Figure 4.28. Gamma ULD at second TCG (a) and ULD at second TCG with smoothing (b).

4.1.26. Tropical Storm Delta

Delta began as an extratropical low, evolved to a SS, then eventually became classified as a TS (NHC 2015). As extratropical, the system exceeded the wind requirements of 17 m s^{-1}; therefore, the analysis focuses on time of SS transition. Central convection and an inner wind maximum formed by 0900 UTC on 22 November and by 1800 UTC on 22 November 2005 the extratropical low became removed from non-tropical frontal cloud bands, allowing SS classification at 30.7° N, 40.5° W (Knapp et al. 2010, NHC 2015). Convection consolidated the next day and Delta was then listed as a TS (NHC 2015). In Figure 4.29, ULD concentrations occur mainly between 350 hPa and 200 hPa with the most organized concentrations at TCG –12 hours and minor organization at TCG +6 hours.

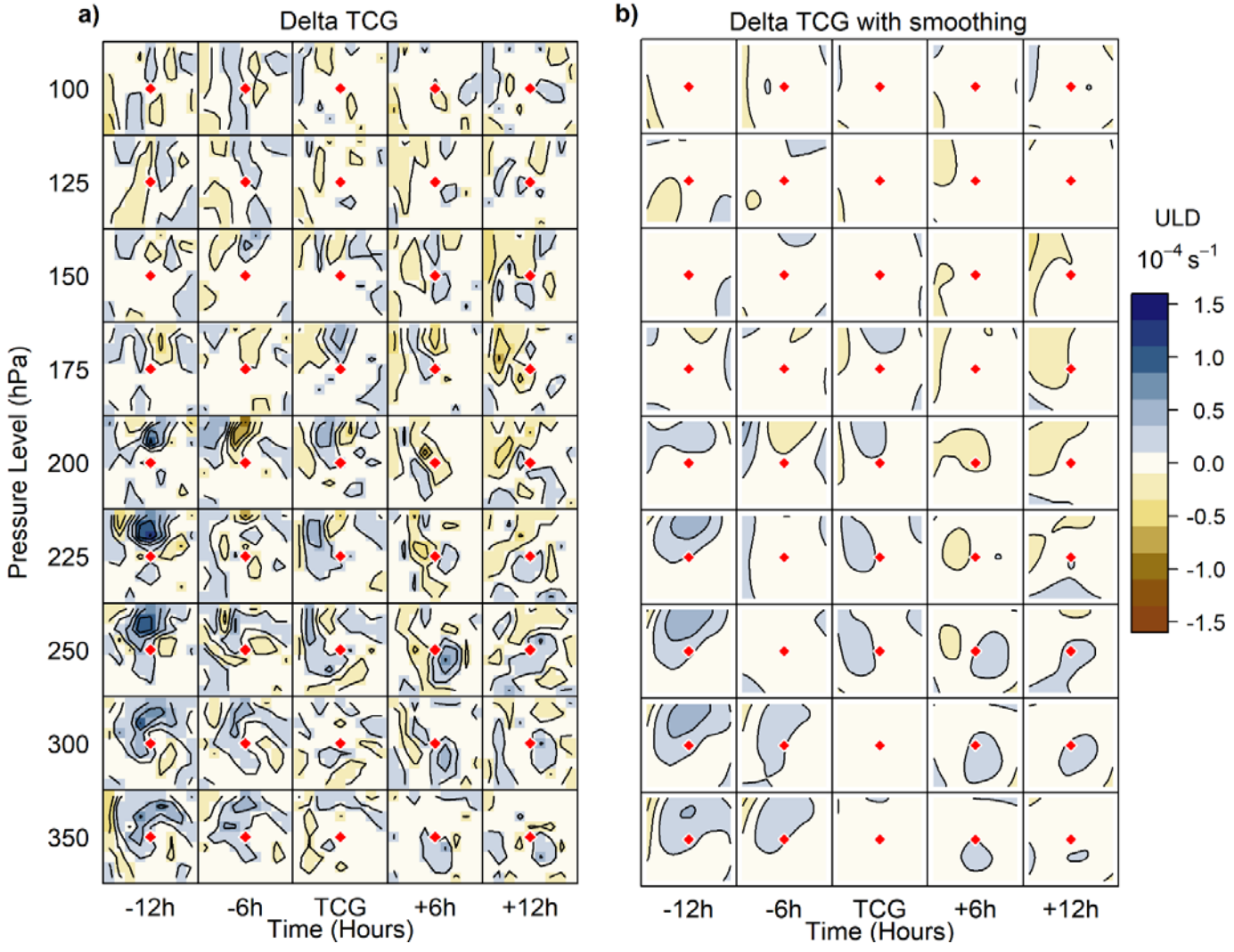

Figure 4.29. Delta ULD at TCG (a) and ULD at TCG with smoothing (b).

4.1.27. Tropical Storm Epsilon

Best track data for Epsilon began 0600 UTC on 29 November 2005 at 31.5° N, 49.2° W (Knapp et al. 2010) when the system was classified as a TS, skipping TD status. Epsilon appeared on satellite as a SS the evening prior as it separated from a frontal zone, but insufficient organization of non-frontal convection was present, thereby precluding classification as a SS (NHC 2015). Coordinates for times prior to TCG were based on available information of storm location. Similar to Delta and beginning with SS characteristics, ULD concentrations for Epsilon occur from 350 hPa to 200 hPa in Figure 4.30. ULD magnitude is greatest prior to TCG but begins to organize near the COC after TCG.

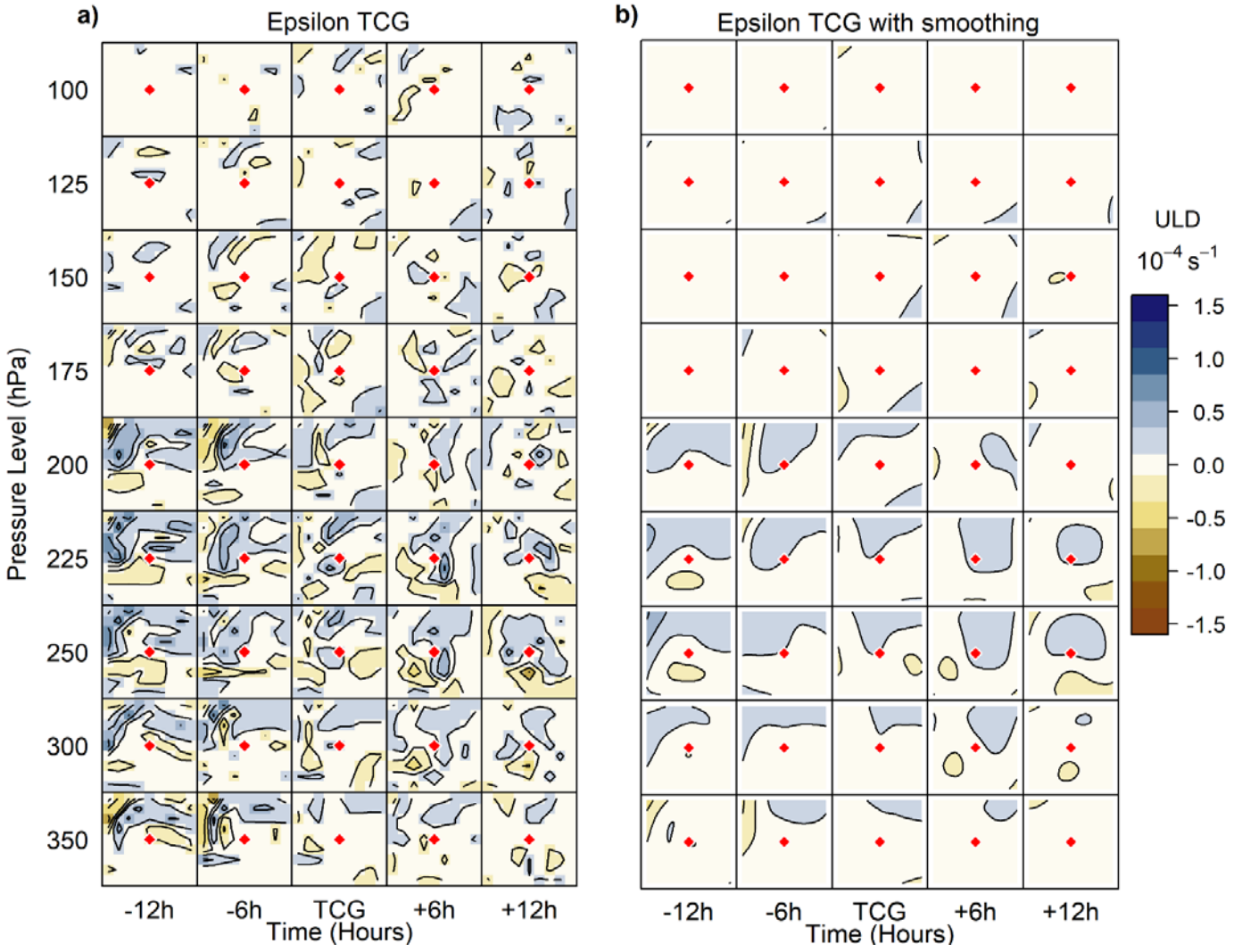

Figure 4.30. Epsilon ULD at TCG (a) and ULD at TCG with smoothing (b).

4.1.28. Tropical Storm Zeta

Zeta began when enough increased and organized thunderstorm activity occurred near the center of a closed low late 29 December that warranted TD classification early on 30 December (NHC 2015). TS designation occurred at 0600 UTC on 30 December 2005 at 24.2° N, 36.1° W (Knapp et al. 2010) as rapidly developing convection banding encircled the low-level center (NHC 2015). TCG –12 hour coordinates were estimated based on the slow-moving system's TCG –6 hour coordinates. The cyclone continued to strengthen throughout the time analyzed and ULD increased near and east of the COC between 250 hPa and 175 hPa after TCG (Figure 4.31).

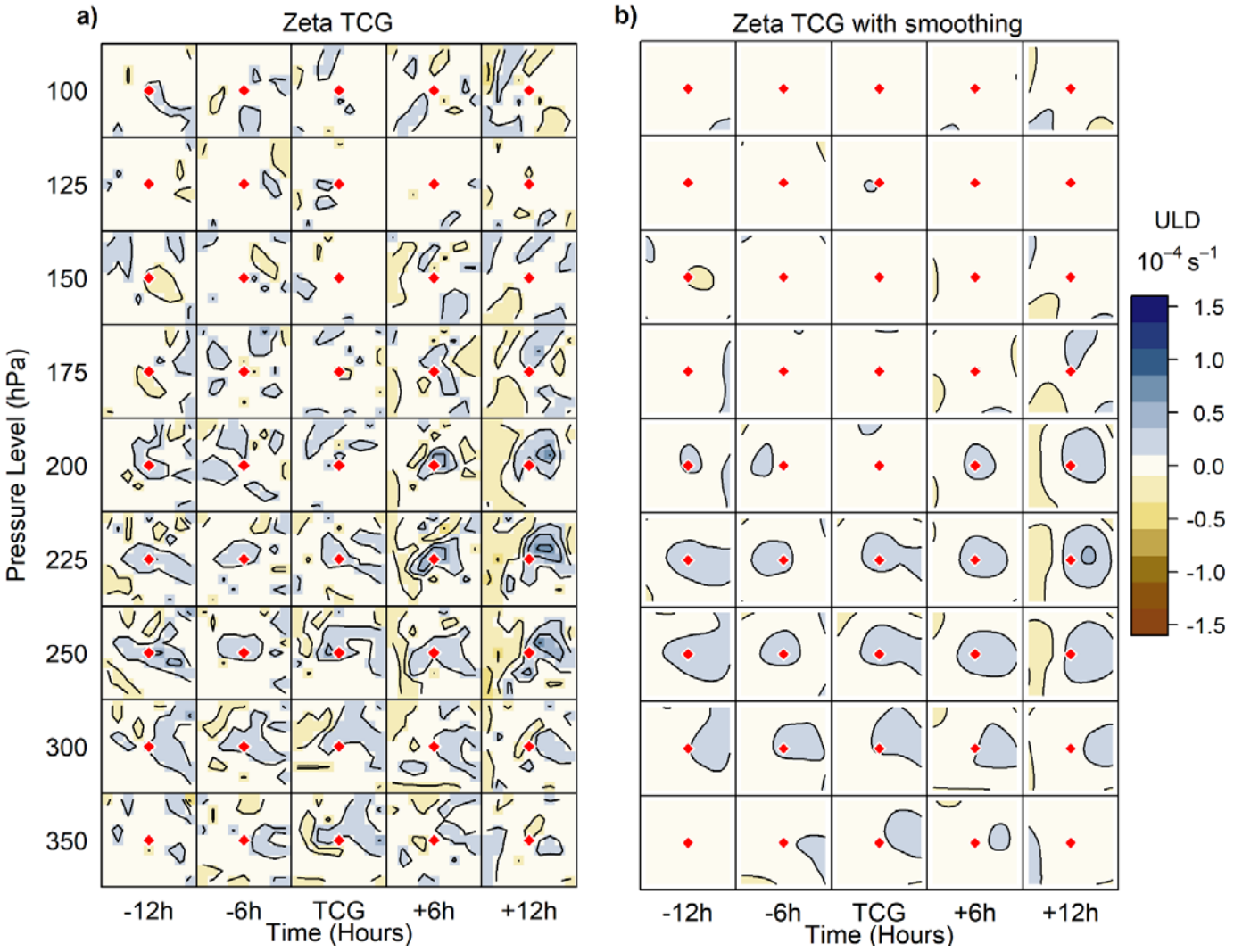

Figure 4.31. Zeta ULD at TCG (a) and ULD at TCG with smoothing (b).

4.2. Maximum ULD

A histogram displaying the percentage contribution of the maximum 2% of ULD values per TCG occurrence is shown in Figure 4.32. The figure shows only levels 200 hPa to 150 hPa since these three vertical levels represent ~70% of the maximum ULD values. The smallest contribution of the three levels is from 200 hPa. A more complete version of this histogram including all levels can be found in the Appendix Figure A.1. Percentages displayed below are in relation to all nine levels and five times. Results show that of the 2187 cases, maximum ULD values are found most commonly at 175 hPa (29.0%), followed by 150 hPa (21.41%), and 200 hPa (19.41%). Over half of maximum ULD in this study is found above 200 hPa.

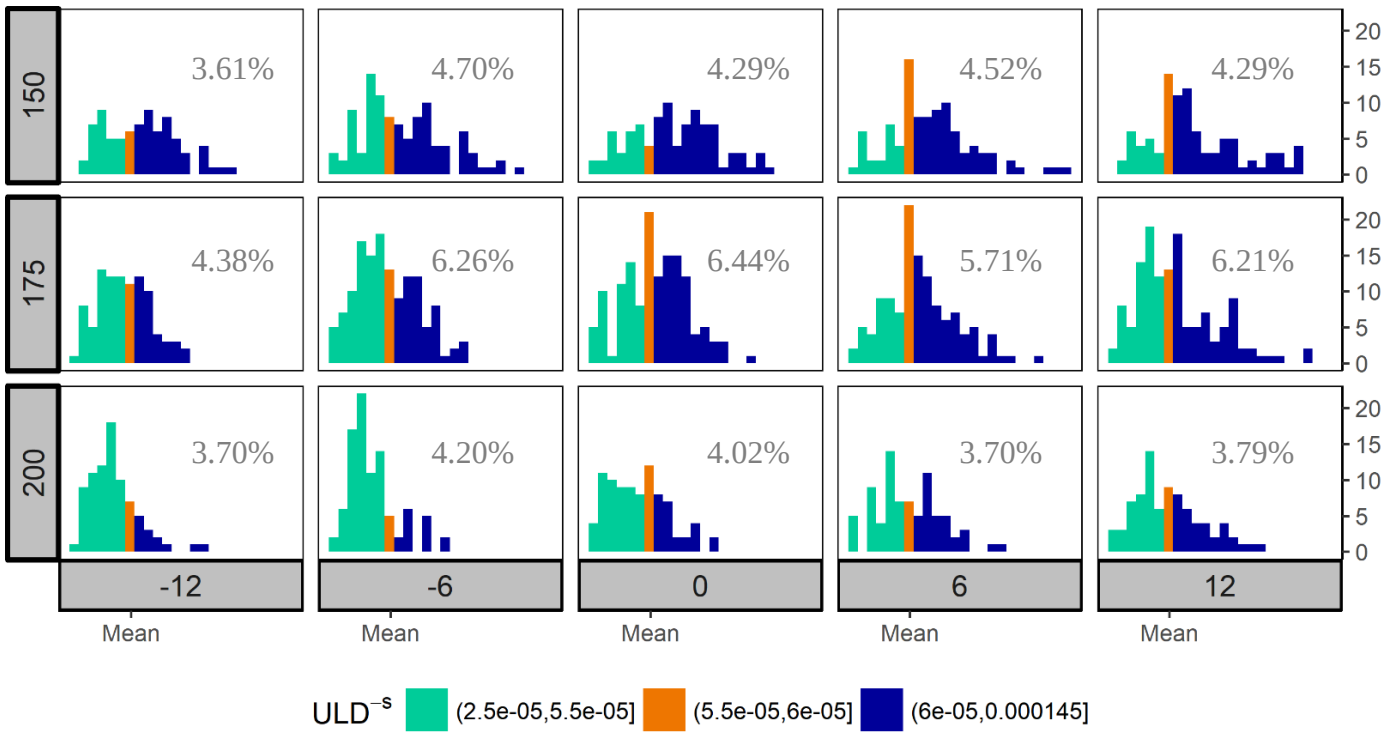

Figure 4.32. Histogram of greatest 2% ULD values between levels 200 hPa and 150 hPa per TCG occurrence for the 2005 season. Time on the bottom x-axis (TCG –12 hours, TCG –6 hours, TCG, TCG +6 hours, TCG +12 hours) and mean of highest 2% ULD values labeled at tick mark. Vertical level in hPa is listed on the left y-axis and count on the right y-axis. Bin width is 5.0 x 10^{-6} s^{-1}, ranging from 2.5 x 10^{-5} s^{-1} to 1.45 x 10^{-4} s^{-1}. Colors (green, orange, dark blue) indicate relation to the mean (below, mean, above).

The maximum 2% ULD per individual TCG (i.e., top 73 ULD values during each of the 30 TCG occurrences) between the 350 and 100 hPa level is displayed in Figure 4.33. LOESS is applied to identify the maximum ULD values as they vary within the five time stamps throughout TCG. The percentage of ULD

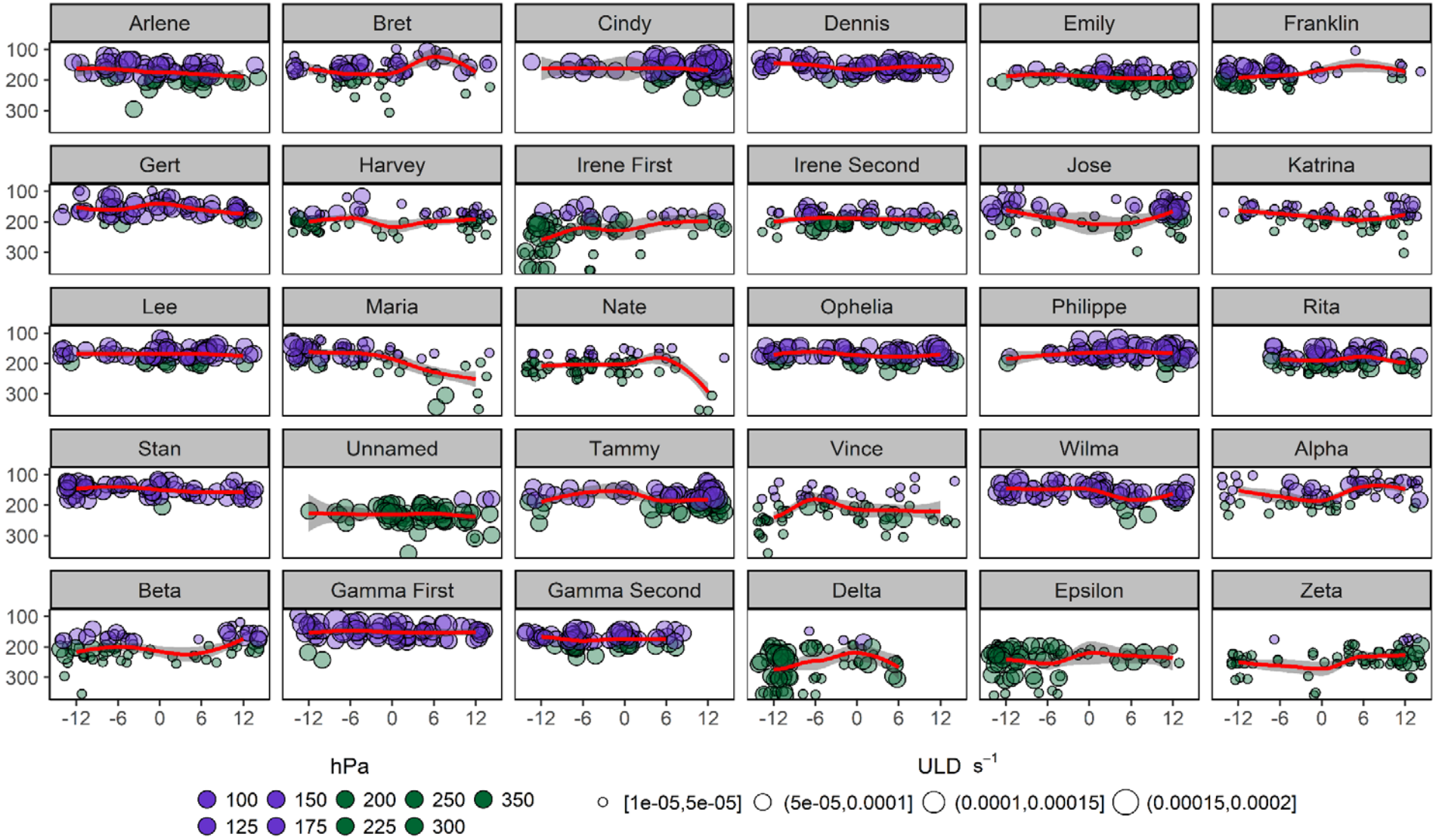

Figure 4.33. Top 2% of ULD values per TCG occurrence. ULD between levels 350 hPa and 100 hPa with LOESS smoothing in red and 95% confidence interval shaded in grey. Time is on each x-axis (TCG –12 hours, TCG –6 hours, TCG, TCG +6 hours, TCG +12 hours) and vertical pressure level in hPa is on each y-axis. Bin width is 5.0 x 10^{-5} s^{-1}, with a range from 1.0 x 10^{-5} s^{-1} to 2.0 x 10^{-4} s^{-1}. Purple (green) represents above 200 hPa (includes 200 hPa and below). Larger (smaller) ULD symbol size indicates higher (lower) rates per second. Plot uses jitter and increased transparency on points to prevent "overplotting."

values distributed per TCG is the highest in the range above the 200 hPa (purple) level (i.e., compared with values at or below 200 hPa (green)).

An evaluation of the top 2% maxima (not shown) of ULD for the total season (i.e., not per TCG) indicates the majority of top ULD observations occur above the 200 hPa vertical level. Calculations show nearly 60% of the ULD maxima reaching above 200 hPa. Additional review of the total season maxima when dispersed by TCG occurrence (not shown) shows an immense variation in individual TCG contribution to the whole. Contributions range from Nate, which during the 24 hours evaluated, did not exhibit any ULD values strong enough to be included in the assessment of total season top 2% values, to Gamma, which not only holds the two largest single ULD values in the study, but its second TCG occurrence contains the largest percentage of the maxima.

In a similar evaluation of the top 1% ULD values (not shown), the same three levels appear to comprise the vast majority of the greatest ULD magnitudes (1080 values), containing 73.1% of maximum values. The 200 hPa level contributes only 17.7% of the maximum ULD, while the 175 hPa (29.5%) and 150 hPa (25.9%) levels together represent over 55% of the highest 1% of ULD during TCG based on the 2005 Atlantic season. It is interesting to note that the 150 hPa level substantially increases its contribution to the whole, as a smaller and smaller tail of the distribution is analyzed.

4.3. Mean ULD

Mean values of ULD show 175 hPa as the optimum level to analyze ULD during TCG. That said, Figure 4.34 (a) and (b) clearly show that limiting ULD to only one level would provide a less than optimal representation. While keeping in mind each TCG is unique, the mean itself represents a variation that cannot be narrowed down to one atmospheric "slice." The vertical evolution of ULD appears to be significant throughout pressure levels 250 hPa to 125 hPa and temporally appears to organize and strengthen until it levels off at TCG +12 hours. A slight decrease in the elevation of largest ULD magnitude occurs at 125 hPa during TCG. Most notable is ULD becoming more organized between 200 hPa and 150 hPa during times TCG to TCG +12 hours. Mean ULD also clusters to the north and east of the COC. This could be significant, as

research tends to focus more on areas in or around the COC and generally relative to the radius of maximum winds.

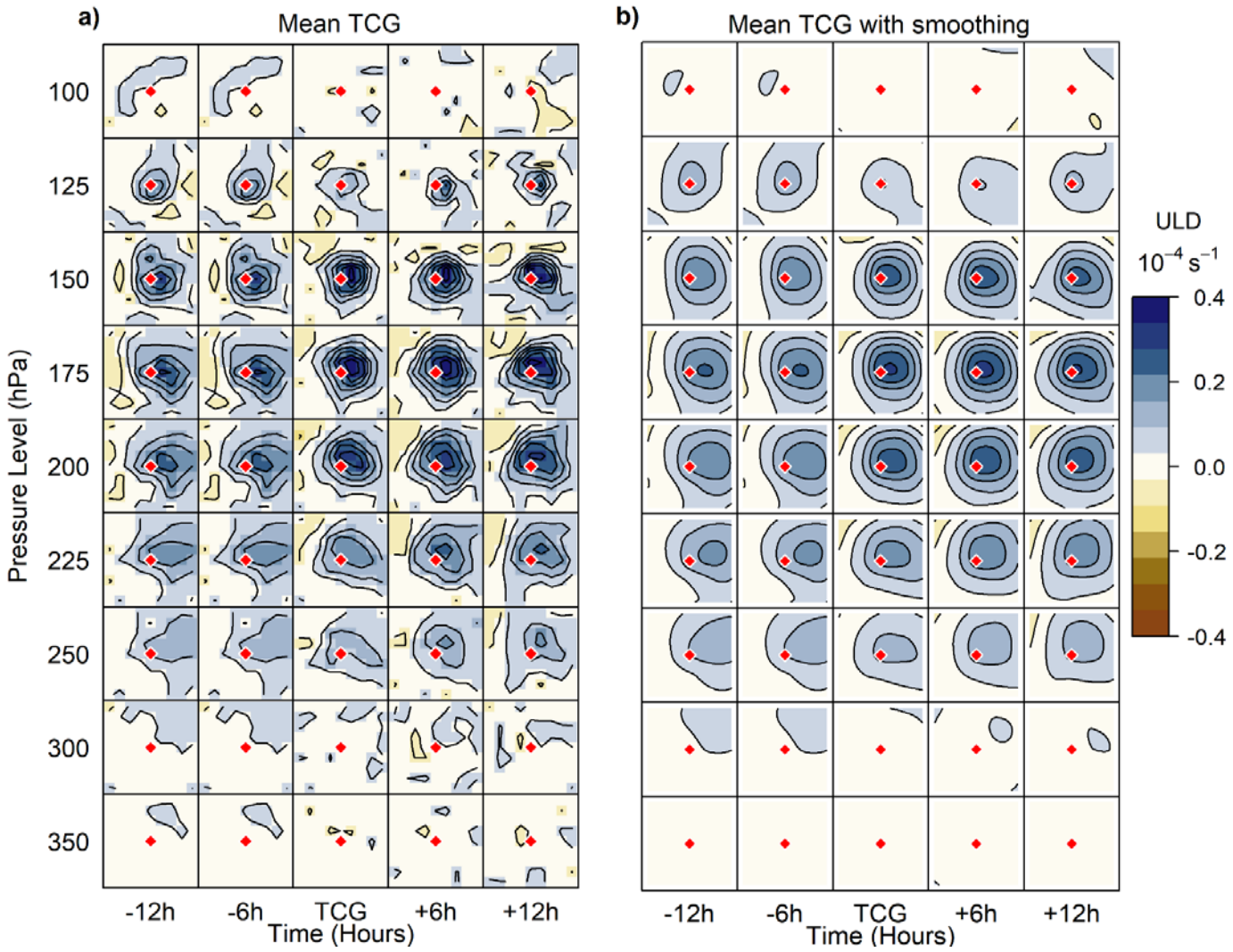

Figure 4.34. Mean ULD at TCG (a) and ULD at TCG with smoothing (b).

Results show that the maximum clustered ULD values are generally found at the 175 hPa level on average. Illustrated in Figure 4.35 which graphs the top 2% of mean values, maximum ULD is contained between 225 hPa and 150 hPa. A LOESS smoothing curve identifies 175 hPa as the best statistical result for the location of ULD through all studied times. This result is consistent through calculations applied to all 30 TCG occurrences together, but each storm displays a unique variation through time and pressure level (See Section 4.1), suggesting that vertically and temporally, the ULD field is dynamic.

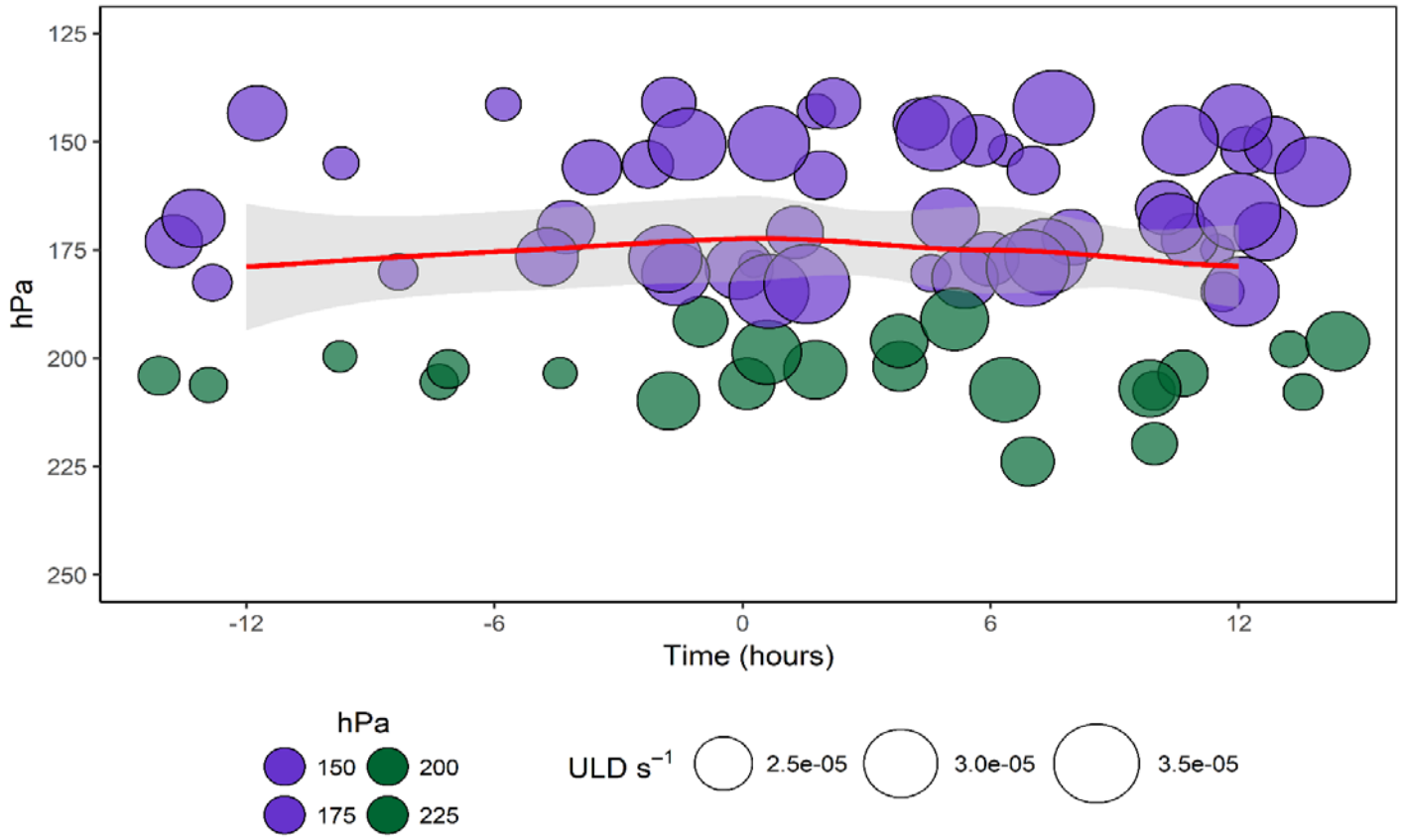

Figure 4.35. Same as Figure 4.33 but a single plot of top 2% mean ULD values (73). Circle size indicates minimum, mean, and maximum with a bin width of 5.0 x 10^{-6} s^{-1} for scale.

4.4. Data Set Comparison

Due to the recent availability of the ERA-Interim Project with ULD on a 0.7° latitude by 0.7° longitude spatial grid (ECMWF 2009, Berrisford et al. 2011), the following is a brief comparison of JRA-55 and ERA-Interim Project data sets. All available atmospheric levels (i.e., 37) are used to create a full visualization of divergence through the entire atmospheric depth for each evaluated time. Figure 4.36 for JRA-55 and Figure 4.37 for ERA-Interim Project show the (a) west-to-east and (b) south-to-north vertical cross section view of mean ULD through the COC.

All TCGs are included in the mean analysis and the highest magnitudes of ULD are located above the 200 hPa level (red dotted line) for each time stamp. Both (a) and (b) in Figure 4.36 using JRA-55 data, show increased ULD concentrations above 200 hPa. In Figure 4.37 using ERA-Interim data, mean ULD in (b) appears closer along the 200 hPa level in comparison to (a). Although one set of analysis (Figure 4.37 (b)) out of the four suggests ULD clustering closer to 200 hPa, all plots show the mean vertical location of the ULD

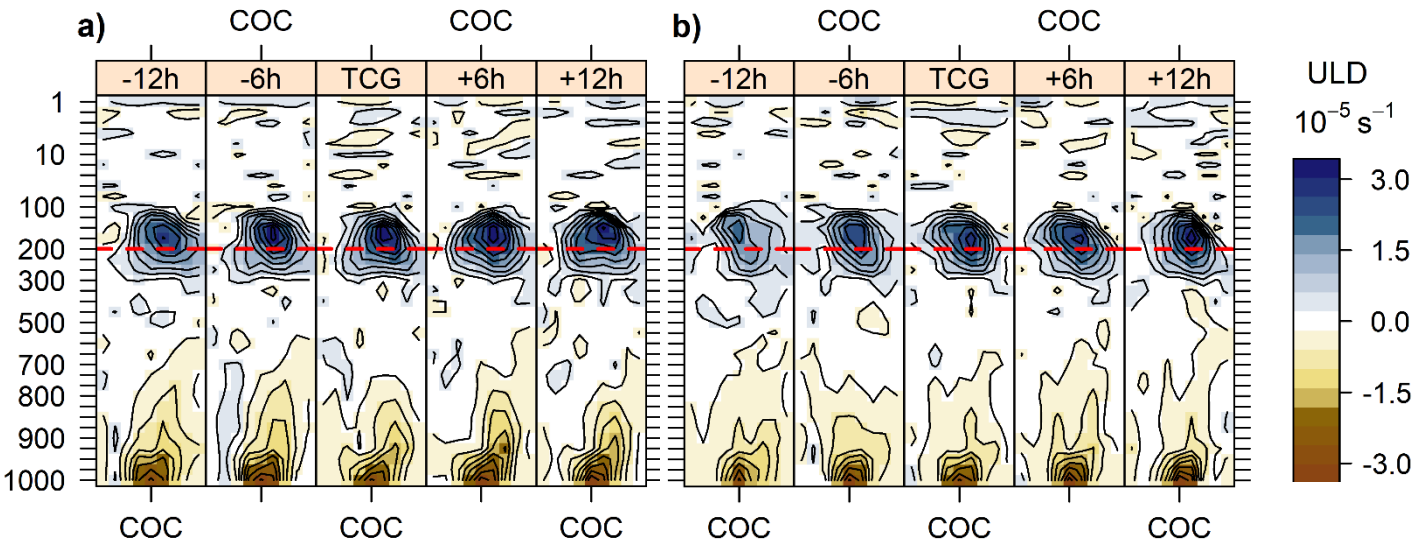

Figure 4.36. Cross section of mean ULD for JRA-55 data, (a) west-to-east and (b) south-to-north through COC (tick mark) for each time (top x-axis). Red dotted line represents 200 hPa.

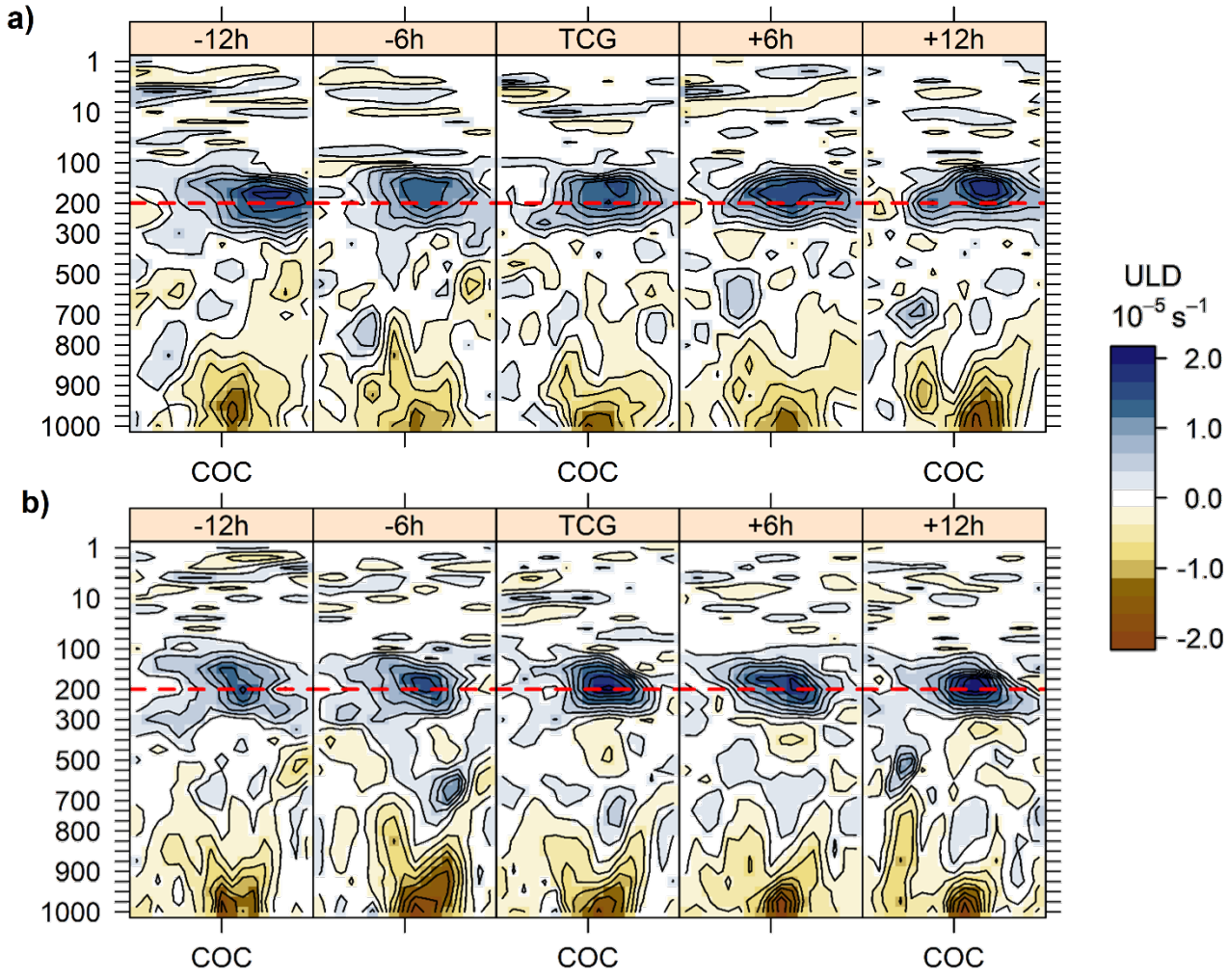

Figure 4.37. Same as Figure 4.36 but for ERA-Interim Project data.

field to be vertically and spatially widespread and mainly located between the 250 hPa to 100 hPa levels. Temporally, the mean does not show significant variation.

Comparison of mean ULD between the two data sets shows values for ERA-Interim ULD are smaller as a whole but the trends are very similar and in close agreement with JRA-55. Concentrations of the divergence field are closer to 200 hPa for the ERA-Interim data analysis (Figure 4.38) than the JRA-55 data analysis (Figure 4.34), but the range of levels from 250 hPa to 125 hPa is the same. The temporal evolution shows a general trend of ULD becoming more organized and strengthening or maintaining magnitude during and post TCG when compared to pre-TCG in Figures 4.34 (a) and 4.38 (a). Analysis of both data sets

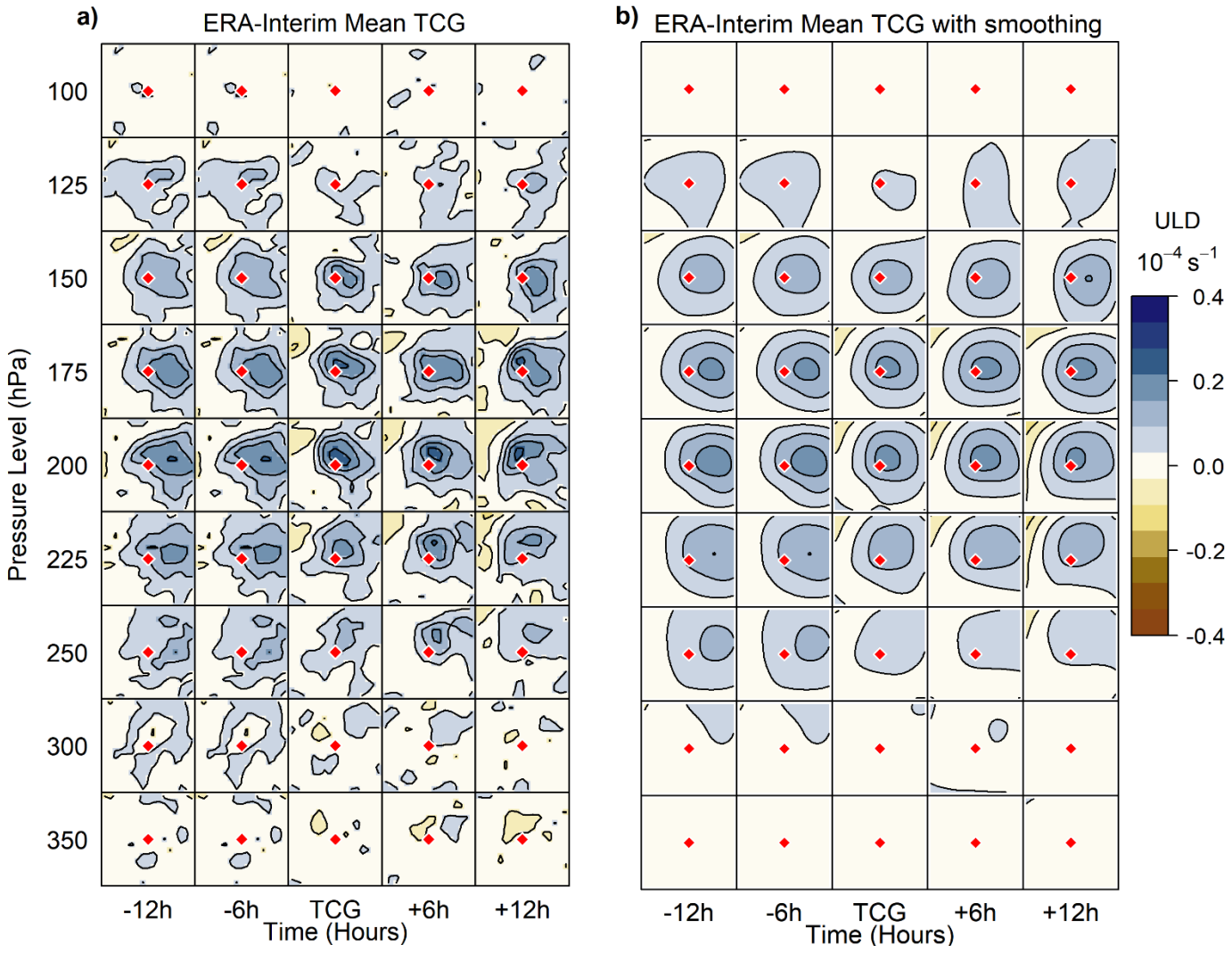

Figure 4.38. Same as Figure 4.34 but for ERA-Interim Project data.

indicates changes in magnitude and frequency of ULD through a wide range of atmospheric levels over time, confirming that ULD maxima cannot be assumed to occur at only one level.

4.5. Summary

This chapter has provided a detailed look at individual TCG occurrences and the ULD associated with them. It reviewed the 30 individual TCGs, the season's overall mean, and the highest percentages of maximum ULD. Visualization of the data and results were displayed throughout the chapter to provide a clearer understanding of the results. A brief comparison of available data sets concludes the chapter. The next chapter will conclude the research and tie it together with the research questions in Chapter 1.

5. CONCLUSIONS

5.1. Upper-Level Divergence at Tropical Cyclogenesis

Understanding the complex dynamics involved with TC formation and intensification as related to the evolution of ULD is pertinent to a more complete investigation of tropical systems. Prediction of TCs is improving rapidly as scientific understanding of the atmospheric and oceanic conditions that characterize TCG, along with tools available for measuring the associated variables, are becoming more advanced and widespread. Literature shows that ULD is assumed to occur at the atmospheric pressure level of 200 hPa. But in reality, ULD is a dynamic variable as with all other atmospheric variables and should not be assumed to exist at a single, predetermined atmospheric level, especially now that better observations and models to depict ULD are advancing. Evolution of the ULD field during intensification to TS classification shows maximum values generally reaching higher in the troposphere than 200 hPa of atmospheric pressure. Although maximum values of divergence identify ~175 hPa as the average ULD level, it is also clear that using an average level is not the most significant in all cases. Each TCG condition is unique and should be evaluated individually.

Davidson and Kar (2002) suggested that absence of enhanced ULD during intensification could mean that it may not be crucial to intensification. They also noted the absence could possibly be due to the issue of measuring ULD accurately at the time of the study (Davidson and Kar 2002). Boyle (1994) reported that a 200 hPa ULD signal can be weak or nonexistent, but on average is associated with cyclones. The present research suggests that while the signal may be "weak or nonexistent" at 200 hPa, it can be more robust at other vertical levels and lateral locations with respect to the COC. These results support the Persing et al. (2002) findings of ULD patterns above 200 hPa in Hurricane Opal (1995) with "[u]pper-level divergence exhibits significant vertical structure, such that single-level or layer-average analysis techniques do not capture the divergence signature aloft." A few examples of why ULD analysis should not be confined to one pressure level are seen in the individual TCG occurrences of Dennis, Gert, Stan, Wilma, and Gamma's first TCG, registering significant clustered ULD higher in the atmosphere than 200 hPa. Occurrences during Vince, Delta, and Zeta reflect significant ULD clustering lower in the atmosphere than 200 hPa. Investigating many of the other

TCGs in 2005 shows that restricting ULD data analysis to 200 hPa would not encompass the full ULD range but represent only a fraction of ULD extent, thereby limiting its contribution in models and research.

Temporal evolution of ULD during the five evaluated times reveals a different pattern for each TCG. Comparing a few of the above-mentioned TCG occurrences in relation to the time series, Wilma's ULD reduced in magnitude and moved lower in the atmosphere as TCG progressed, while Gert's strongest and Stan's weakest ULD field both occurred at TCG –6 hours. The mean temporal evolution maintains a steady increase in magnitude until TCG +12 hours at which point it appears to level off. Additional analysis is needed to further explore the significance of ULD leveling off after TCG.

In comparing JRA-55 and ERA-Interim modeled data sets, a strong agreement is evident that ULD is dynamic and fluctuates vertically, temporally, and spatially during TCG. Additional comparative analysis (not shown) of these data sets also supports these research findings.

With an increasing amount of research recognizing the significance of the secondary circulation and TC outflow, it would seem that it is time to establish new parameters for the examination of TCs. For example, storm intensification is sensitive to the distribution of vertical levels used in Pennsylvania State University–National Center for Atmospheric Research Mesoscale Model (MM5), and Kimball and Dougherty (2006) showed that the outflow layer must be even better-resolved than the inflow layer, to depict a TC correctly. In a study of Ophelia's genesis, Houze et al. (2009) observed substantial outflow at approximately 14 km (i.e., ~150 hPa) which is supported by this research (Figure 4.17). Chen and Zhang (2013) attributed the high elevation of Wilma's ULD to the record-breaking strength it experienced. According to Barrett et al. (2016), radial ULD movement "is critically related to both TC track and intensity." Ge et al. (2008) showed that ULD could possibly influence TC size. In an overview of outflow in TCs using ERA-Interim reanalysis (Dee et al. 2011) from 1979 to 2014, Ditchek et al. (2017) recognized the 175 hPa to 150 hPa level as the location of peak ULD.

It is essential to understand the height and spatial distribution of ULD required for formation, development, and intensification of TCs. An evaluation across spatial (including both vertical and horizontal)

and temporal scales of ULD is important for producing a useful analysis or forecasting product. It is clear that in all scientific research, assumptions must be made on variables that are unavailable for detailed analysis. Emanuel et al. (2004) references this approach while discussing applied data parameterization: "[w]e make no assertion that the 850–200-hPa wind shear is the optimal quantity to use; it is merely expedient to use these values until and unless superior measures are developed." ULD is no longer unavailable and outflow values analyzed throughout the upper troposphere should be included in future models. Likewise, further research is necessary for more accurate outcomes.

6. FUTURE RESEARCH

Exploring further into the conditions necessary for the ULD to increase and maintain itself during any portion of a TC life cycle is important for improvements in modeling. Future research can analyze ULD during any stage of development of a TC or as it progresses throughout the entire life cycle. ULD correlation with other atmospheric conditions and variables would prove to be useful in understanding the precise contribution of ULD to TC stability, strength, and growth. Analysis of latitudinal and basin position, time of occurrence (i.e., diurnal and monthly), and vertical height of the tropopause with the ULD would increase the accuracy of TC forecasting.

If storms provide a "signature" in terms of their ULD field that precedes intensity changes, then TC intensity forecasting can be improved substantially. The advent of higher-resolution data sets, improved geospatial analytic techniques, and more precise animations of the temporal evolution of three-dimensional mapped ULD may facilitate the identification of such a signature. As Gehne and Kleeman (2012) mentioned, direct global observations are not available for certain dynamical variables (i.e., wind, divergence, geopotential). Therefore, use of reanalysis products is required in the absence of direct measurements. One prospective in situ data source for divergence analysis in future research could be the U. S. Naval Research Laboratory Marine Meteorology Division (2012) and their work with NASA using unmanned aircraft to measure the hurricane outflow layer environmental conditions in the Atlantic "at higher altitudes than routine hurricane research and reconnaissance aircraft can reach." Options to apply such data to analysis are limitless.

7. REFERENCES

Aberson, S. D. (2008). Large forecast degradations due to synoptic surveillance during the 2004 and 2005 hurricane seasons. Monthly Weather Review, 136(8), 3138–3150.

Abish, B., Joseph, P. V., and Johannessen, O. M. (2015). Climate change in the subtropical jetstream during 1950–2009. Advances in Atmospheric Sciences, 32(1), 140–148. doi:10.1007/s00376-014-4156-6.

Agudelo, P. A., Hoyos, C. D., Curry, J. A., and Webster, P. J. (2011). Probabilistic discrimination between large-scale environments of intensifying and decaying African easterly waves. Climate Dynamics, 36(7–8), 1379–1401. doi:10.1007/s00382-010-0851-x.

Arpe, K. (1989). Impacts of changes in the ECMWF analysis-forecasting scheme on the systematic error of the model. Proc. Ten Years of Medium-Range Weather Forecasting, 1, 466–474.

Babu, S. R., Ratnam, M. V., Basha, G., Krishnamurthy, B. V., and Venkateswararao, B. (2015). Effect of tropical cyclones on the tropical tropopause parameters observed using COSMIC GPS RO data. Atmospheric Chemistry and Physics, 15(18), 10239–10249. doi:10.5194/acp-15-10239-2015.

Baker, E. J. (1979). Predicting response to hurricane warnings - reanalysis of data from 4 Studies. Mass Emergencies, 4(1), 9–24.

Baray, J. L., Ancellet, G., Randriambelo, T., and Baldy, S. (1999). Tropical cyclone Marlene and stratosphere-troposphere exchange. Journal of Geophysical Research-Atmospheres, 104(D11), 13953–13970. doi:10.1029/1999jd900028.

Barrett, B. S., Sanabia, E. R., Reynolds, S. C., Stapleton, J. K., and Borrego, A. L. (2016). Evolution of the upper tropospheric outflow in Hurricanes Iselle and Julio (2014) in the Navy Global Environmental Model (NAVGEM) analyses and in satellite and dropsonde observations. Journal of Geophysical Research-Atmospheres, 121(22), 13273–13286. doi:10.1002/2016jd025656.

Bell, G., Blake, E., Landsea, C., Mo, K., Pasch, R., Chelliah, M., and Goldenberg, S. (2006). The 2005 North Atlantic hurricane season. A climate perspective. http://www.cpc.ncep.noaa.gov/products/expert_assessment/hurrsummary_2005.pdf.

Bender, M. A. (1997). The effect of relative flow on the asymmetric structure in the interior of hurricanes. Journal of the Atmospheric Sciences, 54(6), 703–724. doi:10.1175/1520-0469(1997)054<0703:teorfo>2.0.co;2.

Bentley, A. M., Bosart, L. F., and Keyser, D. (2017). Upper-tropospheric precursors to the formation of subtropical cyclones that undergo tropical transition in the North Atlantic Basin. Monthly Weather Review, 145(2), 503–520. doi:10.1175/mwr-d-16-0263.1.

Berrisford, P., Dee, D., Poli, P., Brugge, R., Fielding, K., Fuentes, M., … Simmons, A.. (2011). The ERA-Interim archive [Version 2.0]. European Centre for Medium Range Weather Forecasts, Shinfield Park. Reading, Berkshire RG2 9AX, United Kingdom.

Beven, J. L., Avila, L. A., Blake, E. S., Brown, D. P., Franklin, J. L., Knabb, R. D., … Stewart, S. R. (2008). Atlantic hurricane season of 2005. Monthly Weather Review, 136(3), 1109–1173.

Bhatia, K. T., and Nolan, D. S. (2013). Relating the skill of tropical cyclone intensity forecasts to the synoptic environment. Weather and Forecasting, 28(4), 961–980. doi:10.1175/waf-d-12-00110.1.

Bhowmik, S. K. R., and Kotal, S. D. (2010). A dynamical statistical model for prediction of a tropical cyclone. Marine Geodesy, 33(4), 412–423. doi:10.1080/01490419.2010.518073.

Black, P. G., and Anthes, R. A. (1971). Asymmetric structure of tropical cyclone outflow layer. Journal of the Atmospheric Sciences, 28(8), 1348–1366. doi:10.1175/1520-0469(1971)028<1348:otasot>2.0.co;2.

Bosart, L. F., Velden, C. S., Bracken, W. E., Molinari, J., and Black, P. G. (1999). Environmental influences on the rapid intensification of Hurricane Opal (1995) over the Gulf of Mexico. Monthly Weather Review, 128(2), 322–352.

Boyle, J. S. (1994). The northern wintertime divergence extrema at 200 hPa and MSLP cyclones as simulated in the AMIP integration by the ECMFW general-circulation model. Journal of Climate, 7(1), 24–32. doi:10.1175/1520-0442(1994)007<0024:tnwdea>2.0.co;2.

Bracken, W. E., and Bosart, L. F. (2000). The role of synoptic-scale flow during tropical cyclogenesis over the North Atlantic Ocean. Monthly Weather Review, 128(2), 353–376.

Brammer, A., and Thorncroft, C. D. (2015). Variability and evolution of African easterly wave structures and their relationship with tropical cyclogenesis over the Eastern Atlantic. Monthly Weather Review, 143(12), 4975–4995. doi:10.1175/mwr-d-15-0106.1.

Braun, S. A., Montgomery, M. T., and Pu, Z. X. (2006). High-resolution simulation of Hurricane Bonnie (1998). Part I: The organization of eyewall vertical motion. Journal of the Atmospheric Sciences, 63(1), 19–42. doi:10.1175/jas3598.1.

Brayshaw, D. J., Hoskins, B., and Blackburn, M. (2009). The basic ingredients of the North Atlantic storm track. Part I: Land-sea contrast and orography. Journal of the Atmospheric Sciences, 66(9), 2539–2558. doi:10.1175/2009jas3078.1.

Brayshaw, D. J., Hoskins, B., and Blackburn, M. (2011). The basic ingredients of the North Atlantic storm track. Part II: Sea surface temperatures. Journal of the Atmospheric Sciences, 68(8), 1784–1805. doi:10.1175/2011jas3674.1.

Briegel, L. M., and Frank, W. M. (1997). Large-scale influences on tropical cyclogenesis in the western North Pacific. Monthly Weather Review, 125(7), 1397–1413. doi:10.1175/1520-0493(1997)125<1397:LSIOTC>2.0.CO;2.

Businger, S., Graziano, T. M., Kaplan, M. L., and Rozumalski, R. A. (2005). Cold-air cyclogenesis along the Gulf-Stream front: investigation of diabatic impacts on cyclone development, frontal structure, and track. Meteorology and Atmospheric Physics, 88(1–2), 65–90. doi:10.1007/s00703-003-0050-y.

Camargo, S. J., Emanuel, K. A., and Sobel, A. H. (2007a). Use of a genesis potential index to diagnose ENSO effects on tropical cyclone genesis. Journal of Climate, 20(19), 4819–4834. doi:10.1175/jcli4282.1.

Camargo, S. J., Sobel, A. H., Barnston, A. G., and Emanuel, K. A. (2007b). Tropical cyclone genesis potential index in climate models. Tellus Series a-Dynamic Meteorology and Oceanography, 59(4), 428–443. doi:10.1111/j.1600-0870.2007.00238. x.

Chan, J. C. L., and Kwok, R. H. F. (1999). Tropical cyclone genesis in a global numerical weather prediction model. Monthly Weather Review, 127(5), 611–624. doi:10.1175/1520-0493(1999)127<0611:tcgiag>2.0.co;2.

Chand, S. S., and Walsh, K. J. E. (2009). Tropical cyclone activity in the Fiji region: Spatial patterns and relationship to large-scale circulation. Journal of Climate, 22(14), 3877–3893. doi:10.1175/2009jcli2880.1.

Chen, H., and Zhang, D. L. (2013). On the rapid intensification of Hurricane Wilma (2005). Part II: Convective bursts and the upper-level warm core. Journal of the Atmospheric Sciences, 70(1), 146–162. doi:10.1175/jas-d-12-062.1.

Cheung, K. K. W. (2004). Large-scale environmental parameters associated with tropical cyclone formations in the western North Pacific. Journal of Climate, 17(3), 466–484. doi:10.1175/1520-0442(2004)017<0466:lepawt>2.0.co;2.

Chiodi, A. M., and Harrison, D. E. (2008). Hurricane alley SST variability in 2005 and 2006. Journal of Climate, 21(18), 4710–4722. doi:10.1175/2008jcli2084.1.

Choi, K. S., Cha, Y., Kim, H. D., and Kang, S. D. (2016). Possible relationship between East Asian summer monsoon and western North Pacific tropical cyclone genesis frequency. Theoretical and Applied Climatology, 124(1–2), 81–90. doi:10.1007/s00704-015-1383-4.

Christy, J. R., Herman, B., Pielke, R., Klotzbach, P., McNider, R. T., Hnilo, J. J., Spencer, R. W., Chase, T., Douglass, D. (2010). What do observational datasets say about modeled tropospheric temperature trends since 1979? Remote Sensing, 2(9), 2148–2169. doi:10.3390/rs2092148.

Colbert, A. J., and Soden, B. J. (2012). Climatological variations in North Atlantic tropical cyclone tracks. Journal of Climate, 25(2), 657–673. doi:10.1175/jcli-d-11-00034.1.

Colón, J. A., and Nightingale, L. C. W. R., and Navy, U. (1963). Development of tropical cyclones in relation to circulation patterns at the 200-millibar level. Monthly Weather Review. Monthly Weather Review, 91(7), 329–336.

Corbosiero, K. L., and Molinari, J. (2002). The effects of vertical wind shear on the distribution of convection in tropical cyclones. Monthly Weather Review, 130(8), 2110–2123. doi:10.1175/1520-0493(2002)130<2110:teovws>2.0.co;2.

Climate Prediction Center (CPC 2017). Climate Diagnostics Bulletin. NOAA. National Weather Service. NOAA Center for Weather and Climate Prediction. http://www.cpc.ncep.noaa.gov/products/CDB/Tropics/figt24.shtml.

Czajkowski, J., and Done, J. (2014). As the wind blows? Understanding hurricane damages at the local level through a case study analysis. Weather Climate and Society, 6(2), 202–217. doi:10.1175/wcas-d-13-00024.1.

Daloz, A. S., Chauvin, F., Walsh, K., Lavender, S., Abbs, D., and Roux, F. (2012). The ability of general circulation models to simulate tropical cyclones and their precursors over the North Atlantic main development region. Climate Dynamics, 39(7–8), 1559–1576. doi:10.1007/s00382-012-1290-7.

Davidson, N. E. (1995). Vorticity budget for AMEX. 1. Diagnostics. Monthly Weather Review, 123(6), 1620–1635. doi:10.1175/1520–0493(1995)123<1620:vbfapi>2.0.co;2.

Davidson, N. E., and Kar, S. K. (2002). Upper-tropospheric flow transitions during rapid tropical cyclone intensification. Quarterly Journal of the Royal Meteorological Society, 128(581), 861–891. doi:10.1256/0035900021643728.

Davidson, N. E. (2010). On the intensification and recurvature of tropical cyclone Tracy (1974). Australian Meteorological and Oceanographic Journal, 60(3), 169–177.

Davis, C. A. (2015). The formation of moist vortices and tropical cyclones in idealized simulations. Journal of the Atmospheric Sciences, 72(9), 3499–3516. doi:10.1175/jas-d-15-0027.1.

Davis, C. A., and Bosart, L. F. (2003). Baroclinically induced tropical cyclogenesis. Monthly Weather Review, 131(11), 2730–2747. doi:10.1175/1520-0493(2003)131<2730:bitc>2.0.co;2.

De Bellevue, J. L., Baray, J. L., Baldy, S., Ancellet, G., Diab, R., and Ravetta, F. (2007). Simulations of stratospheric to tropospheric transport during the tropical cyclone Marlene event. Atmospheric Environment, 41(31), 6510–6526. doi:10.1016/j.atmosenv.2007.04.040.

Dee, D. P., Uppala, S. M., Simmons, A. J., Berrisford, P., Poli, P., Kobayashi, S., . . . Vitart, F. (2011). The ERA-Interim reanalysis: Configuration and performance of the data assimilation system. Quarterly Journal of the Royal Meteorological Society, 137(656), 553–597. doi:10.1002/qj.828.

DeMaria, M., and Kaplan, J. (1994). A Statistical Hurricane Intensity Prediction Scheme (SHIPS) for the Atlantic Basin. Weather and Forecasting, 9(2), 209–220. doi:10.1175/1520-0434(1994)009<0209:ashipS>2.0.co;2.

DeMaria, M., and Kaplan, J. (1999). An updated Statistical Hurricane Intensity Prediction Scheme (SHIPS) for the Atlantic and eastern North Pacific basins. Weather and Forecasting, 14(3), 326–337. doi:10.1175/1520-0434(1999)014<0326:aushipS>2.0.co;2.

DeMaria, M., Knaff, J. A., and Connell, B. H. (2001). A tropical cyclone genesis parameter for the Tropical Atlantic. Weather and Forecasting, 16(2), 219–233. doi:10.1175/1520-0434(2001)016<0219:atcgpf>2.0.co;2.

DeMaria, M., Mainelli, M., Shay, L. K., Knaff, J. A., and Kaplan, J. (2005). Further improvements to the Statistical Hurricane Intensity Prediction Scheme (SHIPS). Weather and Forecasting, 20(4), 531–543. doi:10.1175/waf862.1.

Dengler, K., and Reeder, M. J. (1997). The effects of convection and baroclinicity on the motion of tropical-cyclone-like vortices. Quarterly Journal of the Royal Meteorological Society, 123(539), 699–725.

Denur, J. (2011). The apparent "super-Carnot" efficiency of hurricanes: Nature's steam engine versus the steam locomotive. American Journal of Physics, 79(6), 631–643. doi:10.1119/1.3534841.

Dessler, A. E. (2002). The effect of deep, tropical convection on the tropical tropopause layer. Journal of Geophysical Research, 107(D3). doi:10.1029/2001jd000511.

Didlake, A. C., Jr., and Houze, R. A., Jr. (2013). Convective-scale variations in the inner-core rainbands of a tropical cyclone. Journal of the Atmospheric Sciences, 70(2), 504–523. doi:10.1175/jas-d-12-0134.1.

Ditchek, S. D., Molinari, J., and Vollaro, D. (2017). Tropical cyclone outflow-layer structure and balanced response to eddy forcings. Journal of the Atmospheric Sciences, 74(1), 133–149. doi:10.1175/jas-d-16-0117.1.

Dolling, K., and Barnes, G. M. (2014). The evolution of Hurricane Humberto (2001). Journal of the Atmospheric Sciences, 71(4), 1276–1291. doi:10.1175/jas-d-13-0164.1.

Done, J. M., Bruyere, C. L., Ge, M., and Jaye, A. (2014). Internal variability of North Atlantic tropical cyclones. Journal of Geophysical Research-Atmospheres, 119(11), 6506–6519. doi:10.1002/2014jd021542.

Druyan, L. M., Lonergan, P., and Eichler, T. (1999). A GCM investigation of global warming impacts relevant to tropical cyclone genesis. International Journal of Climatology, 19(6), 607617. doi:10.1002/(sici)1097–0088(199905)19:6<607::aid-joc383>3.0.co;2-m.

Dunkerton, T. J., Montgomery, M. T., and Wang, Z. (2009). Tropical cyclogenesis in a tropical wave critical layer: Easterly waves. Atmospheric Chemistry and Physics, 9(15), 5587–5646. doi:10.5194/acp-9-5587-2009.

Durden, S. L. (2013). Observed tropical cyclone eye thermal anomaly profiles extending above 300 hPa. Monthly Weather Review, 141(12), 4256–4268. doi:10.1175/mwr-d-13-00021.1.

Ebita, A., Kobayashi, S., Ota, Y., Moriya, M., Kumabe, R., Onogi, K., ... and Kamahori, H. (2011). The Japanese 55-year Reanalysis “JRA-55”: An interim report. Sola, 7, 149–152.

Ellrod, G. P., and Knapp, D. I. (1992). An objective clear-air turbulence forecasting technique–Verification and operational use. Weather and Forecasting, (1), 150–165. doi:10.1175/1520-0434(1992)007<0150:aocatf>2.0.co;2.

Elsberry, R. L., and Jeffries, R. A. (1996). Vertical wind shear influences on tropical cyclone formation and intensification during TCM-92 and TCM-93. Monthly Weather Review, 124(7), 1374–1387. doi:10.1175/1520-0493(1996)124<1374:vwsiot>2.0.co;2.

Elsberry, R. L., and Stenger, R. A. (2008). Advances in understanding of tropical cyclone wind structure changes. Asia-Pacific Journal of Atmospheric Sciences, 44(1), 11–24.

Emanuel, K. A. (1986). An air sea interaction theory for tropical cyclones. 1. Steady-state maintenance. Journal of the Atmospheric Sciences, 43(6), 585–604. doi:10.1175/1520-0469(1986)043<0585:aasitf>2.0.co;2.

Emanuel, K., DesAutels, C., Holloway, C., and Korty, R. (2004). Environmental control of tropical cyclone intensity. Journal of the Atmospheric Sciences, 61(7), 843–858. doi:10.1175/1520-0469(2004)061<0843:ecotci>2.0.co;2.

ESRI. (2017). World Physical Map. Source: U.S. National Park Service. ArcGIS Online Data. Contributors: Esri, HERE, FAO, NOAA. http://www.arcgis.com/home/webmap/viewer.html?layers=c4ec722a1cd34cf0a23904aadf8923a0anduseExisting=1.

European Centre for Medium-Range Weather Forecasts. ECMWF. (2009). ERA-Interim Project. Research Data Archive at the National Center for Atmospheric Research, Computational and Information Systems Laboratory, Boulder, CO. [Available online at https://doi.org/10.5065/D6CR5RD9.] Accessed† 30 June 2017.

Fang, J. A., and Zhang, F. Q. (2011). Evolution of multiscale vortices in the development of Hurricane Dolly (2008). Journal of the Atmospheric Sciences, 68(1), 103–122. doi:10.1175/2010jas3522.1.

Farris, G.S., Smith, G.J., Crane, M.P., Demas, C.R., Robbins, L.L., and Lavoie, D.L., eds., (2007). Science and the storms—the USGS response to the hurricanes of 2005: U.S. Geological Survey Circular 1306, 283 p. Website: https://pubs.usgs.gov/circ/1306/.

Finocchio, P. M., and Majumdar, S. J. (2017). A statistical perspective on wind profiles and vertical wind shear in tropical cyclone environments of the Northern Hemisphere. Monthly Weather Review, 145(1), 361–378. doi:10.1175/mwr-d-16-0221.1.

Fischer, M. S., Tang, B. H., and Corbosiero, K. L. (2017). Assessing the influence of upper-tropospheric troughs on tropical cyclone intensification rates after genesis. Monthly Weather Review, 145(4), 1295–1313. doi:10.1175/mwr-d-16-0275.1.

Fitzpatrick, P. J., Knaff, J. A., Landsea, C. W., and Finley, S. V. (1995). Documentation of a systematic bias in the Aviation Model's forecast of the Atlantic tropical upper-tropospheric trough - Implications for tropical cyclone forecasting. Weather and Forecasting, 10(2), 433–446. doi:10.1175/1520-0434(1995)010<0433:doasbi>2.0.co;2.

Foltz, G. R., and McPhaden, M. J. (2006). Unusually warm sea surface temperatures in the tropical North Atlantic during 2005. Geophysical Research Letters, 33, L19703 doi:10.1029/2006gl027394.

Frank, W. M., and Ritchie, E. A. (2001). Effects of vertical wind shear on the intensity and structure of numerically simulated hurricanes. Monthly Weather Review, 129(9), 2249–2269. doi:10.1175/1520-0493(2001)129<2249:eovwso>2.0.co;2.

Fu, B., Peng, M. S., Li, T., and Stevens, D. E. (2012). Developing versus nondeveloping disturbances for tropical cyclone formation. Part II: western North Pacific. Monthly Weather Review, 140(4), 1067–1080. doi:10.1175/2011mwr3618.1.

Galarneau, T. J., McTaggart-Cowan, R., Bosart, L. F., and Davis, C. A. (2015). Development of North Atlantic tropical disturbances near upper-level potential vorticity streamers. Journal of the Atmospheric Sciences, 72(2), 572–597. doi:10.1175/jas-d-14-0106.1.

Ge, X., Li, T., Wang, Y., and Peng, M. S. (2008). Tropical cyclone energy dispersion in a three-dimensional primitive equation model: Upper-tropospheric influence. Journal of the Atmospheric Sciences, 65(7), 2272–2289. doi:10.1175/2007jas2431.1.

Ge, X., Li, T., and Peng, M. S. (2010). Cyclogenesis simulation of Typhoon Prapiroon (2000) associated with Rossby wave energy dispersion. Monthly Weather Review, 138(1), 42–54. doi:10.1175/2009mwr3005.1.

Gehne, M., and Kleeman, R. (2012). Spectral analysis of tropical atmospheric dynamical variables using a linear shallow-water modal decomposition. Journal of the Atmospheric Sciences, 69(7), 2300–2316. doi:10.1175/jas-d-10-05008.1.

Georgiadis, A. P., and Bigg, G. (2007). Environmental links to reduced tropical cyclogenesis over the south-east Caribbean. International Journal of Climatology, 27(8), 989–1001. doi:10.1002/joc.1451.

Goldenberg, S. B., Landsea, C. W., Mestas-Nunez, A. M., and Gray, W. M. (2001). The recent increase in Atlantic hurricane activity: Causes and implications. Science, 293(5529), 474–479. doi:10.1126/science.1060040.

Gollan, G., and Greatbatch, R. J. (2015). On the extratropical influence of variations of the upper-tropospheric equatorial zonal-mean zonal wind during boreal winter. Journal of Climate, 28(1), 168–185. doi:10.1175/jcli-d-14-00185.1.

Gopalakrishnan, S. G., Marks, F., Zhang, X. J., Bao, J. W., Yeh, K. S., and Atlas, R. (2011). The experimental HWRF System: A study on the influence of horizontal resolution on the structure and intensity changes in tropical cyclones using an idealized framework. Monthly Weather Review, 139(6), 1762–1784. doi:10.1175/2010mwr3535.1.

Grams, C. M., Wernli, H., Bottcher, M., Campa, J., Corsmeier, U., Jones, S., Keller, J., Lenz, C., Wiegand, L. (2011). The key role of diabatic processes in modifying the upper-tropospheric wave guide: a North Atlantic case-study. Quarterly Journal of the Royal Meteorological Society, 137(661), 2174–2193. doi:10.1002/qj.891.

Gray, W. M. (1968). Global view of origin of tropical disturbances and storms. Monthly Weather Review, 96(10), 669-700. doi:10.1175/1520–0493(1968)096<0669:gvotoo>2.0.co;2.

Gray, W. M. (1998). The formation of tropical cyclones. Meteorology and Atmospheric Physics, 67(1–4), 37–69. doi:10.1007/bf01277501.

Hanley, D., Molinari, J., and Keyser, D. (2001). A composite study of the interactions between tropical cyclones and upper-tropospheric troughs. Monthly Weather Review, 129(10), 2570-2584. doi:10.1175/1520-0493(2001)129<2570:acsoti>2.0.co;2.

Harada, Y., Kamahori, H., Kobayashi, C., Endo, H., Kobayashi, S., Ota, Y., Onoda, H., Onogi, K., Miyaoka, K., Takahashi, K. (2016). The JRA-55 Reanalysis: Representation of Atmospheric Circulation and Climate Variability. Journal of the Meteorological Society of Japan, 94(3), 269-302. doi:10.2151/jmsj.2016-015.

Hendricks, E. A., Peng, M. S., Fu, B., and Li, T. (2010). Quantifying environmental control on tropical cyclone intensity change. Monthly Weather Review, 138(8), 3243–3271. doi:10.1175/2010mwr3185.1.

Hennon, C. C., and Hobgood, J. S. (2003). Forecasting tropical cyclogenesis over the Atlantic basin using large-scale data. Monthly Weather Review, 131(12), 2927–2940. doi:10.1175/1520-0493(2003)131<2927:ftcota>2.0.co;2.

Heymsfield, G. M., Halverson, J., Ritchie, E., Simpson, J., Molinari, J., and Tian, L. (2006). Structure of highly sheared Tropical Storm Chantal during CAMEX-4. Journal of the Atmospheric Sciences, 63(1), 268–287. doi:10.1175/jas3602.1.

Holton, J. R., and Colton, D. E. (1972). Diagnostic study of vorticity balance at 200 mb in tropics during northern summer. Journal of the Atmospheric Sciences, 29(6), 1124–1128. doi:10.1175/1520–0469(1972)029<1124:adsotv>2.0.co;2.

Houze, R. A. (1997). Stratiform precipitation in regions of convection: A meteorological paradox? Bulletin of the American Meteorological Society, 78(10), 2179–2196. doi:10.1175/1520-0477(1997)078<2179:spiroc>2.0.co;2.

Houze, R. A., Jr., Lee, W.-C., and Bell, M. M. (2009). Convective contribution to the genesis of Hurricane Ophelia (2005). Monthly Weather Review, 137(9), 2778–2800. doi:10.1175/2009mwr2727.1.

Hulme, A. L., and Martin, J. E. (2009). Synoptic- and frontal-scale influences on tropical transition events in the Atlantic basin. Part II: Tropical transition of Hurricane Karen. Monthly Weather Review, 137(11), 3626–3650. doi:10.1175/2009mwr2803.1.

Hunt, B. G., and Watterson, I. G. (2010). The temporal and spatial characteristics of surrogate tropical cyclones from a multi-millenial simulation. Climate Dynamics, 34(5), 699–718. doi:10.1007/s00382-009-0627-3.

Hurricane Research Division (HRD 2011). Frequently Asked Questions. What is a tropical disturbance, a tropical depression, or a tropical storm? Atlantic Oceanographic and Meteorological Laboratory. Contributed by Chris Landsea (NHC).

Japan Meteorological Agency/Japan (2013), JRA-55: Japanese 55-year Reanalysis, Daily 3-hourly and 6-hourly data, https://doi.org/10.5065/D6HH6H41, Research Data Archive at the National Center for Atmospheric Research, Computational and Information Systems Laboratory, Boulder, CO (updated monthly), Accessed Oct 2014.

Jeevarekha, A., and Philominathan, P. (2016). A nonlinear approach to analyse the development of tropical disturbances. Pramana-Journal of Physics, 86(5), 1031–1042. doi:10.1007/s12043-015-1131-4.

Jeong, D., Min, K. H., Lee, G., and Kim, K. E. (2014). A case study of mesoscale convective band (MCB) development and evolution along a quasi-stationary front. Advances in Atmospheric Sciences, 31(4), 901–915. doi:10.1007/s00376-013-3089-9.

Jones, S. C., Harr, P. A., Abraham, J., Bosart, L. F., Bowyer, P. J., Evans, J. L., Hanley, D.E., Hanstrum, B. N., Hart, R.E., Lalaurette, F., Sinclair, M. R., Smith, R. K., and Thorncroft, C. (2003). The extratropical transition of tropical cyclones: Forecast challenges, current understanding, and future directions. Weather and Forecasting, 18(6), 1052–1092. doi:10.1175/1520-0434(2003)018<1052:tetotc>2.0.co;2.

Jordan, E. S. (1952). An observational study of the upper wind-circulation around tropical storms. Journal of Meteorology, 9(5), 340–346. doi:10.1175/1520-0469(1952)009<0340:aosotu>2.0.co;2.

Kalnay, E., Kanamitsu, M., Kistler, R., Collins, W., Deaven, D., Gandin, L., . . . and Joseph, D. (1996). The NCEP/NCAR 40-year reanalysis project. Bulletin of the American Meteorological Society, 77(3), 437–471. doi:10.1175/1520-0477(1996)077<0437:tnyrp>2.0.co;2. NCEP Reanalysis data provided by the NOAA/OAR/ESRL PSD, Boulder, CO, USA, from http://www.esrl.noaa.gov/psd/.

Kaplan, J., DeMaria, M., and Knaff, J. A. (2010). A revised tropical cyclone rapid intensification index for the Atlantic and Eastern North Pacific basins. Weather and Forecasting, 25(1), 220–241. doi:10.1175/2009waf2222280.1.

Karyampudi, V. M., and Pierce, H. F. (2002). Synoptic-scale influence of the Saharan air layer on tropical cyclogenesis over the eastern Atlantic. Monthly Weather Review, 130(12), 3100–3128. doi:10.1175/1520-0493(2002)130<3100:ssiots>2.0.co;2.

Kasahara, A., Mizzi, A. P., and Donner, L. J. (1994). Diabatic initialization for improvement in the tropical analysis of divergence and moisture using satellite radiometric imagery data. Tellus Series A-Dynamic Meteorology and Oceanography, 46(3), 242–264. doi:10.1034/j.1600-0870.1994.t01-2-00002.x.

Kerns, B., Greene, K., and Zipser, E. (2008). Four years of Tropical ERA-40 vorticity maxima tracks. Part I: Climatology and vertical vorticity structure. Monthly Weather Review, 136(11), 4301–4319. doi:10.1175/2008mwr2390.1.

Kerns, B. W., and Chen, S. S. (2013). Cloud clusters and tropical cyclogenesis: Developing and nondeveloping systems and their large-scale environment. Monthly Weather Review, 141(1), 192–210. doi:10.1175/mwr-d-11-00239.1.

Kerns, B. W., and Chen, S. S. (2015). Subsidence warming as an underappreciated ingredient in tropical cyclogenesis. Part I: Aircraft observations. Journal of the Atmospheric Sciences, 72(11), 4237–4260. doi:10.1175/jas-d-14-0366.1.

Kidder, S. Q., Goldberg, M. D., Zehr, R. M., DeMaria, M., Purdom, J. F. W., Velden, C. S., Grody, N. C., and Kusselson, S. J. (2000). Satellite analysis of tropical cyclones using the Advanced Microwave Sounding Unit (AMSU). Bulletin of the American Meteorological Society, 81(6), 1241–1259. doi:10.1175/1520-0477(2000)081<1241:saotcu>2.3.co;2.

Kim, S. H., Chun, H. Y., and Jang, W. (2014). Horizontal divergence of typhoon-generated gravity waves in the upper troposphere and lower stratosphere (UTLS) and its influence on typhoon evolution. Atmospheric Chemistry and Physics, 14(7), 3175–3182. doi:10.5194/acp-14-3175-2014.

Kimball, S. K., and Dougherty, F. C. (2006). The sensitivity of idealized hurricane structure and development to the distribution of vertical levels in MM5. Monthly Weather Review, 134(7), 1987–2008. doi:10.1175/mwr3171.1.

Kitabatake, N. (2002). Extratropical transformation of Typhoon Vicki (9807): Structural change and the role of upper-tropospheric disturbances. Journal of the Meteorological Society of Japan, 80(2), 229–247. doi:10.2151/jmsj.80.229.

Klotzbach, P. J. (2011). Forecasting October-November Caribbean hurricane days. Journal of Geophysical Research-Atmospheres, 116, 9. doi:10.1029/2011jd016146.

Klotzbach, P. J., and Gray, W. M. (2006). Causes of the unusually destructive 2004 Atlantic basin hurricane season. Bulletin of the American Meteorological Society, 87(10), 1325-1333. doi:10.1175/bams-87-10-1325.

Klotzbach, P. J., and Gray, W. M. (2009). Twenty-five years of Atlantic basin seasonal hurricane forecasts (1984–2008). Geophysical Research Letters, 36, L09711. doi:10.1029/2009gl037580.

Knaff, J. A., Kossin, J. P., and DeMaria, M. (2003). Annular hurricanes. Weather and Forecasting, 18(2), 204–223. doi:10.1175/1520-0434(2003)018<0204:ah>2.0.co;2.

Knaff, J. A., Seseske, S. A., DeMaria, M., and Demuth, J. L. (2004). On the influences of vertical wind shear on symmetric tropical cyclone structure derived from AMSU. Monthly Weather Review, 132(10), 2503–2510. doi:10.1175/1520-0493(2004)132<2503:otiovw>2.0.co;2.

Knapp, K. R., Kruk, M. C., Levinson, D. H., Diamond, H. J., and Neumann, C. J. (2010). The international best track archive for climate stewardship (IBTrACS) unifying tropical cyclone data. Bulletin of the American Meteorological Society, 91(3), 363–376.

Kobayashi, S., National Center for Atmospheric Research Staff (Eds) (2017). Last modified 18 August 2016. The Climate Data Guide: JRA-55. Retrieved from https://climatedataguide.ucar.edu/climate-data/jra-55.

Kodama, K. R., and Businger, S. (1998). Weather and forecasting challenges in the Pacific Region of the National Weather Service. Weather and Forecasting, 13(3), 523–546. doi:10.1175/1520-0434(1998)013<0523:wafcit>2.0.co;2.

Komaromi, W. A., and Majumdar, S. J. (2014). Ensemble-based error and predictability metrics associated with tropical cyclogenesis. Part I: Basinwide perspective. Monthly Weather Review, 142(8), 2879–2898. doi:10.1175/mwr-d-13-00370.1.

Komaromi, W. A., and Majumdar, S. J. (2015). Ensemble-based error and predictability metrics associated with tropical cyclogenesis. Part II: Wave-relative framework. Monthly Weather Review, 143(5), 1665–1686. doi:10.1175/mwr-d-14-00286.1.

Komaromi, W. A., and Doyle, J. D. (2017). Tropical cyclone outflow and warm core structure as revealed by HS3 dropsonde data. Monthly Weather Review, 145(4), 1339–1359. doi:10.1175/mwr-d-16-0172.1.

Korty, R. L., Camargo, S. J., and Galewsky, J. (2012). Variations in tropical cyclone genesis factors in simulations of the Holocene Epoch. Journal of Climate, 25(23), 8196–8211. doi:10.1175/jcli-d-12-00033.1.

Kotal, S. D., and Bhowmik, S. K. R. (2013). Large-scale characteristics of rapidly intensifying tropical cyclones over the Bay of Bengal and a Rapid Intensification (RI) index. Mausam, 64(1), 13–24.

Krishnamurti, T. N. (1971a). Observational study of the tropical upper tropospheric motion field during the Northern Hemisphere summer. Journal of Applied Meteorology, 10(6), 1066–1096.

Krishnamurti, T. N. (1971b). Tropical east-west circulations during northern summer. Journal of the Atmospheric Sciences, 28(8), 1342-1347. doi:10.1175/1520-0469(1971)028<1342:tewcdt>2.0.co;2.

Kubokawa, H., Fujiwara, M., Nasuno, T., Miura, M., Yamamoto, M. K., and Satoh, M. (2012). Analysis of the tropical tropopause layer using the Nonhydrostatic Icosahedral Atmospheric Model (NICAM): 2. An experiment under the atmospheric conditions of December 2006 to January 2007. Journal of Geophysical Research-Atmospheres, 117. doi:10.1029/2012jd017737.

Laing, A., and Evans, J. L. (2011). Introduction to Tropical Meteorology 2nd edition. A Comprehensive Online and Print Textbook, Version 2.0, October 2011. University Corporation for Atmospheric Research, Boulder, CO.

Landsea, C. W., Bell, G. D., Gray, W. M., and Goldenberg, S. B. (1998). The extremely active 1995 Atlantic hurricane season: Environmental conditions and verification of seasonal forecasts. Monthly Weather Review, 126(5), 1174-1193. doi:10.1175/1520-0493(1998)126<1174:teaahs>2.0.co;2.

Landsea, C. W., Pielke, R. A., Mestas-Nunez, A., and Knaff, J. A. (1999). Atlantic basin hurricanes: Indices of climatic changes. Climatic Change, 42(1), 89–129. doi:10.1023/a:1005416332322.

Landsea, C. W., Vecchi, G. A., Bengtsson, L., and Knutson, T. R. (2010). Impact of Duration Thresholds on Atlantic Tropical Cyclone Counts. Journal of Climate, 23(10), 2508-2519. doi:10.1175/2009jcli3034.1.

Lee, C.-Y., Tippett, M. K., Camargo, S. J., and Sobel, A. H. (2015). Probabilistic multiple linear regression modeling for tropical cyclone intensity. Monthly Weather Review, 143(3), 933–954. doi:10.1175/mwr-d-14-00171.1.

Leppert, K. D., Cecil, D. J., and Petersen, W. A. (2013). Relation between tropical easterly waves, convection, and tropical cyclogenesis: A Lagrangian perspective. Monthly Weather Review, 141(8), 2649–2668. doi:10.1175/mwr-d-12-00217.1.

Leppert, K. D., II, and Petersen, W. A. (2010). Electrically active hot towers in African easterly waves prior to tropical cyclogenesis. Monthly Weather Review, 138(3), 663–687. doi:10.1175/2009mwr3048.1.

Leroux, M. D., Plu, M., Barbary, D., Roux, F., and Arbogast, P. (2013). Dynamical and physical processes leading to tropical cyclone intensification under upper-level trough forcing. Journal of the Atmospheric Sciences, 70(8), 2547–2565. doi:10.1175/jas-d-12-0293.1.

Leroux, M.-D., Plu, M., and Roux, F. (2016). On the sensitivity of tropical cyclone intensification under upper-level trough forcing. Monthly Weather Review, 144(3), 1179–1202. doi:10.1175/mwr-d-15-0224.1.

Li, Y., Cheung, K. K. W., and Chan, J. C. L. (2014). Numerical study on the development of asymmetric convection and vertical wind shear during tropical cyclone landfall. Quarterly Journal of the Royal Meteorological Society, 140(683), 1866–1877. doi:10.1002/qj.2259.

Liu, C.C., Shyu, T.Y., Chao, C.C., and Lin, Y.F. (2009). Analysis on Typhoon Longwang intensity changes over the ocean via satellite data. Journal of Marine Science and Technology–Taiwan, 17(1), 23–28.

Liu, Y. B., Zhang, D. L., and Yau, M. K. (1997). Multiscale numerical study of Hurricane Andrew (1992). 1. Explicit simulation and verification. Monthly Weather Review, 125(12), 3073–3093. doi:10.1175/1520-0493(1997)125<3073:amnsoh>2.0.co;2.

Liu, Y. B., Zhang, D. L., and Yau, M. K. (1999). A multiscale numerical study of Hurricane Andrew (1992). Part II: Kinematics and inner-core structures. Monthly Weather Review, 127(11), 2597–2616. doi:10.1175/1520-0493(1999)127<2597:amnsoh>2.0.co;2.

Lowag, A., Black, M. L., and Eastin, M. D. (2008). Structural and intensity changes of Hurricane Bret (1999). Part I: Environmental influences. Monthly Weather Review, 136(11), 4320–4333. doi:10.1175/2008mwr2438.1.

Mallard, M. S., Lackmann, G. M., Aiyyer, A., and Hill, K. (2013a). Atlantic hurricanes and climate change. Part I: Experimental design and isolation of thermodynamic effects. Journal of Climate, 26(13), 4876–4893. doi:10.1175/jcli-d-12-00182.1.

Mallard, M. S., Lackmann, G. M., and Aiyyer, A. (2013b). Atlantic hurricanes and climate change. Part II: Role of thermodynamic changes in decreased hurricane frequency. Journal of Climate, 26(21), 8513–8528. doi:10.1175/jcli-d-12-00183.1.

Marks, F. D., and Houze, R. A. (1987). Inner core structure of Hurricane Alicia from airborne Doppler radar observations. Journal of the Atmospheric Sciences, 44(9), 1296–1317. doi:10.1175/1520-0469(1987)044<1296:icsoha>2.0.co;2.

Mauk, R. G., and Hobgood, J. S. (2012). Tropical cyclone formation in environments with cool SST and high wind shear over the northeastern Atlantic Ocean. Weather and Forecasting, 27(6), 1433–1448. doi:10.1175/waf-d-11-00048.1.

McBride, J. L., and Gray, W. M. (1980). Mass divergence in tropical weather systems. 1. Diurnal-variation. Quarterly Journal of the Royal Meteorological Society, 106(449), 501–516. doi:10.1002/qj.49710644908.

McBride, J. L., and Zehr, R. (1981). Observational analysis of tropical cyclone formation. 2. Comparison of non-developing versus developing systems. Journal of the Atmospheric Sciences, 38(6), 1132–1151. doi:10.1175/1520-0469(1981)038<1132:oaotcf>2.0.co;2.

McFarquhar, G. M., Jewett, B. F., Gilmore, M. S., Nesbitt, S. W., and Hsieh, T. L. (2012). Vertical velocity and microphysical distributions related to rapid intensification in a simulation of Hurricane Dennis (2005). Journal of the Atmospheric Sciences, 69(12), 3515-3534. doi:10.1175/jas-d-12-016.1.

McGauley, M. G., and Nolan, D. S. (2011). Measuring environmental favorability for tropical cyclogenesis by statistical analysis of threshold parameters. Journal of Climate, 24(23), 5968-5997. doi:10.1175/2011jcli4176.1.

McTaggart-Cowan, R., Bosart, L. F., Gyakum, J. R., and Atallah, E. H. (2007a). Hurricane Katrina (2005). Part I: Complex life cycle of an intense tropical cyclone. Monthly Weather Review, 135(12), 3905–3926. doi:10.1175/2007mwr1875.1.

McTaggart-Cowan, R., Bosart, L. F., Gyakum, J. R., and Atallah, E. H. (2007b). Hurricane Katrina (2005). Part II: Evolution and hemispheric impacts of a diabatically generated warm pool. Monthly Weather Review, 135(12), 3927–3949. doi:10.1175/2007mwr2096.1.

McTaggart-Cowan, R., Deane, G. D., Bosart, L. F., Davis, C. A., and Galarneau, T. J. (2008). Climatology of tropical cyclogenesis in the North Atlantic (1948–2004). Monthly Weather Review, 136(4), 1284-1304. doi:10.1175/2007mwr2245.1.

McTaggart-Cowan, R., Galarneau, T. J., Jr., Bosart, L. F., Moore, R. W., and Martius, O. (2013). A global climatology of baroclinically influenced tropical cyclogenesis. Monthly Weather Review, 141(6), 1963–1989. doi:10.1175/mwr-d-12-00186.1.

Mecikalski, J. R., and Tripoli, G. J. (2003). Influence of upper-tropospheric inertial stability on the convective transport of momentum. Quarterly Journal of the Royal Meteorological Society, 129(590), 1537–1563. doi:10.1256/qj.00.08.

Merrill, R. T., and Velden, C. S. (1996). A three-dimensional analysis of the outflow layer of supertyphoon Flo (1990). Monthly Weather Review, 124(1), 47–63. doi:10.1175/1520-0493(1996)124<0047:atdaot>2.0.co;2.

Misra, V., DiNapoli, S., and Powell, M. (2013). The track integrated kinetic energy of Atlantic tropical cyclones. Monthly Weather Review, 141(7), 2383–2389. doi:10.1175/mwr-d-12-00349.1.

Molinari, J., Lombardo, K., and Vollaro, D. (2007). Tropical cyclogenesis within an equatorial Rossby wave packet. Journal of the Atmospheric Sciences, 64(4), 1301–1317. doi:10.1175/jas3902.1.

Molinari, J., and Vollaro, D. (1989). External influences on hurricane intensity. 1. Outflow layer eddy angular-momentum fluxes. Journal of the Atmospheric Sciences, 46(8), 1093–1105. doi:10.1175/1520-0469(1989)046<1093:eiohip>2.0.co;2.

Molinari, J., Vollaro, D., and Robasky, F. (1992). Use of ECMWF operational analyses for studies of the tropical cyclone environment. Meteorology and Atmospheric Physics, 47(2–4), 127–144. doi:10.1007/bf01025613.

Möller, J. D., and Shapiro, L. J. (2002). Balanced contributions to the intensification of hurricane Opal as diagnosed from a GFDL model forecast. Monthly Weather Review, 130(7), 1866–1881. doi:10.1175/1520-0493(2002)130<1866:bcttio>2.0.co;2.

Moon, I. J., Kim, S. H., Klotzbach, P., and Chan, J. C. L. (2015). Roles of interbasin frequency changes in the poleward shifts of the maximum intensity location of tropical cyclones. Environmental Research Letters, 10(10), 9. doi:10.1088/1748-9326/10/10/104004.

Munsell, E. B., Sippel, J. A., Braun, S. A., Weng, Y., and Zhang, F. (2015). Dynamics and predictability of Hurricane Nadine (2012) evaluated through convection-permitting ensemble analysis and forecasts. Monthly Weather Review, 143(11), 4514–4532. doi:10.1175/mwr-d-14-00358.1.

Murakami, H. (2014). Tropical cyclones in reanalysis data sets. Geophysical Research Letters, 41(6), 2133-2141. doi:10.1002/2014gl059519.

NASA image courtesy Jeff Schmaltz, MODIS Rapid Response Team, Goddard Space Flight Center. Instrument(s): Terra – MODIS. Web: Nov. 1, 2017.

National Hurricane Center (NHC 2015). Tropical Cyclone Climatology and Tropical Cyclone Reports 2005 Atlantic Hurricane Season. National Oceanic and Atmospheric Administration (NOAA). Web 2014–2017. http://www.nhc.noaa.gov/climo/ and http://www.nhc.noaa.gov/data/tcr/index.php?season=2005andbasin=atl.

Neumann, B., Vafeidis, A. T., Zimmermann, J., and Nicholls, R. J. (2015). Future coastal population growth and exposure to sea-level rise and coastal flooding - A global assessment (vol 10, e0118571, 2015). PLoS One, 10(6), 1. doi:10.1371/journal.pone.0131375.

Nolan, D. S. (2007). What is the trigger for tropical cyclogenesis? Australian Meteorological Magazine, 56(4), 241–266.

Ooyama, K. V. (1982). Conceptual evolution of the theory and modeling of the tropical cyclone. Journal of the Meteorological Society of Japan, 60(1), 369–380.

Owens, B. F., and Landsea, C. W. (2003). Assessing the skill of operational Atlantic seasonal tropical cyclone forecasts. Weather and Forecasting, 18(1), 45–54. doi:10.1175/1520-0434(2003)018<0045:atsooa>2.0.co;2.

Ozawa, H., and Shimokawa, S. (2015). Thermodynamics of a tropical cyclone: Generation and dissipation of mechanical energy in a self-driven convection system. Tellus Series A ―Dynamic Meteorology and Oceanography, 67. doi:10.3402/tellusa.v67.24216.

Paterson, L. A., Hanstrum, B. N., Davidson, N. E., and Weber, H. C. (2005). Influence of environmental vertical wind shear on the intensity of hurricane-strength tropical cyclones in the Australian region. Monthly Weather Review, 133(12), 3644-3660. doi:10.1175/mwr3041.1.

Peevey, T. R., Gille, J. C., Homeyer, C. R., and Manney, G. L. (2014). The double tropopause and its dynamical relationship to the tropopause inversion layer in storm track regions. Journal of Geophysical Research-Atmospheres, 119(17). doi:10.1002/2014jd021808.

Peng, M. S., Fu, B., Li, T., and Stevens, D. E. (2012). Developing versus nondeveloping disturbances for tropical cyclone formation. Part I: North Atlantic. Monthly Weather Review, 140(4), 1047–1066. doi:10.1175/2011mwr3617.1.

Persing, J., Montgomery, M. T., and Tuleya, R. E. (2002). Environmental interactions in the GFDL hurricane model for Hurricane Opal. Monthly Weather Review, 130(2), 298-317. doi:10.1175/1520-0493(2002)130<0298:eiitgh>2.0.co;2.

Pino, J. V. (2015). Impacts of the Three-Dimensional Oceanic Thermal Structure and Translation Speed on Tropical Cyclogenesis and Intensity Fluctuations during the 2005 North Atlantic Hurricane Season. LSU Master's Theses. 1644. https://digitalcommons.lsu.edu/gradschool_theses/1644.

Prasad, M. H. (2016). Weather and climatic conditions over tropical regions. Imperial Journal of Interdisciplinary Research, 2(12), 206–212.

Qian, Y.-K., Liang, C.-X., Liang, Q., Lin, L., and Yuan, Z. (2011). On the forced tangentially-averaged radial-vertical circulation within vortices. Part II: The transformation of Tropical Storm Haima (2004). Advances in Atmospheric Sciences, 28(5), 1143-1158. doi:10.1007/s00376-010-0060-x.

Qian, Y. K., Liang, C. X., Peng, S. Q., Chen, S. M., and Wang, S. H. (2016a). A Horizontal Index for the Influence of Upper-Level Environmental Flow on Tropical Cyclone Intensity. Weather and Forecasting, 31(1), 237-253. doi:10.1175/waf-d-15-0091.1.

Qian, Y. K., Liang, C. X., Yuan, Z. J., Peng, S. Q., Wu, J. J., and Wang, S. H. (2016b). Upper-tropospheric environment-tropical cyclone interactions over the western North Pacific: A statistical study. Advances in Atmospheric Sciences, 33(5), 614-631. doi:10.1007/s00376-015-5148-x.

R project for Statistical Computing and IDE R Studio. (2014). https://www.r-project.org/ https://www.rstudio.com/products/rstudio/. Complete programming code for all research analysis written by Sara A. Ates. 2014–2017.

Rai, D., Pattnaik, S., and Rajesh, P. V. D. (2016). Sensitivity of tropical cyclone characteristics to the radial distribution of sea surface temperature. Journal of Earth System Science, 125(4), 691–708. doi:10.1007/s12040-016-0687-9.

Randel, W. J., Wu, F., and Forster, P. (2007a). The extratropical tropopause inversion layer: Global observations with GPS data, and a radiative forcing mechanism. Journal of the Atmospheric Sciences, 64(12), 4489–4496. doi:10.1175/2007jas2412.1.

Randel, W. J., Seidel, D. J., and Pan, L. L. (2007b). Observational characteristics of double tropopauses. Journal of Geophysical Research-Atmospheres, 112(D7), 13. doi:10.1029/2006jd007904.

Rappin, E. D., Morgan, M. C., and Tripoli, G. J. (2011). The impact of outflow environment on tropical cyclone intensification and structure. Journal of the Atmospheric Sciences, 68(2), 177–194. doi:10.1175/2009jas2970.1.

Raynak, C. S. (2009). Statistical-dynamical forecasting of tropical cyclogenesis in the north Atlantic at intraseasonal lead times. A Thesis. Naval Postgraduate School, Monterey, CA. June 2009.

Reader, M. C., and Moore, G. W. K. (1995). Stratosphere-troposphere interactions associated with a case of explosive cyclogenesis in the Labrador-Sea. Tellus Series a-Dynamic Meteorology and Oceanography, 47(5), 849-863. doi:10.1034/j.1600-0870.1995.00124.x.

Reed, R. J., and Recker, E. E. (1971). Structure and properties of synoptic-scale wave disturbances in equatorial Western Pacific. Journal of the Atmospheric Sciences, 28(7), 1117-1133. doi:10.1175/1520-0469(1971)028<1117:saposs>2.0.co;2.

Ren, D. D., Lynch, M., Leslie, L. M., and Lemarshall, J. (2014). Sensitivity of tropical cyclone tracks and intensity to ocean surface temperature: Four cases in four different basins. Tellus Series A — Dynamic Meteorology and Oceanography, 66(1), 24212. doi:10.3402/tellusa.v66.2421.

Reynolds, C. A., Langland, R., Pauley, P. M., and Velden, C. (2013). Tropical cyclone data impact studies: Influence of model bias and synthetic observations. Monthly Weather Review, 141(12), 4373–4394. doi:10.1175/mwr-d-12-00300.1.

Riehl, H. (1948). On the formation of typhoons. Journal of Meteorology, 5(6), 247-264. doi:10.1175/1520-0469(1948)005<0247:otfot>2.0.co;2.

Riemer, M., and Jones, S. C. (2010). The downstream impact of tropical cyclones on a developing baroclinic wave in idealized scenarios of extratropical transition. Quarterly Journal of the Royal Meteorological Society, 136(648), 617–637. doi:10.1002/qj.605.

Riemer, M., Montgomery, M. T., and Nicholls, M. E. (2010). A new paradigm for intensity modification of tropical cyclones: thermodynamic impact of vertical wind shear on the inflow layer. Atmospheric Chemistry and Physics, 10(7), 3163-3188.

Riemer, M., and Laliberté, F. (2015). Secondary circulation of tropical cyclones in vertical wind shear: Lagrangian diagnostic and pathways of environmental interaction. Journal of the Atmospheric Sciences, 72(9), 3517–3536. doi:10.1175/jas-d-14-0350.1.

Rios-Berrios, R., Torn, R. D., and Davis, C. A. (2016a). An ensemble approach to investigate tropical cyclone intensification in sheared environments. Part I: Katia (2011). Journal of the Atmospheric Sciences, 73(1), 71–93. doi:10.1175/jas-d-15-0052.1.

Rios-Berrios, R., Torn, R. D., and Davis, C. A. (2016b). An ensemble approach to investigate tropical cyclone intensification in sheared environments. Part II: Ophelia (2011). Journal of the Atmospheric Sciences, 73(4), 1555–1575. doi:10.1175/jas-d-15-0245.1.

Rodgers, E. B., Olson, W. S., Karyampudi, V. M., and Pierce, H. F. (1998). Satellite-derived latent heating distribution and environmental influences in Hurricane Opal (1995). Monthly Weather Review, 126(5), 1229-1247. doi:10.1175/1520-0493(1998)126<1229:sdlhda>2.0.co;2.

Ruiz-Barradas, A., Carton, J. A., and Nigam, S. (2000). Structure of interannual-to-decadal climate variability in the tropical Atlantic sector. Journal of Climate, 13(18), 3285–3297. doi:10.1175/1520-0442(2000)013<3285:soitdc>2.0.co;2.

Sadler, J. C. (1976). Role of tropical upper tropospheric trough in early season typhoon development. Monthly Weather Review, 104(10), 1266-1278. doi:10.1175/1520-0493(1976)104<1266:arottu>2.0.co;2.

Sall, S. M., Sauvageot, H., Gaye, A. T., Viltard, A., and de Felice, P. (2006). A cyclogenesis index for tropical Atlantic off the African coasts. Atmospheric Research, 79(2), 123–147. doi:10.1016/j.atmosres.2005.05.004.

Sanabia, E. R., Barrett, B. S., and Fine, C. M. (2014). Relationships between tropical cyclone intensity and eyewall structure as determined by radial profiles of inner-core infrared brightness temperature. Monthly Weather Review, 142(12), 4581–4599. doi:10.1175/mwr-d-13-00336.1.

Sandhya, M., Sridharan, S., Devi, M. I., and Gadhavi, H. (2015). Tropical upper tropospheric ozone enhancements due to potential vorticity intrusions over Indian sector. Journal of Atmospheric and Solar-Terrestrial Physics, 132, 147-152. doi:10.1016/j.jastp.2015.07.014.

Schecter, D. A. (2011). Evaluation of a reduced model for investigating hurricane formation from turbulence. Quarterly Journal of the Royal Meteorological Society, 137(654), 155–178. doi:10.1002/qj.729.

Schiemann, R., Luthi, D., and Schar, C. (2009). Seasonality and Interannual Variability of the Westerly Jet in the Tibetan Plateau Region. Journal of Climate, 22(11), 2940-2957. doi:10.1175/2008jcli2625.1.

Schott, T., Landsea, C., Hafele, G., Lorens, J., Taylor, A., Thurm, H., Ward, B., Willis, M., and Zaleski, W., (2012). The Saffir-Simpson Team. National Hurricane Center. http://www.nhc.noaa.gov/pdf/sshws.pdf.

Schumacher, A. B., DeMaria, M., and Knaff, J. A. (2009). Objective estimation of the 24-h probability of tropical cyclone formation. Weather and Forecasting, 24(2), 456–471. doi:10.1175/2008waf2007109.1.

Scowcroft, G., Ginis, I., Knowlton, C., Yablonsky, R., and Morin, H. (2011). Hurricanes: Science and Society. University of Rhode Island (URI) Graduate School of Oceanography (GSO), http://www.hurricanescience.org.

Shapiro, L. J., and Moller, J. D. (2003). Influence of atmospheric asymmetries on the intensification of hurricane opal: Piecewise PV inversion diagnosis of a GFDL model forecast. Monthly Weather Review, 131(8), 1637–1649. doi:10.1175//2552.1.

Shi, J. J., Chang, S., and Raman, S. (1997). Interaction between Hurricane Florence (1988) and an upper-tropospheric westerly trough. Journal of the Atmospheric Sciences, 54(9), 1231–1247. doi:10.1175/1520-0469(1997)054<1231:ibhfaa>2.0.co;2.

Shu, S. J., Zhang, F. Q., Ming, J., and Wang, Y. (2014). Environmental influences on the intensity changes of tropical cyclones over the western North Pacific. Atmospheric Chemistry and Physics, 14(12), 6329-6342. doi:10.5194/acp-14-6329-2014.

Simpson, J., Ritchie, E., Holland, G. J., Halverson, J., and Stewart, S. (1997). Mesoscale interactions in tropical cyclone genesis. Monthly Weather Review, 125(10), 2643-2661. doi:10.1175/1520-0493(1997)125<2643:miitcg>2.0.co;2.

Sippel, J. A., Braun, S. A., and Shie, C. L. (2011). Environmental influences on the strength of Tropical Storm Debby (2006). Journal of the Atmospheric Sciences, 68(11), 2557-2581. doi:10.1175/2011jas3648.1.

Song, P., Zhu, J., Zhong, Z., Qi, L., and Wang, X. (2016). Impact of atmospheric and oceanic conditions on the frequency and genesis location of tropical cyclones over the western North Pacific in 2004 and 2010. Advances in Atmospheric Sciences, 33(5), 599–613. doi:10.1007/s00376-015-5046-2.

Srinivas, C. V., Venkatesan, R., Rao, D. V. B., and Prasad, D. H. (2007). Numerical simulation of Andhra severe cyclone (2003): Model sensitivity to the boundary layer and convection parameterization. Pure and Applied Geophysics, 164(8–9), 1465–1487. doi:10.1007/s00024-007-0228-1.

Srivastava, K., and Bhardwaj, R. (2014). Assimilation of Doppler weather radar data in WRF model for simulation of Tropical Cyclone Aila. Pure and Applied Geophysics, 171(8), 2043–2072. doi:10.1007/s00024-013-0723-5.

Strong, C., and Davis, R. E. (2006). Variability in the altitude of fast upper tropospheric winds over the Northern Hemisphere during winter. Journal of Geophysical Research-Atmospheres, 111(D10), 15. doi:10.1029/2005jd006497.

Sugi, M., Noda, A., and Sato, N. (2002). Influence of the global warming on tropical cyclone climatology: An experiment with the JMA global model. Journal of the Meteorological Society of Japan, 80(2), 249-272. doi:10.2151/jmsj.80.249.

Sun, D. L., Lau, K. M., and Kafatos, M. (2008). Contrasting the 2007 and 2005 hurricane seasons: Evidence of possible impacts of Saharan dry air and dust on tropical cyclone activity in the Atlantic basin. Geophysical Research Letters, 35(15), L15405. doi:10.1029/2008gl034529.

Tang, B., and Emanuel, K. (2010). Midlevel ventilation’s constraint on tropical cyclone intensity. Journal of the Atmospheric Sciences, 67(6), 1817–1830. doi:10.1175/2010jas3318.1.

Tang, B. H. (2017). Coupled dynamic-thermodynamic forcings during tropical cyclogenesis: Part I. Diagnostic framework. Journal of the Atmospheric Sciences, 74(7), 2269-2278. doi:10.1175/JAS-D17-0048.1.

Tao, D. D., and Zhang, F. Q. (2015). Effects of vertical wind shear on the predictability of tropical cyclones: Practical versus intrinsic limit. Journal of Advances in Modeling Earth Systems, 7(4), 1534-1553. doi:10.1002/2015ms000474.

Thompson, R. M., Payne, S. W., Recker, E. E., and Reed, R. J. (1979). Structure and properties of synoptic-scale wave disturbances in the Intertropical Convergence Zone of the Eastern Atlantic. Journal of the Atmospheric Sciences, 36(1), 53–72. doi:10.1175/1520-0469(1979)036<0053:saposs>2.0.co;2.

Tian, F. X., Zhou, T. J., and Zhang, L. X. (2013). Tropical cyclone genesis potential index over the western North Pacific simulated by LASG/IAP AGCM. Acta Meteorologica Sinica, 27(1), 50–62. doi:10.1007/s13351-013-0106-y.

Tippett, M. K., Camargo, S. J., and Sobel, A. H. (2011). A Poisson regression index for tropical cyclone genesis and the role of large-scale vorticity in genesis. Journal of Climate, 24(9), 2335–2357. doi:10.1175/2010jcli3811.1.

Torn, R. D., and Cook, D. (2013). The role of vortex and environment errors in genesis forecasts of Hurricanes Danielle and Karl (2010). Monthly Weather Review, 141(1), 232–251. doi:10.1175/mwr-d-12-00086.1.

U. S. Naval Research Laboratory Marine Meteorology Division (2012). NRL Researchers Use Unmanned Aircraft to Probe Hurricane Outflow Jets. Web article. https://www.nrl.navy.mil/media/news-releases/2012/nrl-researchers-use-unmanned-aircraft-to-probe-hurricane-outflow-jets.

Ventrice, M. J., Thorncroft, C. D., and Janiga, M. A. (2012). Atlantic tropical cyclogenesis: A three-way interaction between an African easterly wave, diurnally varying convection, and a convectively coupled atmospheric Kelvin wave. Monthly Weather Review, 140(4), 1108–1124. doi:10.1175/mwr-d-11-00122.1.

Vizy, E. K., and Cook, K. H. (2009). Tropical storm development from African easterly waves in the eastern Atlantic: A comparison of two successive waves using a regional model as part of NASA AMMA 2006. Journal of the Atmospheric Sciences, 66(11), 3313–3334. doi:10.1175/2009jas3064.1.

Waco, D. E. (1970). Temperatures and turbulence at tropopause levels over Hurricane-Beulah (1967). Monthly Weather Review, 98(10), 749-755. doi:10.1175/1520-0493(1970)098<0749:tatatl>2.3.co;2.

Wang, C. C., and Rogers, J. C. (2001). A composite study of explosive cyclogenesis in different sectors of the North Atlantic. Part I: Cyclone structure and evolution. Monthly Weather Review, 129(6), 1481–1499. doi:10.1175/1520-0493(2001)129<1481:acsoec>2.0.co;2.

Wang, Y. Q. (1998). On the bogusing of tropical cyclones in numerical models: The influence of vertical structure. Meteorology and Atmospheric Physics, 65(3–4), 153–170. doi:10.1007/bf01030785.

Willoughby, H. E. (1988). The dynamics of the tropical cyclone core. Australian Meteorological Magazine, 36, 183–191.

Willoughby, H. E. (1999). Hurricane heat engines. Nature, 401(6754), 649–650. doi:10.1038/44287.

Wood, K. M., and Ritchie, E. A. (2013). An updated climatology of tropical cyclone impacts on the southwestern United States. Monthly Weather Review, 141(12), 4322–4336. doi:10.1175/mwr-d-13-00078.1.

Wu, C. C., and Emanuel, K. A. (1994). On hurricane outflow structure. Journal of the Atmospheric Sciences, 51(13), 1995–2003. doi:10.1175/1520-0469(1994)051<1995:ohos>2.0.co;2.

Wu, G. X., and Lau, N. C. (1992). A GCM simulation of the relationship between tropical-storm formation and ENSO. Monthly Weather Review, 120(6), 958–977. doi:10.1175/1520-0493(1992)120<0958:agsotr>2.0.co;2.

Wu, L. G., Braun, S. A., Halverson, J., and Heymsfield, G. (2006). A numerical study of Hurricane Erin (2001). Part I: Model verification and storm evolution. Journal of the Atmospheric Sciences, 63(1), 65–86. doi:10.1175/jas3597.1.

Xu, J., and Wang, Y. Q. (2010). Sensitivity of tropical cyclone inner-core size and intensity to the radial distribution of surface entropy flux. Journal of the Atmospheric Sciences, 67(6), 1831–1852. doi:10.1175/2010jas3387.1.

Yan, Q., Korty, R., and Zhang, Z. S. (2015). Tropical cyclone genesis factors in a simulation of the last two millennia: Results from the Community Earth System Model. Journal of Climate, 28(18), 7182–7202. doi:10.1175/jcli-d-15-0054.1.

Yi, M., Fu, Y., Liu, P., and Zheng, Z. (2015). Deep convective clouds over the northern Pacific and their relationship with oceanic cyclones. Advances in Atmospheric Sciences, 32(6), 821–830. doi:10.1007/s00376-014-4056-9.

Yoo, J., Collins, J. M., and Rohli, R. V. (2014). Tropical cyclogenesis in the Intra-Americas Sea: Hurricane Cindy (2005). Professional Geographer, 66(3), 511–524. doi:10.1080/00330124.2013.805628.

Yu, Z. F., and Yu, H. (2011). Relation of the second type thermal helicity to precipitation of landfalling typhoons: A case study of Typhoon Talim. Acta Meteorologica Sinica, 25(2), 224–237. doi:10.1007/s13351-011-0029-4.

Zehr, R. (1992). Tropical Cyclogenesis in the Western North Pacific. NOAA Technical Report NESDIS, 16, 181.

Zhang, W., Leung, Y., and Wang, Y. F. (2013). Cluster analysis of post-landfall tracks of landfalling tropical cyclones over China. Climate Dynamics, 40(5–6), 1237–1255. doi:10.1007/s00382-012-1519-5.

Zhao, H., Yoshida, R., and Raga, G. B. (2015). Impact of the Madden–Julian Oscillation on Western North Pacific tropical cyclogenesis associated with large-scale patterns. Journal of Applied Meteorology and Climatology, 54(7), 1413–1429. doi:10.1175/jamc-d-14-0254.1.

Zhao, M., and Held, I. M. (2012). TC-permitting GCM simulations of hurricane frequency response to sea surface temperature anomalies projected for the late-twenty-first century. Journal of Climate, 25(8), 2995–3009. doi:10.1175/jcli-d-11-00313.1.

Zhao, M., Held, I. M., and Lin, S. J. (2012). Some counterintuitive dependencies of tropical cyclone frequency on parameters in a GCM. Journal of the Atmospheric Sciences, 69(7), 2272–2283. doi:10.1175/jas-d-11-0238.1.

Zhu, L., Zhang, D.-L., Cecelski, S. F., and Shen, X. (2015). Genesis of Tropical Storm Debby (2006) within an African easterly wave: Roles of the bottom-up and midlevel pouch processes. Journal of the Atmospheric Sciences, 72(6), 2267–2285. doi:10.1175/jas-d-14-0217.1.

8. APPENDIX: EXPANDED TABLES AND ANALYSIS

Table A.1. List of 200 hPa uses in literature for upper-level variable.

Author(s)	Year	Variable at 200 hPa
Abish et al.	2015	Mean zonal wind
Barrett et al.	2016	Outflow winds
Bell et al.	2006	Wind
Bhatia and Nolan	2013	Vertical wind shear
Bhowmik and Kotal	2010	Divergence
Black and Anthes	1971	Divergence
Bosart et al.	1999	Divergence
Boyle	1994	Divergence
Bracken and Bosart	2000	Divergence
Brammer and Thorncroft	2015	Divergence
Braun et al.	2006	Divergence
Businger et al.	2005	Divergence
Camargo et al.	2007a	Vertical wind shear
Camargo et al.	2007b	Vertical wind shear
Chan and Kwok	1999	Vertical wind shear
Chand and Walsh	2009	Divergence
Cheung	2004	Divergence
Choi et al.	2016	Divergence
Christy et al.	2010	Divergence
Colbert and Soden	2012	Wind
Colón and Nightingale	1963	Divergence
Corbosiero and Molinari	2002	Vertical wind shear
Daloz et al.	2012	Vertical wind shear
Davidson	2010	Divergence
Davidson and Kar	2002	Divergence
Davis	2015	Wind
Davis and Bosart	2003	Vertical wind shear
De Bellevue et al.	2007	Horizontal winds
DeMaria and Kaplan	1994	Vertical wind shear
DeMaria and Kaplan	1999	Divergence
DeMaria et al.	2001	Vertical wind shear
DeMaria et al.	2005	Divergence
Didlake and Houze	2013	Vertical wind shear
Dolling and Barnes	2014	Vertical wind shear
Done et al.	2014	Horizontal wind shear
Druyan et al.	1999	Vertical wind shear
Dunkerton et al.	2009	Divergence
Durden	2013	Divergence
Ellrod and Knapp	1992	Wind

(table cont'd.)

Author(s)	Year	Variable at 200 hPa
Elsberry and Jefferies	1996	Vertical wind shear
Elsberry and Stenger	2008	Outflow temperatures
Finocchio and Majumdar	2017	Wind
Fischer et al.	2017	Vertical wind shear
Fitzpatrick et al.	1995	Wind
Frank and Ritchie	2001	Potential vorticity
Fu et al.	2012	Divergence
Galarneau et al.	2015	Divergence
Georgiadis and Bigg	2007	Wind shear absolute intensity
Goldenberg et al.	2001	Vertical wind shear
Gollan and Greatbatch	2015	Divergence
Grams et al.	2011	Potential vorticity
Gray	1968	Divergence
Gray	1998	Streamline Winds
Hanley et al.	2001	Divergence
Hendricks et al.	2010	Divergence
Hennon and Hobgood	2003	Wind
Heymsfield et al.	2006	Vertical wind shear
Holton and Colton	1972	Divergence
Hulme and Martin	2009	Wind
Hunt and Watterson	2010	Vertical wind shear
Jeevarekha and Philominathan	2016	Vertical wind shear
Jeong et al.	2014	Wind
Jones et al.	2003	Divergence
Kaplan et al.	2010	Wind
Karyampudi and Pierce	2002	Divergence
Kerns and Chen	2013	Vertical wind shear
Kerns et al.	2008	Vorticity
Klotzbach	2011	Wind
Klotzbach and Gray	2006	Wind
Klotzbach and Gray	2009	Wind
Knaff et al.	2003	Divergence
Knaff et al.	2004	Vertical wind shear
Kodama and Businger	1998	Wind
Komaromi and Majumdar	2014	Divergence
Komaromi and Majumdar	2015	Divergence
Korty et al.	2012	Vertical wind shear
Kotal and Bhowmik	2013	Divergence
Krishnamurti	1971a	Divergence
Krishnamurti	1971b	Divergence
Landsea et al.	1998	Wind
Landsea et al.	2010	Wind

(table cont'd.)

Author(s)	Year	Variable at 200 hPa
Lee et al.	2015	Divergence
Leppert and Petersen	2010	Divergence
Leppert et al.	2013	Divergence
Leroux et al.	2013	Divergence
Leroux et al.	2016	Divergence
Li et al.	2014	Wind
Lowag et al.	2008	Vertical wind shear
Mallard et al.	2013a	Vertical wind shear
Mallard et al.	2013b	Vertical wind shear
Mauk and Hobgood	2012	Vertical wind shear
McBride and Gray	1980	Divergence
McBride and Zehr	1981	Divergence
McFarquhar et al.	2012	Vertical wind shear
McGauley and Nolan	2011	Vertical wind shear
McTaggart-Cowan	2007a	Wind
McTaggart-Cowan	2007b	Wind
McTaggart-Cowan	2008	Q-Vector divergence
McTaggart-Cowan	2013	Potential vorticity
Misra et al.	2013	Vertical wind shear
Molinari and Vollaro	1989	Outflow layer
Molinari et al.	2007	Vertical wind shear
Molinari et al.	1992	Wind
Moon et al.	2015	Vertical wind shear
Munsell et al.	2015	Vertical wind shear
Nolan	2007	Divergence
Owens and Landsea	2003	Wind
Paterson et al.	2005	Divergence
Peevey et al.	2014	Latitude of the maximum wind
Peng et al.	2012	Divergence
Qian et al.	2011	Wind
Qian et al.	2016a	Wind
Qian et al.	2016b	Wind
Randel et al.	2007b	Vorticity
Randel et al.	2007a	Vorticity
Rappin et al.	2011	Vertical wind shear
Raynak	2009	Divergence
Reader and Moore	1995	Wind
Ren et al.	2014	Outflow
Reynolds et al.	2013	Model bias
Riehl	1948	Wind
Riemer and Jones	2010	Wind
Riemer et al.	2010	Vertical wind shear

(table cont'd.)

Author(s)	Year	Variable at 200 hPa
Rios-Berrios et al.	2016a	Vertical wind shear
Rios-Berrios et al.	2016b	Vertical wind shear
Rodgers et al.	1998	Outflow
Ruiz-Barradas et al.	2000	Divergence
Sall et al.	2006	Vertical wind shear
Sanabia et al.	2014	Vertical wind shear
Sandhya et al.	2015	Wind
Schiemann et al.	2009	Wind
Schumacher et al.	2009	Vertical wind shear
Shi et al.	1997	Divergence
Shu et al.	2014	Wind
Simpson et al.	1997	Wind
Sippel et al.	2011	Vertical wind shear
Song et al.	2016	Divergence
Srinivas et al.	2007	Divergence
Srivastava and Bhardwaj	2014	Divergence
Strong and Davis	2006	Wind
Sugi et al.	2002	Potential Temperature
Tao and Zhang	2015	Vertical wind shear
Tian et al.	2013	Divergence
Tippett et al.	2011	Vertical wind shear
Torn and Cook	2013	Divergence
Ventrice et al.	2012	Wind anomalies
Vizy and Cook	2009	Divergence
Wu and Emanuel	1994	Outflow fields
Wu and Lau	1992	Divergence
Wu et al.	2006	Divergence
Yan et al.	2015	Vertical wind shear
Yi et al.	2015	Divergence
Yu and Yu	2011	Divergence
Zehr	1992	Divergence
Zhang et al.	2013	Divergence
Zhao and Held	2012	Vertical wind shear
Zhao et al.	2012	Vertical wind shear
Zhao et al.	2015	Vertical wind shear
Zhu et al.	2015	Divergence

Table A.2. Extended version of Table 3.1 with manual Pre-TD coordinates listed.

TCG	Name	Classification	Lat °N	Long °W	Date 2005	Time	Lat °N (NN)	Long °W (NN)
1	Arlene	TD	16.90	84.00	08-Jun	18:00	17.50	83.75
1	Arlene	TD	17.40	83.90	09-Jun	00:00	17.50	83.75
1	Arlene	TCG	18.20	83.90	09-Jun	06:00	18.75	83.75
1	Arlene	TS	19.00	84.00	09-Jun	12:00	18.75	83.75
1	Arlene	TS	19.70	84.10	09-Jun	18:00	20.00	83.75
2	Bret	Disturbance	20.00	95.00	28-Jun	12:00	20.00	95.00
2	Bret	TD	19.70	95.40	28-Jun	18:00	20.00	95.00
2	Bret	TCG	20.00	95.80	29-Jun	00:00	20.00	96.25
2	Bret	TS	20.40	96.40	29-Jun	06:00	20.00	96.25
2	Bret	TS	20.80	97.30	29-Jun	12:00	21.25	97.50
3	Cindy	TD	22.30	89.00	04-Jul	18:00	22.50	88.75
3	Cindy	TD	23.90	89.70	05-Jul	00:00	23.75	90.00
3	Cindy	TCG	25.10	90.20	05-Jul	06:00	25.00	90.00
3	Cindy	TS	26.40	90.40	05-Jul	12:00	26.25	90.00
3	Cindy	TS	27.60	90.50	05-Jul	18:00	27.50	90.00
4	Dennis	TD	12.20	62.50	05-Jul	00:00	12.50	62.50
4	Dennis	TD	12.50	64.20	05-Jul	06:00	12.50	63.75
4	Dennis	TCG	13.00	65.90	05-Jul	12:00	12.50	66.25
4	Dennis	TS	13.60	67.30	05-Jul	18:00	13.75	67.50
4	Dennis	TS	14.30	68.50	06-Jul	00:00	13.75	68.75
5	Emily	TD	10.90	44.40	11-Jul	12:00	11.25	45.00
5	Emily	TD	11.00	45.40	11-Jul	18:00	11.25	45.00
5	Emily	TCG	11.00	46.80	12-Jul	00:00	11.25	46.25
5	Emily	TS	11.00	48.50	12-Jul	06:00	11.25	48.75
5	Emily	TS	11.00	50.20	12-Jul	12:00	11.25	50.00
6	Franklin	Disturbance	25.00	75.00	21-Jul	12:00	25.00	75.00
6	Franklin	TD	25.00	75.00	21-Jul	18:00	25.00	75.00
6	Franklin	TCG	25.70	75.90	22-Jul	00:00	26.25	76.25
6	Franklin	TS	26.20	76.40	22-Jul	06:00	26.25	76.25
6	Franklin	TS	26.60	76.80	22-Jul	12:00	26.25	76.25
7	Gert	TD	19.30	92.90	23-Jul	18:00	18.75	92.50
7	Gert	TD	19.80	93.80	24-Jul	00:00	20.00	93.75
7	Gert	TCG	20.80	95.00	24-Jul	06:00	21.25	95.00
7	Gert	TS	21.00	95.80	24-Jul	12:00	21.25	96.25
7	Gert	TS	21.40	96.60	24-Jul	18:00	21.25	96.25
8	Harvey	TD	28.20	68.80	02-Aug	18:00	28.75	68.75
8	Harvey	TD	28.90	68.70	03-Aug	00:00	28.75	68.75
8	Harvey	TCG	29.50	68.60	03-Aug	06:00	30.00	68.75
8	Harvey	TS	30.30	68.30	03-Aug	12:00	30.00	68.75
8	Harvey	TS	30.90	67.70	03-Aug	18:00	31.25	67.50
9	Irene (1)	TD	19.30	43.50	07-Aug	00:00	18.75	43.75
9	Irene (1)	TD	19.70	44.20	07-Aug	06:00	20.00	43.75
9	Irene (1)	TCG	20.20	45.00	07-Aug	12:00	20.00	45.00
9	Irene (1)	TS	20.80	46.00	07-Aug	18:00	21.25	46.25
9	Irene (1)	TS	21.30	47.20	08-Aug	00:00	21.25	47.50
10	Irene (2)	TD	22.40	57.20	10-Aug	12:00	22.50	57.50

(table cont'd.)

TCG	Name	Classification	Lat °N	Long °W	Date 2005	Time	Lat °N (NN)	Long °W (NN)
10	Irene (2)	TD	22.80	58.10	10-Aug	18:00	22.50	57.50
10	Irene (2)	TCG	23.30	59.30	11-Aug	00:00	23.75	58.75
10	Irene (2)	TS	23.90	60.40	11-Aug	06:00	23.75	60.00
10	Irene (2)	TS	24.70	61.70	11-Aug	12:00	25.00	61.25
11	Jose	Disturbance	19.40	94.50	22-Aug	06:00	20.00	95.00
11	Jose	TD	19.40	94.50	22-Aug	12:00	20.00	95.00
11	Jose	TCG	19.60	95.00	22-Aug	18:00	20.00	95.00
11	Jose	TS	19.70	95.70	23-Aug	00:00	20.00	96.25
11	Jose	TS	19.70	96.70	23-Aug	06:00	20.00	96.25
12	Katrina	TD	23.40	75.70	24-Aug	00:00	23.75	76.25
12	Katrina	TD	23.80	76.20	24-Aug	06:00	23.75	76.25
12	Katrina	TCG	24.50	76.50	24-Aug	12:00	25.00	76.25
12	Katrina	TS	25.40	76.90	24-Aug	18:00	25.00	77.50
12	Katrina	TS	26.00	77.70	25-Aug	00:00	26.25	77.50
13	Lee	Disturbance	26.90	52.70	31-Aug	00:00	27.50	52.50
13	Lee	TD	28.00	51.60	31-Aug	06:00	27.50	51.25
13	Lee	TCG	29.00	50.40	31-Aug	12:00	28.75	50.00
13	Lee	TS	30.10	50.10	31-Aug	18:00	30.00	50.00
13	Lee	TD	31.10	50.30	01-Sep	00:00	31.25	50.00
14	Maria	TD	19.90	47.20	02-Sep	00:00	20.00	47.50
14	Maria	TD	20.50	48.30	02-Sep	06:00	20.00	48.75
14	Maria	TCG	21.10	49.40	02-Sep	12:00	21.25	50.00
14	Maria	TS	21.50	50.20	02-Sep	18:00	21.25	50.00
14	Maria	TS	22.00	51.00	03-Sep	00:00	22.50	51.25
15	Ophelia	TD	26.80	78.30	06-Sep	18:00	26.25	78.75
15	Ophelia	TD	27.40	78.50	07-Sep	00:00	27.50	78.75
15	Ophelia	TCG	27.90	78.80	07-Sep	06:00	27.50	78.75
15	Ophelia	TS	28.70	79.20	07-Sep	12:00	28.75	78.75
15	Ophelia	TS	28.80	79.30	07-Sep	18:00	28.75	78.75
16	Nate	Disturbance	28.40	67.00	05-Sep	12:00	28.75	67.50
16	Nate	TD	28.40	67.00	05-Sep	18:00	28.75	67.50
16	Nate	TCG	28.40	66.60	06-Sep	00:00	28.75	66.25
16	Nate	TS	28.50	66.50	06-Sep	06:00	28.75	66.25
16	Nate	TS	28.50	66.50	06-Sep	12:00	28.75	66.25
17	Philippe	Disturbance	13.30	54.50	17-Sep	06:00	13.75	55.00
17	Philippe	TD	13.30	54.50	17-Sep	12:00	13.75	55.00
17	Philippe	TCG	13.50	54.90	17-Sep	18:00	13.75	55.00
17	Philippe	TS	13.90	55.10	18-Sep	00:00	13.75	55.00
17	Philippe	TS	14.40	55.30	18-Sep	06:00	15.00	55.00
18	Rita	TD	21.60	70.70	18-Sep	06:00	21.25	71.25
18	Rita	TD	21.90	71.50	18-Sep	12:00	22.50	71.25
18	Rita	TCG	22.20	72.30	18-Sep	18:00	22.50	72.50
18	Rita	TS	22.40	73.00	19-Sep	00:00	22.50	72.50
18	Rita	TS	22.60	73.80	19-Sep	06:00	22.50	73.75
19	Stan	TD	19.10	86.20	01-Oct	18:00	18.75	86.25
19	Stan	TD	19.30	86.70	02-Oct	00:00	18.75	86.25
19	Stan	TCG	19.50	87.20	02-Oct	06:00	20.00	87.50

(table cont'd.)

TCG	Name	Classification	Lat °N	Long °W	Date 2005	Time	Lat °N (NN)	Long °W (NN)
19	Stan	TS	19.80	87.90	02-Oct	12:00	20.00	87.50
19	Stan	TS	20.30	88.80	02-Oct	18:00	20.00	88.75
20	Unnamed	Disturbance	33.80	31.80	04-Oct	00:00	33.75	31.25
20	Unnamed	SD	34.80	30.20	04-Oct	06:00	35.00	30.00
20	Unnamed	TCG	35.90	28.50	04-Oct	12:00	36.25	28.75
20	Unnamed	STS	37.10	26.70	04-Oct	18:00	37.50	26.25
20	Unnamed	STS	38.80	25.00	05-Oct	00:00	38.75	25.00
21	Tammy	Disturbance	26.70	79.20	04-Oct	18:00	26.25	78.75
21	Tammy	Disturbance	27.30	79.70	05-Oct	00:00	27.50	80.00
21	Tammy	TCG	27.30	79.70	05-Oct	06:00	27.50	80.00
21	Tammy	TS	28.30	80.20	05-Oct	12:00	28.75	80.00
21	Tammy	TS	29.50	80.90	05-Oct	18:00	30.00	81.25
22	Vince	Disturbance	32.50	20.60	07-Oct	18:00	32.50	20.00
22	Vince	Disturbance	32.90	20.60	08-Oct	00:00	32.50	20.00
22	Vince	TCG	32.90	20.60	08-Oct	06:00	32.50	20.00
22	Vince	SS	33.00	20.30	08-Oct	12:00	32.50	20.00
22	Vince	SS	33.10	20.10	08-Oct	18:00	32.50	20.00
23	Wilma	TD	17.50	79.40	16-Oct	18:00	17.50	80.00
23	Wilma	TD	17.40	79.60	17-Oct	00:00	17.50	80.00
23	Wilma	TCG	16.90	79.60	17-Oct	06:00	17.50	80.00
23	Wilma	TS	16.30	79.70	17-Oct	12:00	16.25	80.00
23	Wilma	TS	16.00	79.80	17-Oct	18:00	16.25	80.00
24	Alpha	Disturbance	15.80	67.50	22-Oct	06:00	16.25	67.50
24	Alpha	TD	15.80	67.50	22-Oct	12:00	16.25	67.50
24	Alpha	TCG	16.50	68.50	22-Oct	18:00	16.25	68.75
24	Alpha	TS	17.30	69.60	23-Oct	00:00	17.50	70.00
24	Alpha	TS	17.80	70.50	23-Oct	06:00	17.50	70.00
25	Beta	TD	10.40	80.90	26-Oct	18:00	10.00	81.25
25	Beta	TD	10.70	81.10	27-Oct	00:00	11.25	81.25
25	Beta	TCG	11.00	81.30	27-Oct	06:00	11.25	81.25
25	Beta	TS	11.30	81.30	27-Oct	12:00	11.25	81.25
25	Beta	TS	11.60	81.30	27-Oct	18:00	11.25	81.25
26	Gamma (1)	TD	14.10	64.20	14-Nov	18:00	13.75	63.75
26	Gamma (1)	TD	14.20	65.00	15-Nov	00:00	13.75	65.00
26	Gamma (1)	TCG	14.30	66.00	15-Nov	06:00	13.75	66.25
26	Gamma (1)	TS	14.40	67.10	15-Nov	12:00	15.00	67.50
26	Gamma (1)	TD	14.70	68.40	15-Nov	18:00	15.00	68.75
27	Gamma (2)	Disturbance	15.70	84.80	18-Nov	06:00	16.25	85.00
27	Gamma (2)	Disturbance	15.50	85.50	18-Nov	12:00	15.00	85.00
27	Gamma (2)	TCG	15.70	85.60	18-Nov	18:00	16.25	85.00
27	Gamma (2)	TS	16.00	85.60	19-Nov	00:00	16.25	85.00
27	Gamma (2)	TS	16.10	85.60	19-Nov	06:00	16.25	85.00
28	Delta	Extratropical	31.40	39.90	22-Nov	06:00	31.25	40.00
28	Delta	Extratropical	31.20	39.80	22-Nov	12:00	31.25	40.00
28	Delta	TCG	30.70	40.50	22-Nov	18:00	31.25	40.00
28	Delta	SS	29.90	40.90	23-Nov	00:00	30.00	41.25
28	Delta	SS	28.80	41.30	23-Nov	06:00	28.75	41.25

(table cont'd.)

TCG	Name	Classification	Lat °N	Long °W	Date 2005	Time	Lat °N (NN)	Long °W (NN)
29	Epsilon	Disturbance	31.50	47.00	28-Nov	18:00	31.25	47.50
29	Epsilon	Disturbance	31.50	48.00	29-Nov	00:00	31.25	47.50
29	Epsilon	TCG	31.50	49.20	29-Nov	06:00	31.25	48.75
29	Epsilon	TS	31.60	50.00	29-Nov	12:00	31.25	50.00
29	Epsilon	TS	31.40	50.80	29-Nov	18:00	31.25	51.25
30	Zeta	Disturbance	23.90	35.60	29-Dec	18:00	23.75	35.00
30	Zeta	TD	23.90	35.60	30-Dec	00:00	23.75	35.00
30	Zeta	TCG	24.20	36.10	30-Dec	06:00	23.75	36.25
30	Zeta	TS	24.70	36.60	30-Dec	12:00	25.00	36.25
30	Zeta	TS	25.20	37.00	30-Dec	18:00	25.00	37.50

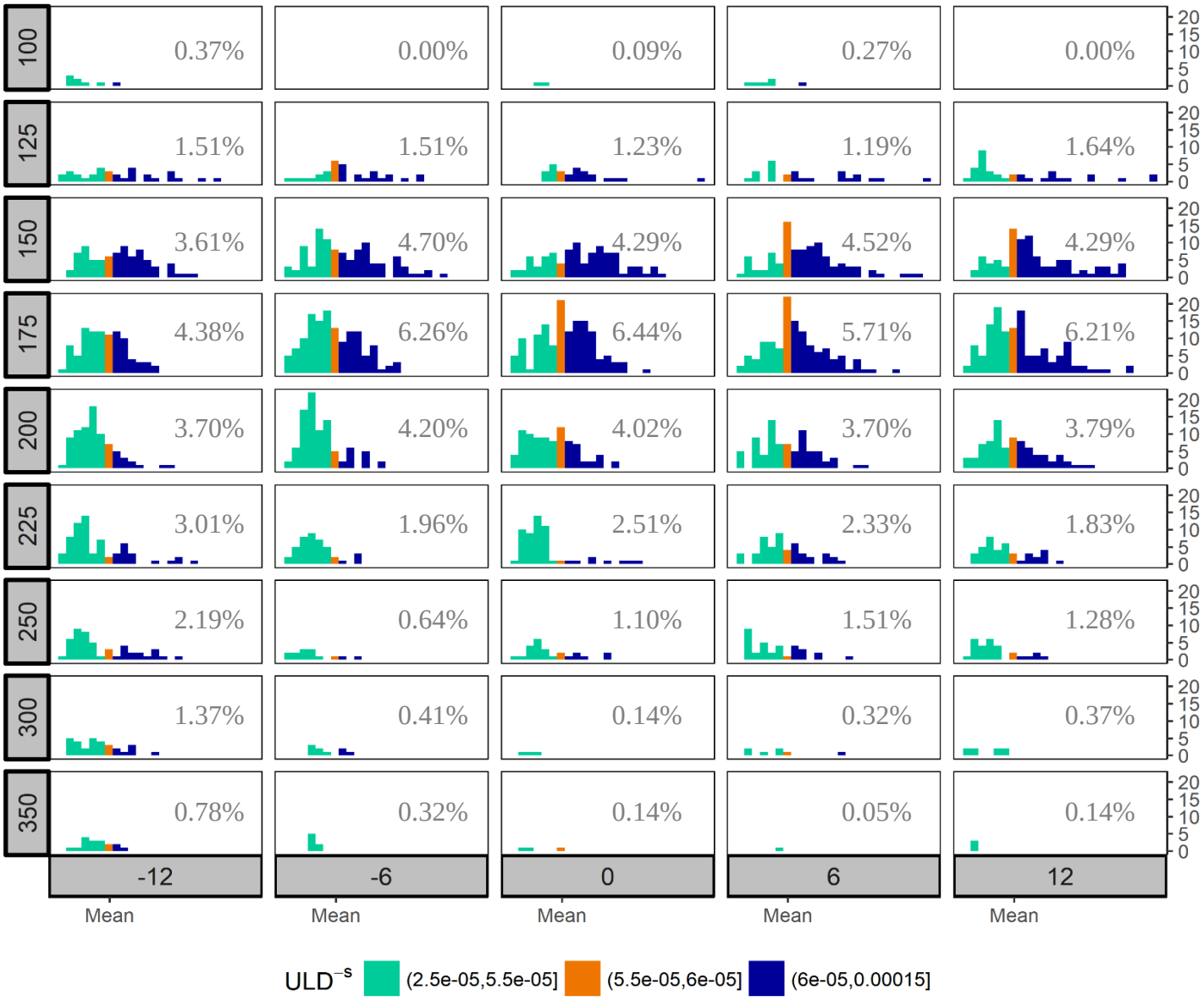

Figure A.1. Same as Figure 4.32 but for all levels included in study.

VITA

Sara Ann Rackett Ates was born in Alexandria, Louisiana. Always inquisitive about the Earth-ocean-atmosphere system, she decided to attend college in 2010 after raising four daughters and completed her B.S. degree in Geology and Geophysics at Louisiana State University (LSU) in May 2014. Sara also earned a double minor in Geography and Disaster Science and Management. She then entered the M.S. program in Geography at LSU and she is a candidate to graduate in May 2018. She has developed new interests and skills in geospatial technologies, analysis, and statistical programming. Sara will begin her Ph.D. program at LSU in the Department of Oceanography and Coastal Sciences in January 2018.